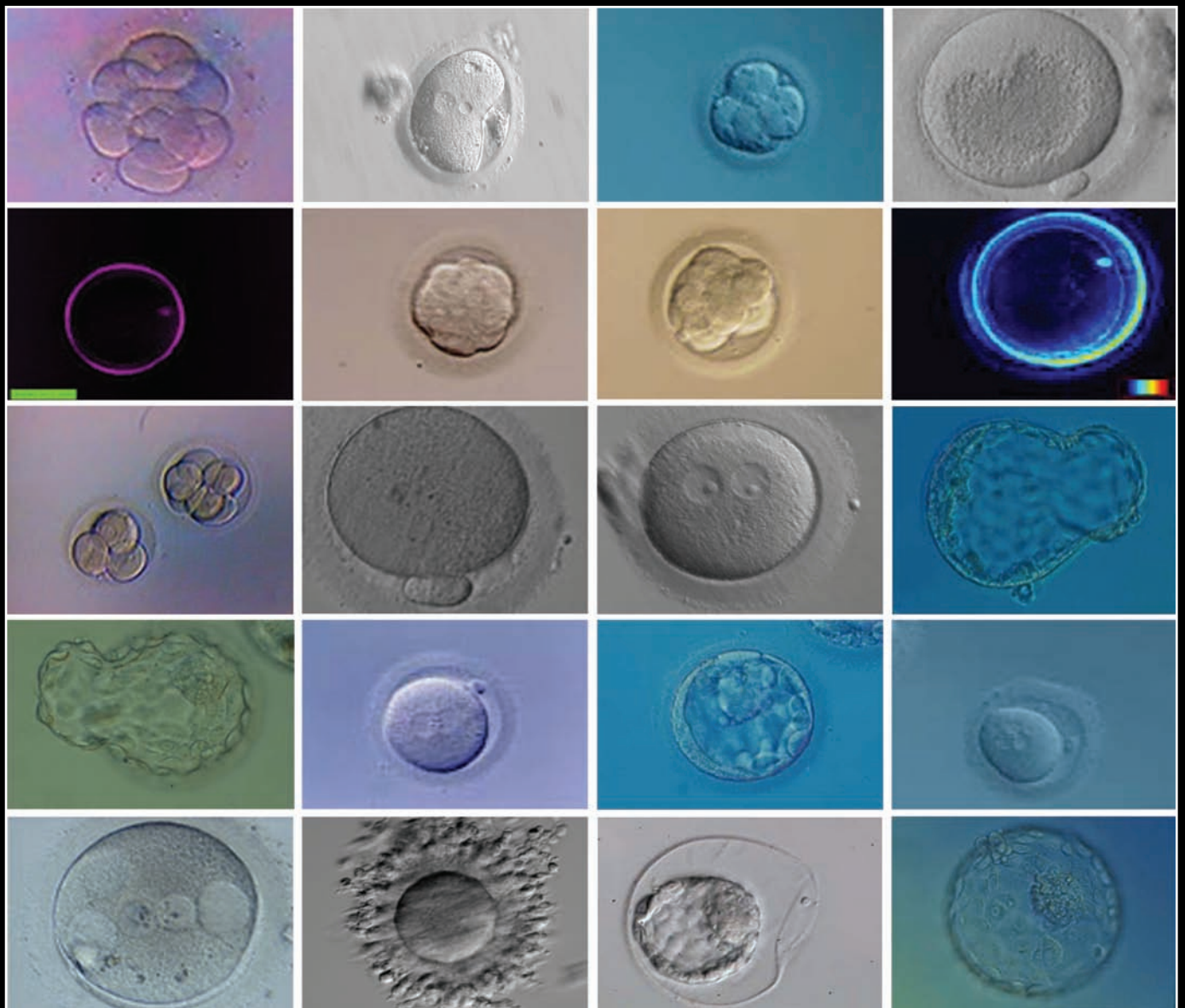


Atlas of Human Embryology: from Oocytes to Preimplantation Embryos

M. Cristina Magli, Gayle M. Jones, Kersti Lundin, Etienne Van den Abbeel
and The Special Interest Group on Embryology



M.C. Magli, G.M. Jones, K. Lundin and E. Van den Abbeel

Atlas of Human Embryology

Human Reproduction Vol. 27, Suppl. 1, 2012

OXFORD
UNIVERSITY PRESS

Human Reproduction
Volume 27 Supplement 1 August 2012
Oxford University Press

 **eshre**
SCIENCE MOVING
PEOPLE
MOVING SCIENCE

ATLAS OF HUMAN EMBRYOLOGY

**From Oocytes To
Preimplantation Embryos**

Edited by

M. Cristina Magli

Gayle M. Jones

Kersti Lundin

Etienne Van den Abbeel

An ESHRE SIG Embryology Initiative

For Loredana Papale, in memorium. Now her passion for Embryology and her strong belief in Embryologists taking a leading role will last forever

Bibliography for Figures

- Arroyo Cardona G**, Institut Universitari Dexeus, 7508028 Barcelona, Spain: Figures 125, 242, 302
- Balaban B**, American Hospital, Assisted Reproduction Unit, 34365 Istanbul, Turkey: Figures 32, 48-50, 69, 73, 94, 134, 197, 203-204, 207-208
- Barriere P**, CHU Nantes, 44093 Nantes Cedex 01, France: Figures 311, 347
- Biogenesi IVF Lab**, Biogenesi, Istituti Clinici Zucchi, 20900 Monza, Italy: Figure 52
- Castelletti E**, IIRM, 6924 Sorengo, Switzerland: Figures 85-87, 90-92, 103, 109, 115, 120-121, 126, 136-137, 143-146, 148, 150, 158, 162, 164, 167-168, 170-171, 173, 190-192, 196
- Ciray NH**, Bahceci Fulya IVF Center Hakki Yeten, 34439 Istanbul, Turkey: Figures 21-22, 54-56, 58, 60, 67-68
- Debrock S**, Leuven University Fertility Center, UZ Leuven Campus Gasthuisberg, B-3000 Leuven, Belgium: Figures 216-217, 232, 234, 236-238, 248, 251-252, 255, 259-260, 262, 283, 288, 291, 295
- De Pablo Franco JL**, Hospital Quirón Bilbao, 48014 Bilbao, Spain: Figures 95, 163, 185, 200, 209, 213-215, 266, 269, 272, 294
- De Santis L**, IVF Unit, Dept Ob/Gyn, H San Raffaele, 20132 Milano, Italy: Figures 20, 81
- Ebner T**, Landes-Frauen- und Kinderklinik Kinderwunsch Zentrum, A4020 Linz, Austria: Figures 10, 12, 25, 31, 42-44, 46, 63, 66, 74-76, 78-79, 174, 184, 304, 316-317, 344, 356
- Ferrer Robles E**, CREA, Centro Médico de Reproducción Asistida, 46003 Valencia, Spain: Figures 220, 241, 263, 275, 278
- Fiorentino A**, Department of Obstetrical, Gynecological and Urological Science and Reproductive Medicine, University of Naples Federico II, 80131 Napoli, Italy: Figures 17, 30, 35, 189, 193-194, 198, 201-202, 256
- Gago García M**, Clinica Quirúrgica Tambre C, 828002 Madrid, Spain: Figures 122, 296, 298, 300, 336, 373
- Gardner DK**, University of Melbourne, 3010 Parkville, Victoria, Australia: Figures 309, 319, 324, 342
- Gómez Sánchez E**, Tahe Reproducción, 30007 Murcia, Spain: Figures 277, 297
- Greuner M**, GMP Happel/Giebel/Russu/Otte, 66113 Saarbrücken, Germany: Figures 11, 88, 93, 104, 110, 159, 161, 172, 188, 199, 205, 270
- Guerrero Villena J**, Instituto Bernabeu, 03016 Alicante, Spain: Figures 282, 286, 289
- Hardarson T**, Fertilitetscentrum Carlanderska Hospital, 40229 Göteborg, Sweden: Figures 321, 346, 353-354, 363, 376, 389
- Herreros Cuesta J**, Hospital Universitario Madrid-Montepríncipe; Unidad de Reproducción, 28660 Boadilla del Monte (Madrid), Spain: Figures 226, 249, 254, 258, 267, 274, 280, 290
- Huguet Gutiérrez E**, IVI Madrid, 28023 Madrid; Spain: Figures 62, 97-98, 141-142, 187, 221, 250, 264, 276, 301
- Iglesias Núñez M**, Hospital Quiron Madrid, 28223 Pozuelo de Alarcón, Spain: Figure 299
- Jones GM**, Centre for Human Reproduction, Genesis Athens Clinic, 15232 Halandri, Greece; GMJ A.R.T. Solutions, 3051 North Melbourne, Victoria, Australia; Monash Immunology & Stem Cell Laboratories, 3800 Monash University, Clayton, Victoria, Australia: Figures 306, 308, 313-314, 320, 322, 325-326, 328-334, 338-341, 343, 348-349, 355, 357-361, 364-368, 370-372, 377-381, 383-384, 386-388, 390-393, 395-397
- Lemmen J**, Copenhagen University Hospital Rigshospitalet, 2100 Copenhagen O, Denmark: Figures 224, 228, 231, 239-240, 243-244, 247, 285
- Mandelbaum J, de Larrouzière V**, Department of Reproductive Biology, Hôpital Tenon, 75020 Paris, France: Figures 5, 7-9
- Martín Mateos J**, FIV Recoletos Valladolid, 47004 Valladolid, Spain: Figure 225
- Mercader A**, IVI-Valencia, 46015 Valencia, Spain: Figures 337, 345, 362, 394
- Moragas Solanes M**, Hospital Quirón Barcelona; 08023 Barcelona, Spain: Figures 210, 222, 245, 253, 279
- Montag M**, Department of Gynaecological Endocrinology and Fertility Disorders, University of Heidelberg, 69115 Heidelberg, Germany: Figures 27, 89, 96, 101, 108, 131, 135, 138, 149, 154, 156-157, 177, 179, 186
- Múgica A**, IBILAB, 07011 Palma de Mallorca, Islas Baleares, Spain: Figures 246, 271
- Nogueira D**, IFREARES - Laboratoire de Biologie de la Reproduction, Clinique Saint Jean Languedo, 31400 Toulouse, France: Figures 2, 3, 4
- Papale ML**, CRA Centro Riproduzione Assistita, 595128 Catania, Italy: Figures 99-100, 102, 105-107, 112-114, 117-119, 123-124, 127-130, 132-133, 139-140, 147, 151-153, 155, 160, 165-166, 169, 175-176, 178, 180-183, 195
- Pérez Bermejo G**, Hospital Universitario Madrid-Montepríncipe, Unidad de Reproducción, 28660 Boadilla del Monte (Madrid), Spain: Figures 212, 223, 268, 273, 284, 293
- Pons Gatell MC**, Centro Medico Teknon, Unitat de Reproducció Assistida, 08022 Barcelona, Spain: Figures 218, 292
- Prados FJ**, Unidad de Reproducción, Hospital Universitario Madrid-Montepríncipe, 28660 Boadilla del Monte, Spain: Figures 70, 219, 227, 229, 230, 233, 235, 257, 261, 265, 281, 287,
- Rienzi LF**, GENERA Centre for Reproductive Medicine, Clinica Valle Giulia, 00197 Roma, Italy: Figures 1, 14-16, 18-19, 23-24, 28-29, 33, 36-41, 45, 47, 51, 53, 57, 59, 61, 65, 71-72, 80, 82-84, 206, 312, 335
- Restelli L**, UO Sterilità di Coppia, Fondazione Ospedale Maggiore Policlinico Infertility Unit, 620122 Milano, Italy: Figures 6, 13, 34, 64
- Solvás Martínez I**, Centro Medico Teknon, Unitat de Reproducció Assistida, 08022 Barcelona, Spain: Figure 211
- Van Landuyt L**, CRG UZ Brussel ILaarbeeklaan, 1011090 Jette-Brussels, Belgium: Figures 303, 305, 307, 310, 315, 318, 327, 350-352, 369, 374-375, 382, 385
- Yoon SC**, Clinica Santa Maria, 70124 Bari, Italy: Figures 26, 77

The oocyte

Laura Rienzi, Basak Balaban, Thomas Ebner
and Jacqueline Mandelbaum

Contents

- Introduction
- A. Cumulus-enclosed oocyte
- B. Oocyte maturation stage
- C. Oocyte size and shape
- D. Cytoplasmic features
 - D.1 Ooplasm
 - D.2 Metaphase plate
- E. Extracytoplasmic features
 - E.1 Zona pellucida
 - E.2 Perivitelline space
 - E.3 Polar body

Introduction

The female gamete plays a crucial role in determining embryo competence and therefore *in vitro* fertilization (IVF) results. Oocyte quality is not only influenced by the nuclear and mitochondrial genome, but also by the microenvironment provided by the ovary and the pre-ovulatory follicle that influences transcription and translation, and as a consequence, cytoplasmic maturity. In contrast to *in vivo* processes, the application of ovarian hormone stimulation protocols for IVF bypasses the complicated selection procedure that usually occurs during oocyte development and maturation of a single oocyte for ovulation, and allows for the maturation of many oocytes, often with compromised quality.

It has been speculated (Van Blerkom and Henry, 1992) that some morphological irregularities, which can easily be assessed at the light microscopy level, may reflect a compromised developmental ability of the oocytes and could therefore represent a useful tool for selecting competent oocytes prior to fertilization. Oocyte morphological assessment in the laboratory is first based on the presentation of the cumulus–corona cells. For mature oocytes, the cumulus–corona mass should appear as an expanded and mucified layer, due to active secretion of hyaluronic acid. This extracellular matrix molecule interposes between the cumulus cells (CCs), separating them and conferring to the cumulus–corona mass a fluffy ‘cloud-like’ appearance. However, stimulated cycles may be characterized by asynchrony between the nuclear maturation status of the oocyte and the expansion of the cumulus–corona cell mass. This has been suggested to be caused by a different sensitivity of the oocyte and the cumulus–corona mass to the stimulants (Laufer *et al.*, 1984).

Following the removal of the cumulus–corona cells in preparation for intracytoplasmic sperm injection (ICSI), oocyte evaluation is more accurate and is based on the nuclear maturation status, the morphology of the cytoplasm and on the appearance of the extracytoplasmic structures. The presence of the first polar body (PBI) is normally considered to be a marker of oocyte nuclear maturity. However, recent studies using polarized light microscopy have shown that oocytes displaying a polar body may still be immature (Rienzi *et al.*, 2005). Only those displaying a meiotic spindle (MS) can in fact be considered as true, mature, Metaphase II (MII) stage oocytes. The presence, position and retardance of the MS have been suggested to be related to developmental competence. In accordance with a recent meta-analysis (Petersen *et al.*, 2009), however, only *in vitro* development can be related to the morphology of the MS. Analyses of *in vivo* development are relatively rare in the literature and the meta-analysis failed to show significant differences in implantation rates between embryos derived from oocytes displaying a detectable MS and those without.

Nuclear maturity alone is, in fact, not enough to determine the quality of an oocyte. Nuclear and cytoplasmic maturation should be completed in a coordinated manner to ensure optimal conditions for subsequent fertilization. An ideal mature human oocyte, based on morphological characteristics, should have a ‘normal-looking’ cytoplasm, a single polar body, an appropriate zona pellucida (ZP) thickness and proper perivitelline space (PVS; Swain and Pool, 2008). However, the majority of the oocytes retrieved after ovarian hyperstimulation exhibit one or more variations in the described ‘ideal’ morphological criteria (De Sutter *et al.*, 1996; Xia, 1997; Balaban *et al.*, 1998; Mikkelsen and Lindenberg, 2001; Balaban and Urman, 2006; Ebner *et al.*, 2006; Rienzi *et al.*, 2008). This is also true for oocytes obtained from proven fertile donors (Ten *et al.*, 2007). Morphology, moreover, often fails to predict fertilizing ability and developmental competence (Rienzi *et al.*, 2011). Only a few morphologically detectable features of the Metaphase II oocyte indicate compromised developmental ability. According to the Istanbul consensus workshop on embryo assessment (Alpha Scientists in Reproductive Medicine and ESHRE Special Interest Group of Embryology, 2011) extracytoplasmic anomalies (PBI morphology, PVS size, the appearance of the ZP) are simply phenotypic variations often related to *in vitro* culture and/or oocyte aging. On the other hand, a special deviation in the cytoplasmic texture, namely the presence of aggregations of smooth endoplasmic reticulum (SER) is potentially lethal and developmental competence of

these oocytes should be interpreted with caution. Oocyte morphology may also reflect genetic abnormalities. This is the case for giant oocytes that contain one additional set of chromosomes. These oocytes, when observed with polarized light microscopy, display two distinct MS. Although, the occurrence of giant oocytes is relatively rare after ovarian hyperstimulation, the use of these cells for IVF is dangerous.

Owing to the complex mechanisms related to oocyte maturation and acquisition of competence, it is unlikely that a single characteristic (with the exception of oocyte size and the presence of SER aggregates) can adequately reflect the quality of the cell. Accordingly, to obtain information about the competence of the oocyte, morphological assessment should be combined with other approaches (i.e. cumulus–corona cell gene expression, metabolomics and oxygen consumption). Further predictive value could be obtained by combining the oocyte evaluation with evaluations of preimplantation development (pronuclear stage, cleavage stage and blastocyst stage).

A. Cumulus-enclosed oocytes

During follicular antrum formation, granulosa cells (GCs) differentiate into mural GCs, lining the follicular wall, and CCs, surrounding the oocyte. Within the cumulus mass, CCs in close contact with the oocyte (corona cells) develop cytoplasmic projections which cross the ZP and form gap junctions with the oolemma. This organized structure is called the cumulus–oocyte complex (COC; Fig. 1; Albertini *et al.*, 2001). In natural spontaneous cycles, oocyte nuclear maturation runs parallel to the gradual FSH-dependent expansion of the cumulus and corona cells, whereas this synchrony may be disturbed in stimulated cycles (Laufer *et al.*, 1984). Immature COCs (Fig. 2), commonly retrieved from small follicles during *in vitro* maturation (IVM) cycles, show a typically unexpanded cumulus with multilayers of compact GCs adhering to the ZP of an immature oocyte at prophase I [germinal-vesicle stage (GV); Figs 3 and 4]. IVM of such immature COCs aims for expansion of CCs and oocyte nuclear maturation.



Figure 1 Cumulus–oocyte complex obtained following ovarian stimulation. The oocyte is typically surrounded by an expanded cumulus corona cell complex. Note the outer CCs separated from each other by extracellular matrix and the corona cells immediately adjacent to the oocyte becoming less compact and radiating away from the ZP. PBI is located at the 1 o'clock position.

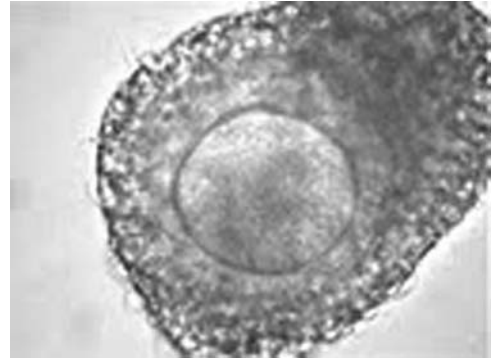


Figure 2 A cumulus–oocyte complex recovered from an IVM cycle showing an oocyte surrounded by unexpanded, compact cumulus and corona cells.

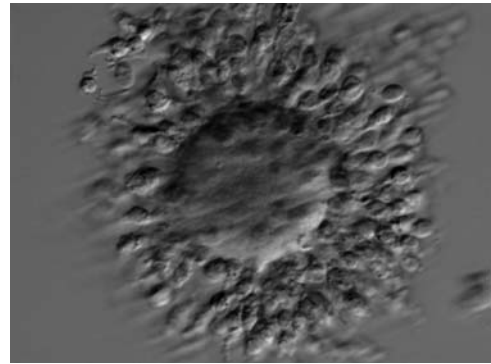


Figure 3 A cumulus–oocyte complex recovered from an IVM cycle. The immature GV oocyte is surrounded by compact GCs. The nucleolus in the GV is visible at the 10 o'clock position.

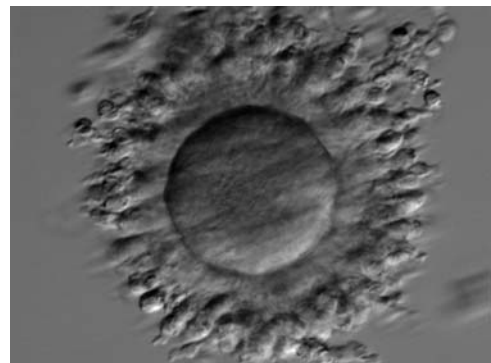


Figure 4 A cumulus–oocyte complex recovered from an IVM cycle. The immature oocyte has a GV at the 3 o'clock position with the nucleolus towards the centre of the oocyte. Compact GCs surround the oocyte.

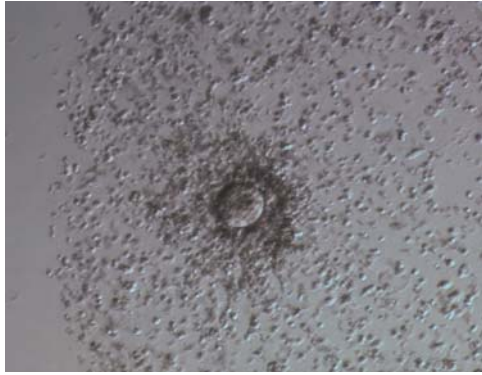


Figure 5 A cumulus oocyte complex at low magnification. The oocyte is surrounded by an expanded cumulus–corona cell complex clearly showing the separation of individual CCs due to the accumulation of hyaluronic acid in the extracellular space.

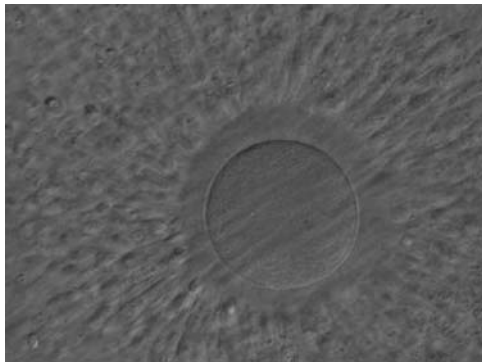


Figure 6 A cumulus–oocyte complex obtained following ovarian stimulation. An expanded cumulus corona cell complex surrounds the oocyte with the outer CCs separated from each other by extracellular matrix. The CCs immediately adjacent to the oocyte become less compact and radiate away from the ZP. The oocyte in the figure can be clearly seen through the surrounding cells at high magnification and no polar body can be seen in the PVS despite the mature status of the cumulus–corona cells.

In stimulated cycles, 34–38 h after triggering ovulation, a typical mature pre-ovulatory COC displays radiating corona cells surrounded by the expanded, loose mass of CCs (Fig. 5). In the majority of expanded COCs, oocytes are mature at the MII stage, although it is possible after gonadotrophin stimulation to find in a mucified cumulus and radiating corona cells an immature oocyte at the GV or metaphase I (MI) stage (Fig. 6). It is common, in stimulated cycles, to recover COCs with an expanded cumulus cell mass but compact, non-radiating corona cells (Figs 7a, 8a and 9a). Indeed, at recovery, the presence of the surrounding cumulus and corona cells usually prevents identification of the PBI in the PVS, an indicator of successful completion of meiosis I with arrest at the MII stage of development (Fig. 1). In preparation for ICSI, oocyte denudation is performed via enzymatic action of hyaluronidase (Figs 7b, 8b and 9b) and

mechanical pipetting, allowing the accurate determination of the oocyte nuclear status (Figs 7c, 8c and 9c).

The Alpha-ESHRE consensus document states that, although there is little corroborated evidence to support a correlation between the appearance of the COC and embryo developmental competence, a binary score (0 or 1) with a 'good' COC (score 1) defined as having an expanded cumulus and a radiating corona should be documented (Alpha Scientists in Reproductive Medicine and ESHRE Special Interest Group of Embryology, 2011).

The bidirectional communication between the oocyte and CCs, crucial for the acquisition of oocyte competence (Gilchrist et al., 2008), might perhaps be investigated in the future, through non-invasive analysis of CCs (pattern of gene expression or protein synthesis), offering new biomarkers of oocyte quality, compensating for the inadequacy of the COC morphological assessment (Feuerstein et al., 2007; Ouandaogo et al., 2011).

B. Oocyte maturation stage

The removal of the cumulus–corona cell mass gives the unique opportunity to evaluate oocyte morphology prior to fertilization, and in particular, the nuclear maturation stage. Oocyte nuclear maturity, as assessed by light microscopy, is assumed to be at the MII stage when the PBI is visible in the PVS (Figs 10 and 11). The MII stage is characterized by the alignment of the homologous chromosomes on the spindle equatorial plate during metaphase of the second meiotic division. It is generally recognized that 85% of the retrieved oocytes following ovarian hyperstimulation display the PBI and are classified as MII, whereas 10% present an intracytoplasmic nucleus called the 'germinal vesicle' (GV; Figs 12–14), characteristic of prophase I of the first meiotic division. Approximately 5% of the oocytes have neither a visible GV nor PBI and these oocytes are generally classified as MI oocytes (Figs 15–17; Rienzi and Ubaldi, 2009). These oocytes may, however, be at the GV breakdown stage where the nuclear envelope has broken down but has not as yet progressed to true MI where the chromosomes are aligned on the metaphase plate in preparation for the completion of the first meiotic division.

Additional information on oocyte nuclear status can be obtained with the use of polarized light microscopy combined with software for image processing for the non-invasive visualization of the MS and other oocyte birefringent structures. The MS is a microtubular structure involved in chromosome segregation, and therefore is crucial in the sequence of events leading to the correct completion of meiosis and subsequent fertilization. Parallel-aligned MS microtubules are birefringent and able to shift the plane of polarized light inducing a retardance; these properties enable the system to generate contrast and image the MS structure (Oldenbourg, 1999; Fig. 18). The presence of the MS gives more accurate information about the nuclear stage of the oocyte. In particular, some oocytes can be immature (at the stage of early telophase I) when observed with polarized light microscopy, despite the presence of PBI in the PVS. At this stage, in fact, there is continuity between the ooplasm of the oocyte and the forming PBI and the MS is interposed between the two separating cells (Figs 19–22). This condition normally has a duration of 75–90 min. The MS has been found to disappear in late telophase I (Fig. 23), reforming only 40–60 min later (Montag et al., 2011). However, it must be underlined that other factors, such as sub-optimal culture conditions, temperature

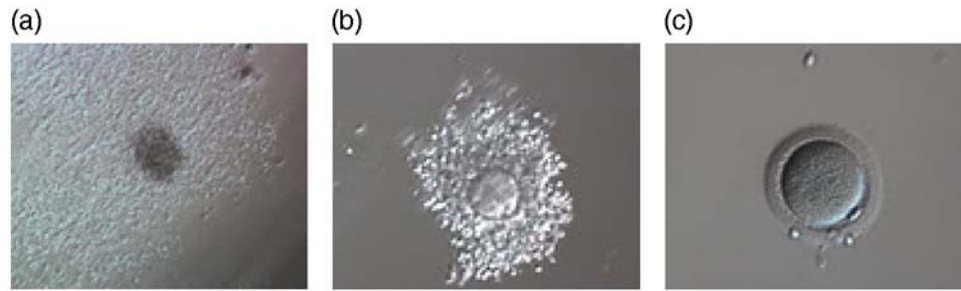


Figure 7 Denudation sequences of a mature oocyte. (a) Cumulus–corona oocyte complex before the denudation process with non-radiating CCs. (100× magnification). (b) Oocyte surrounded by corona cells during hyaluronidase treatment (200× magnification). (c) Denuded oocyte after mechanical stripping, a visible polar body is present in the PVS (200× magnification).



Figure 8 Denudation sequences of a mature oocyte. (a) Cumulus–corona oocyte complex before the denudation process (100× magnification). CCs are abundant. (b) Oocyte surrounded by corona cells during hyaluronidase treatment (200× magnification). Many CCs are still present, but the mature oocyte is already visible with PBI at the 7 o'clock position. (c) Denuded oocyte after mechanical stripping, a visible polar body is present in the PVS (200× magnification).



Figure 9 Denudation sequences of a mature oocyte. (a) Cumulus–corona oocyte complex before the denudation process with compact, non-radiating CCs. (100× magnification). (b) Oocyte surrounded by corona cells during hyaluronidase treatment (200× magnification). (c) Denuded oocyte after mechanical stripping, a visible polar body is present in the PVS (200× magnification).

fluctuations and chemical stress during manipulation, can contribute to MS disassembly (Rienzi and Ubaldi, 2009). Finally, the percentage of oocytes with detectable MS is also related to the time elapsed from HCG administration and is higher after 38 h (Cohen *et al.*, 2004). In general, it is expected that at least 80% of oocytes recovered following ovarian hyperstimulation are MS positive when viewed by polarized light microscopy.

C. Oocyte size and shape

A critical oocyte size is necessary for resumption of meiosis (Otoi *et al.*, 2000). At the beginning of oocyte growth, size is determined by strong adhesion between the oolemma and the inner zona surface (Tartia *et al.*, 2009). Around ovulation GLYT1 is activated

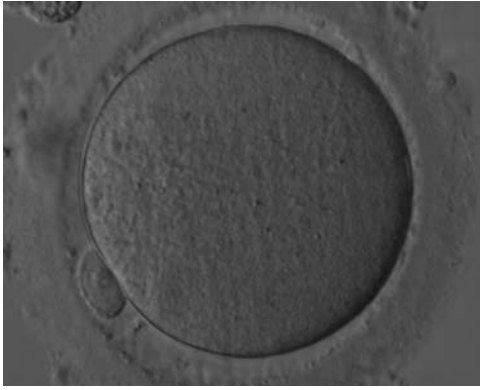


Figure 10 Denuded MII oocyte; an intact PBI is clearly visible in the PVS (400× magnification).



Figure 11 Denuded MII oocyte; the PBI is clearly visible in the narrow PVS (400× magnification).



Figure 12 Denuded GV oocyte. A typical GV oocyte with an eccentrically placed nucleus and a prominent single nucleolus (400× magnification).

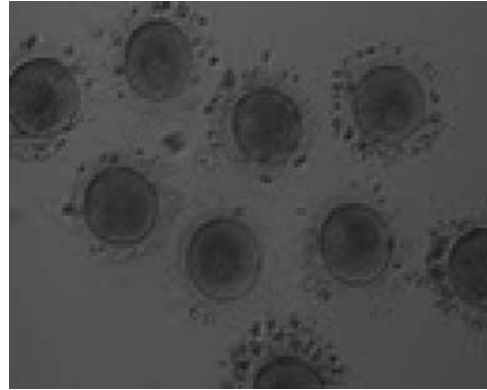


Figure 13 Denuded GV oocytes. Several GV with the organelles condensed centrally within the cytoplasm (200× magnification).

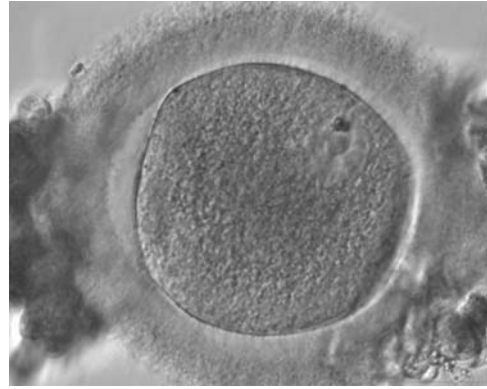


Figure 14 Denuded GV oocyte. A GV oocyte that is possibly approaching GVBD as the nuclear membrane is not distinct over its entirety (400× magnification).

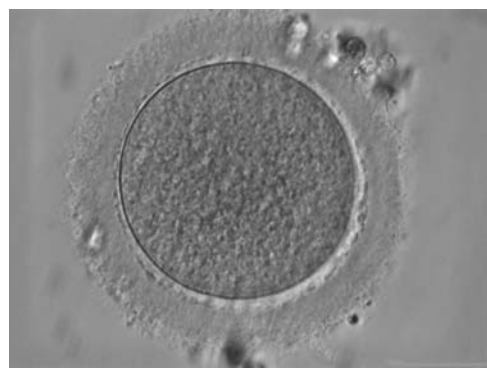


Figure 15 Denuded MI oocyte. This oocyte has no visible nucleus and has not as yet extruded the PBI (400× magnification). PVS is typically narrow.

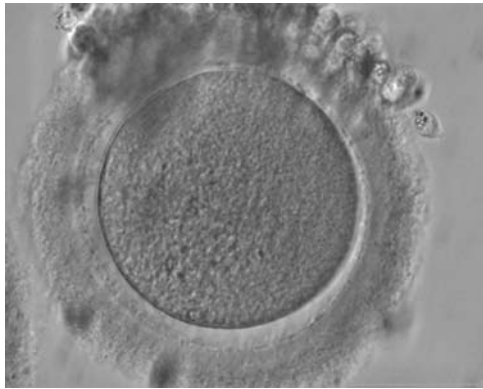


Figure 16 Denuded MI oocyte with no visible nucleus and no PBI (400× magnification). Some CCs are still tightly adhered to the ZP.



Figure 17 Denuded MI oocyte without a visible nucleus or an extruded PBI (400× magnification).

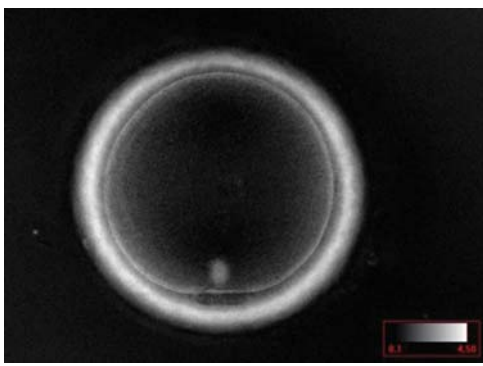


Figure 18 MII oocyte visualized using polarized light microscopy (400× magnification). The polar body is present at the 6 o'clock position in the PVS, and the MS of the second meiotic division is visible in the cytoplasm perfectly aligned to PBI position. This is a fully mature MII oocyte.

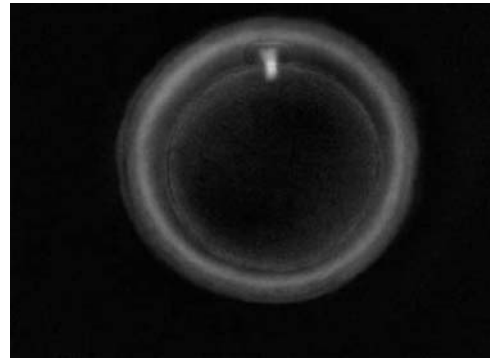


Figure 19 Telophase I oocyte visualized using polarized light microscopy (400× magnification). PBI is present in the PVS; however, the MS can be seen between PBI and the oocyte cytoplasm indicating that this oocyte is still completing the first meiotic division. This is not yet a fully mature MII oocyte.

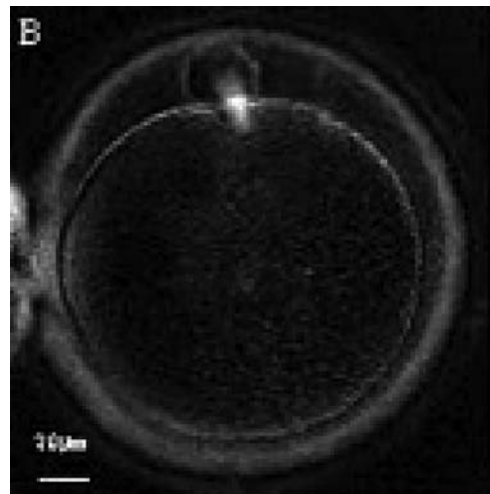


Figure 20 Telophase I oocyte visualized using polarized light microscopy (400× magnification). The MS can be seen between PBI and the oocyte cytoplasm indicating that the first meiotic division is not yet completed.

which mediates glycin accumulation which in turn acts as an osmolyte and thus controls cell volume (Baltz and Tartia, 2009).

The mean ovarian diameter of MII oocytes may vary substantially (Fig. 24) but it is not related to fertilization or developmental quality of human ICSI embryos at the cleavage stage of development (Romão *et al.*, 2010). The situation is different with giant oocytes (Balakier *et al.*, 2002; Rosenbusch *et al.*, 2002). This type of oocyte has about twice the volume of a normal oocyte (about 200 μm) and is tetraploid before meiosis due to their origin, i.e. nuclear but no cytoplasmic division in an oogonium or cytoplasmic fusion of two oogonia. These mechanisms explain the binucleate appearance of

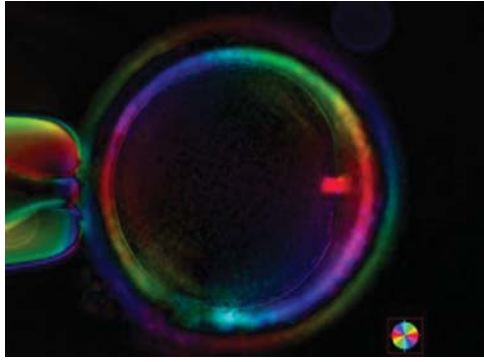


Figure 21 Telophase I oocyte visualized using polarized light microscopy (400× magnification). PBI is present in the PVS at the 3 o'clock position; however, the MS is still bridging PBI and the oocyte cytoplasm indicating that this oocyte is not yet a fully mature MII oocyte.

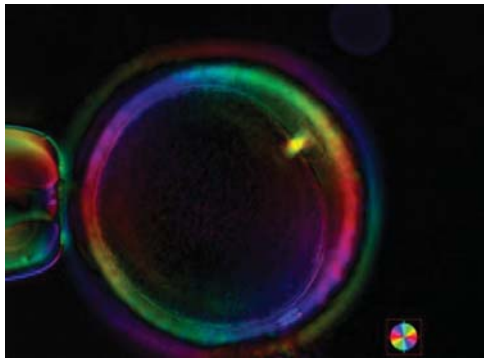


Figure 22 Telophase I oocyte visualized using polarized light microscopy (400× magnification). The MS can be seen between PBI and the oocyte cytoplasm indicating that this oocyte is still completing the first meiotic division despite the extrusion of PBI in the PVS.

prophase I giant eggs (Figs 25 and 26). These oocytes always contribute to digynic triploidy (Figs 27 and 28) and must never be transferred, although the presence of at least one giant oocyte in a cohort of retrieved eggs (Figs 29 and 30) has no effect on treatment outcome (Machtinger et al., 2011).

It is evident that oocytes with extreme forms of shape anomaly exist (Figs 31 and 32; Paz et al., 2004; Esfandiari et al., 2005). Such ova have been shown to be fertilizable and may lead to the birth of healthy babies. While quantifying the degree of the elongation, some authors (Ebner et al., 2008) realized that the dimensions of the shape anomaly were neither correlated with fertilization nor embryo quality. However, when oocytes with ovoid zonae (Figs 33 and 34) develop, day 2 embryos show a flat array of blastomeres rather than the more traditional tetrahedral arrangement and further development is often delayed (Ebner et al., 2008).

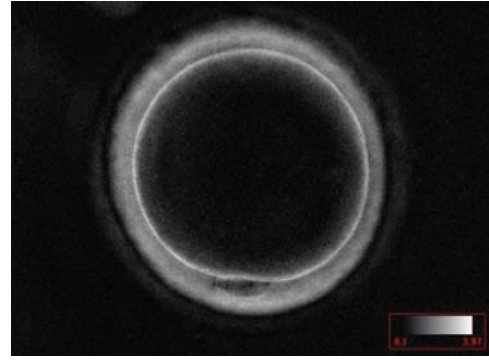


Figure 23 Interphase oocyte (between the first and second meiotic division; Prophase II) visualized using polarized light microscopy (400× magnification). PBI is present in the PVS at the 6 o'clock position; however, the MS of the second meiotic division is not yet visible in the cytoplasm. This is not yet a fully mature MII oocyte.



Figure 24 Small MII oocyte (right) next to a normal-sized MII oocyte (left) from the same cohort (200× magnification).

Rarely, two oocytes can be found within the one follicular complex. Each oocyte is usually surrounded by a ZP but the ZP immediately between the two oocytes is commonly shared rather than duplicated (Fig. 35). It is not uncommon for these conjoined oocytes to show different nuclear maturational states. It has been suggested that such oocytes may play a role in producing dizygotic twins; however, even when both of the conjoined oocytes are mature it is rare that both fertilize and no pregnancies have been reported from such oocytes (Rosenbusch and Hancke, 2012).

D. Cytoplasmic features

D.1 Ooplasm

It has been shown in the literature that severe dysmorphisms of the cytoplasmic texture impairs the developmental and implantation potential of the embryo (Balaban and Urman, 2006). Although a

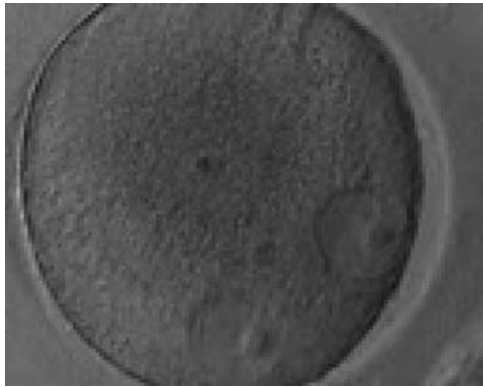


Figure 25 Giant oocyte with two apparent GV's (in an eccentric position). This is a tetraploid oocyte originating from the fusion of two separate oocytes (400 \times magnification).

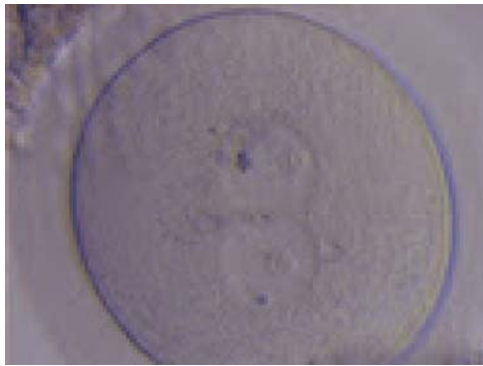


Figure 26 Giant oocyte with two apparent GV's (centrally located and juxtapposed). This tetraploid oocyte originates from the fusion of two separate oocytes and is usually tetraploid (400 \times magnification).

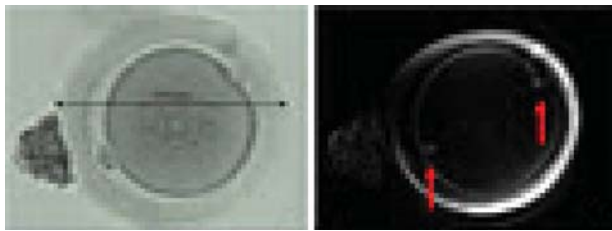


Figure 27 Giant MII oocyte visualized using bright field (left) and polarized light microscopy (right). The oocyte contains two distinct polar bodies and two distinct MSs at opposing poles of the oocyte.

homogeneous, normal cytoplasm is expected in recovered oocytes (Figs 36 and 37), the biological significance of different degrees of heterogeneity in the ooplasm is unknown. Based on current evidence, slightly heterogeneous cytoplasm may only represent normal variability

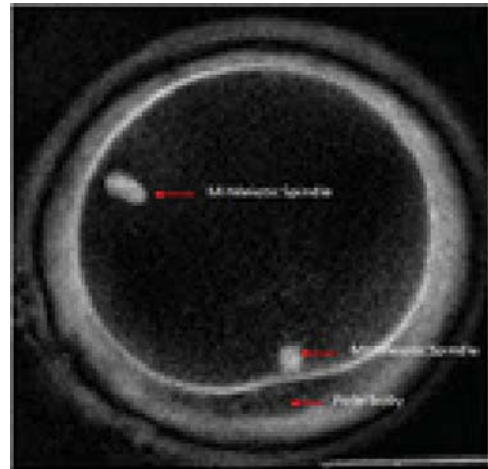


Figure 28 Giant MII oocyte visualized at high power using polarized light microscopy. The two distinct MSs can be observed in the cytoplasm. One MS is from the MI (10 o'clock position) and the other is from MII (6 o'clock position; 400 \times magnification).

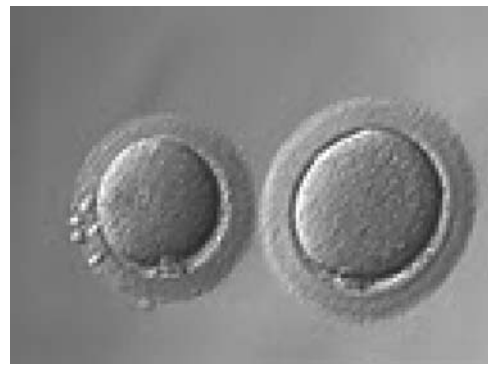


Figure 29 Giant oocyte (right) next to normal-sized oocyte (left; 200 \times magnification).



Figure 30 Giant oocyte (right) next to normal-sized oocyte (left; 200 \times magnification). No PB1 is visible in the giant oocyte.

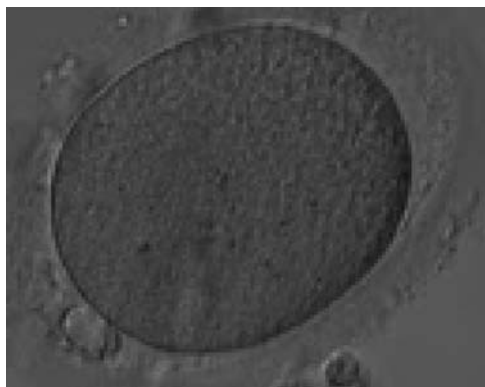


Figure 31 Elongated MII oocyte inside an elongated ZP. Note the PVS appears relatively normal (400× magnification).



Figure 34 Ovoid MII oocyte. Note the ZP is also ovoid in appearance permitting the PVS to remain relatively normal (200× magnification).



Figure 32 Elongated MII oocyte within a grossly distended and irregular ZP (200× magnification).

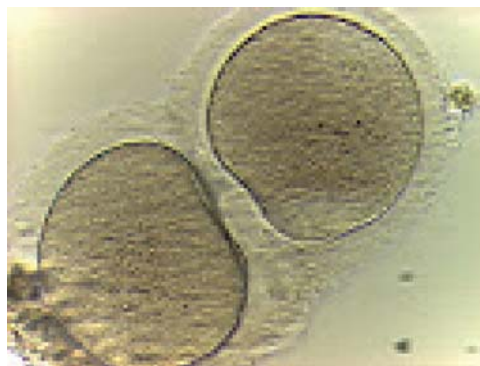


Figure 35 Two oocytes enclosed within a single ZP (400× magnification).



Figure 33 Ovoid MII oocyte. Note the ZP is also ovoid in appearance and the PVS is enlarged at both poles (200× magnification).



Figure 36 Normal homogenous cytoplasm in an MII oocyte (400× magnification).



Figure 37 Normal homogenous cytoplasm in an MII oocyte (400× magnification). ZP is dense and homogeneous.



Figure 38 MII oocyte with granular cytoplasm (400× magnification). ZP is thicker in the lower-left part of the oocyte in this view.



Figure 39 MII oocyte with granular cytoplasm (400× magnification). ZP is also abnormal with marked differences in thickness.



Figure 40 MII oocyte with granular cytoplasm. This figure can be considered as a slight deviation from normal homogeneous cytoplasm (400× magnification).

among retrieved oocytes rather than being an abnormality of developmental significance (Alpha Scientists in Reproductive Medicine and ESHRE Special Interest Group of Embryology, 2011).

Granularities of the cytoplasm (Figs 38–41) are poorly defined in the literature and may depend on the modulation of the optical path used in phase contrast microscopy. These morphological deviations should be carefully distinguished from inclusions such as refractile bodies or lipofuscin bodies (Otsuki *et al.*, 2007; Fig. 42) and organelle clustering which is also described as very condensed centralized granularity detectable by any form of microscopy (Figs 43–45; Alpha Scientists in Reproductive Medicine and ESHRE Special Interest Group of Embryology, 2011).

One of the most important severe cytoplasmic abnormalities of MII oocytes is the appearance of SER clusters (SER discs) within the cytoplasm. SER discs can be identified as translucent vacuole-like structures in the cytoplasm by phase contrast microscopy (Figs 46 and 47). Evidence-based data clearly demonstrates that the embryos derived from oocytes with SER discs are associated with the risk of serious, significantly abnormal outcomes (Balaban and Urman, 2006;



Figure 41 MII oocyte with a high degree of cytoplasmic granularity/degeneration (400× magnification). PBI is larger than normal size.

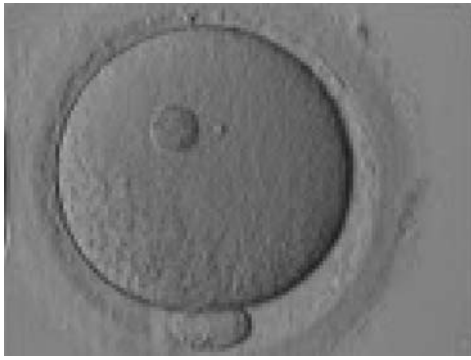


Figure 42 A large refractile body can be seen within the oocyte cytoplasm (400× magnification).



Figure 45 MII oocyte showing organelle clustering forming a large centrally located granular area in the cytoplasm. ZP has an irregular shape.

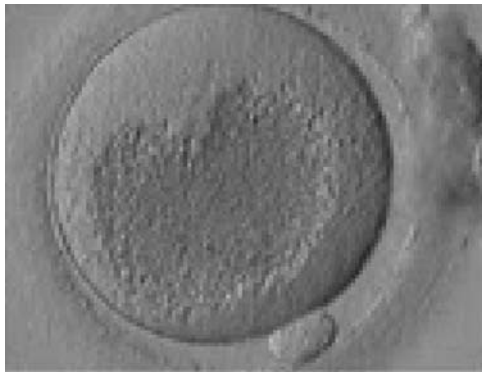


Figure 43 MII oocyte showing a very large centrally located granular area occupying the majority of the cytoplasm. This granularity is typical of organelle clustering.



Figure 46 MII oocyte showing plaques of dilated SER discs in the cytoplasm (400× magnification). The SER discs can be clearly distinguished from the fluid-filled vacuoles pictured in Figs 48–51. The cytoplasm looks heterogeneous with granularity (on the left) and areas devoid of organelles toward the 12 o'clock position in this view.



Figure 44 MII oocyte showing a large centrally located granular area in the cytoplasm denoting organelle clustering.



Figure 47 MII oocyte showing plaques of dilated SER discs in the cytoplasm (400× magnification). The PVS is enlarged and PBI is fragmented.



Figure 48 Vacuolated oocyte. Depicts an oocyte with several small vacuoles distributed throughout the oocyte cytoplasm (200× magnification).



Figure 49 Vacuolated oocyte. This oocyte has a single large vacuole occupying almost half of the oocyte cytoplasm (200× magnification).



Figure 50 Vacuolated oocyte. This oocyte has a single large vacuole in a dark, granular cytoplasm (200× magnification).

Ebner et al., 2006). It is recommended that oocytes with this feature should not be used for injection, and sibling oocytes should be additionally examined for the presence of either a single SER disc or a series of smaller plaques (*Alpha Scientists in Reproductive Medicine and ESHRE Special Interest Group of Embryology, 2011*).

Vacuoles within the cytoplasm are defined as fluid-filled structures which can be more easily noticeable and differ from SER discs (Figs 48–51). Small vacuoles of 5–10 μm in diameter are unlikely to have a biological consequence, whereas large vacuoles $>14 \mu\text{m}$ are associated with fertilization failure. In oocytes that are fertilized, those vacuoles that persist beyond syngamy can interfere with cleavage planes, resulting in a lower blastocyst rate (*Alpha Scientists in Reproductive Medicine and ESHRE Special Interest Group of Embryology, 2011*).

D.2 Metaphase plate

It has been shown that the presence of a detectable birefringent MS inside the oocyte cytoplasm of human MII oocytes (Fig. 52) might be an indicator of oocyte quality such as fertilization and



Figure 51 Vacuolated oocyte. Depicts an oocyte with a single small vacuole in the oocyte cytoplasm (400× magnification).

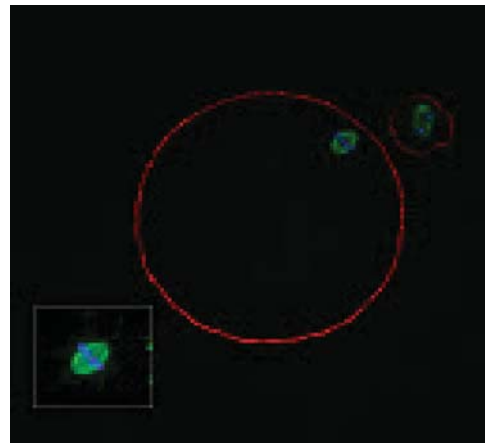


Figure 52 MII oocyte with a normal-shaped MS observed using confocal microscopy.

developmental ability; however, retrospective analysis of results from published articles have been found to be controversial (Borini et al., 2005). A recent meta-analysis showed that although the visibility of the MS of MII oocytes is correlated with fertilization and embryo quality till the blastocyst stage of development, data were insufficient to demonstrate an impairment of the clinical pregnancy and implantation rates (Petersen et al., 2009). The main reason for the controversial findings was that some of the studies did not take into consideration the dynamics of spindle formation that are highly variable during the oocyte maturation stages as well as by confounding technical issues related to oocyte handling. It has been shown that spindle visualization changes during maturation, with a disappearance of the spindle for ~1 h expected during the maturation of MI to PBI extrusion at telophase I and then re-formation at the MII stage. The microtubules of the MS are highly sensitive to chemical (hyaluronidase) and physical changes (temperature and pH variations) that may occur during oocyte handling and a reversible disappearance of the spindle can be expected during these technical preparations (Rienzi et al., 2003; De Santis et al., 2005; Montag et al., 2006).

The spindle structure, when detectable, is not always aligned with the PBI in MII oocytes, and the relationship between the degree of MS deviation from the location of the PBI may also play a role in clinical

outcome (Rienzi et al., 2003, 2005; Figs 53–58). Although it has been shown that there is no relationship between the displacement of the PBI with regard to the MS position on fertilization outcomes and embryo quality (Rienzi et al., 2003; Rama Raju et al., 2007), fertilization is impaired when the displacement is >90% (Rienzi et al., 2003; Figs 59 and 60). Slight shifts in the position of the PBI may also be related to physical displacement during the denudation processes, and can be reversible. However, when the displacement is so great because of inappropriate handling, it could cause irreversible damage to the oocyte structure.

Therefore, a precise sequential analysis of MS imaging should be performed after possible chemical and physical changes and immediately prior to ICSI if MS characteristics are to be used as possible markers of oocyte quality and viability.

E. Extracytoplasmic features

By definition, extracytoplasmic anomalies of the egg include all dysmorphisms related to the ZP, PVS and the polar body of the mature oocyte.

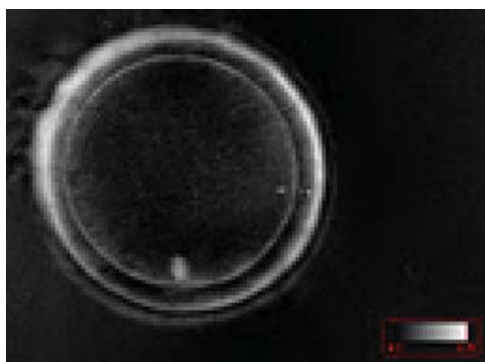


Figure 53 MII oocyte observed using polarized light microscopy with a visible MS just below PBI (400× magnification).

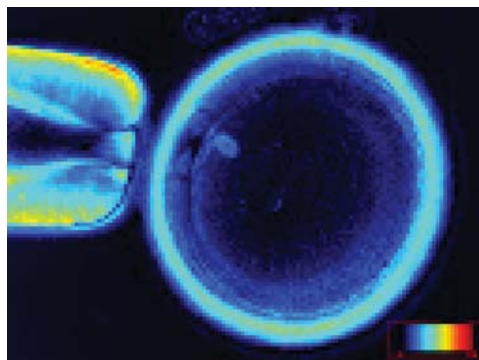


Figure 55 MII oocyte observed using polarized light microscopy with a visible MS just below PBI that appears fragmented (two fragments). (400× magnification).

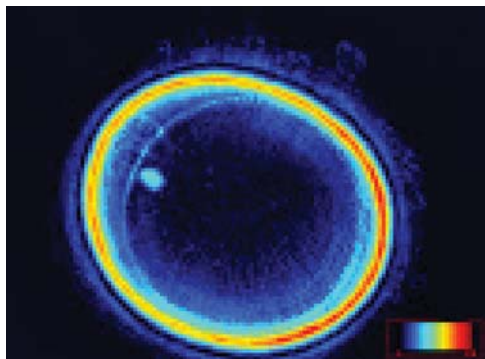


Figure 54 MII oocyte observed using polarized light microscopy with a visible MS near to PBI (400× magnification).

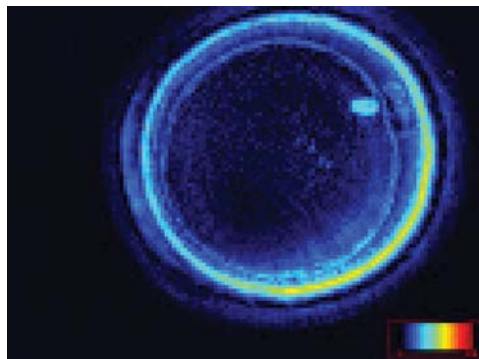


Figure 56 MII oocyte observed using polarized light microscopy. The MS is clearly visible near to PBI (400× magnification).

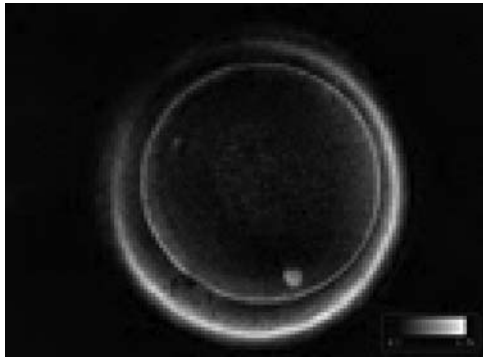


Figure 57 MII oocyte observed using polarized light microscopy with a visible MS slightly dislocated from PB1 at the 7 o'clock position in this view (400× magnification).

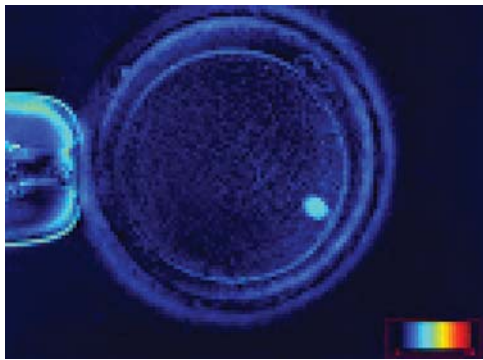


Figure 58 MII oocyte observed using polarized light microscopy with a visible MS dislocated about 80° from PB1 at the 1 o'clock position in this view (400× magnification).

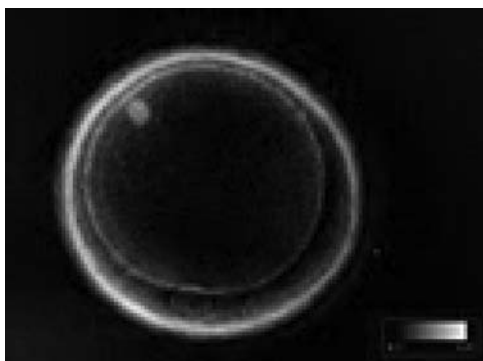


Figure 59 MII oocyte observed using polarized light microscopy with a visible MS highly dislocated (about 135°) from PB1 at the 6 o'clock position in this view (400× magnification).

E.1 Zona pellucida

Any alterations in ZP appearance could be caused by secretion and patterning problems of the glycoprotein matrix (Shen *et al.*, 2005). Since apparent changes in thickness (Figs 61–64) or complete absence of the ZP are extremely rare (Stanger *et al.*, 2001), more subtle changes in the three-dimensional structure are most frequently observed. Since the inner layer of the zona is highly ordered, it can clearly be visualized using polarized light (Figs 65–68; Pelletier *et al.*, 2004). Embryos with a good prognosis in terms of blastocyst formation and pregnancy can be predicted when viewed using polarized light (Montag *et al.*, 2008; Ebner *et al.*, 2010).

The degree to which discoloration of the ZP contributes to the birefringence of the outer shell is not known; however, it has been suggested that successful fertilization, embryo development and pregnancy can be achieved after transfer of embryos derived from brown zonae (Figs 63 and 64; Esfandiari *et al.*, 2006).

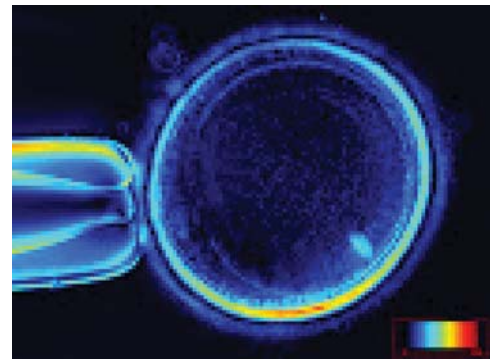


Figure 60 MII oocyte observed using polarized light microscopy with a visible MS highly dislocated (slightly more than 90°) from PB1 at the 8 o'clock position in this view (400× magnification).



Figure 61 MII oocyte with a thick and dense ZP (200× magnification).



Figure 62 MII oocyte with a thick ZP (200× magnification).

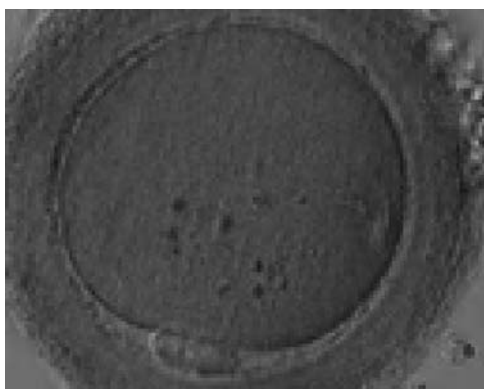


Figure 63 MII oocyte with a thick and dark ZP. Some inclusions are visible in the ooplasm.



Figure 64 MII oocyte with a thick and dark ZP whose thickness is not homogeneous

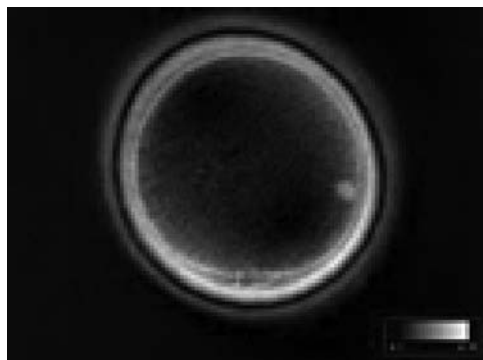


Figure 65 MII oocyte observed using polarized light microscopy with a clear birefringent ZP inner layer. The MS is dislocated from PBI by almost 90°.

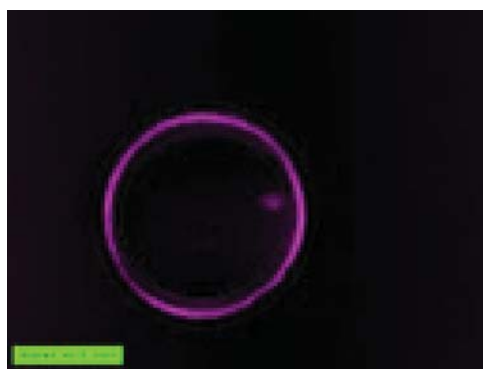


Figure 66 MII oocyte observed using polarized light microscopy with a clear birefringent ZP inner layer. The MS is also clearly visible at the 3 o'clock position in this view.

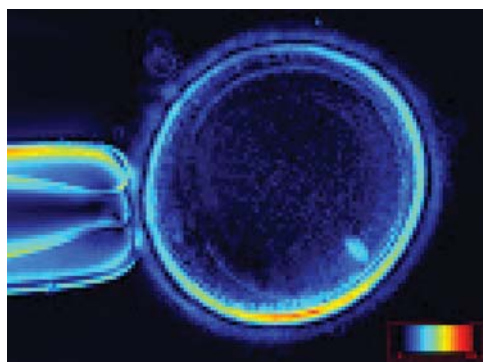


Figure 67 MII oocyte showing different degrees of ZP inner layer birefringence. The figure has a high degree of birefringence.

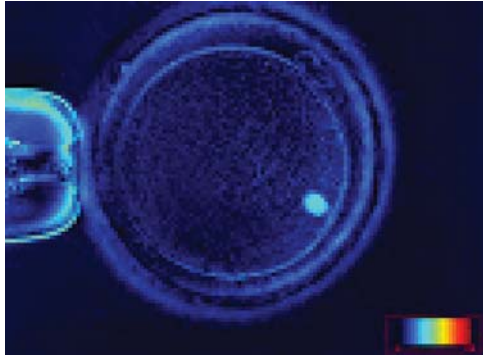


Figure 68 MII oocyte showing different degrees of ZP inner layer birefringence. The figure has a low degree of birefringence.



Figure 69 Oocyte with an abnormally shaped ZP and with what appears to be a duplication of, or tears in, the ZP. The oocyte has an irregular shape and cytoplasmic appearance with a large sized PBI.



Figure 70 Oocyte with an abnormally shaped ZP and with what appears to be a duplication of, or tears in, the ZP. The oocyte is highly dysmorphic with no evident PBI in the PVS.

Another rare finding is grossly abnormally shaped ZP with what could be either duplication of the inner layer of the ZP or a tear in the layers of the ZP creating an intrazonal space (Figs 69–71).

E.2 Perivitelline space

Several authors have noted that approximately one-third of all ova show a large PVS, a dysmorphism that was found to be negatively correlated with fertilization rate and embryo quality (Xia, 1997; Rienzi *et al.*, 2008). Data from the literature indicate that a large PVS (Figs 72–74) may be ascribed to over-mature eggs (Mikkelsen and Lindenberg, 2001; Miao *et al.*, 2009). In other words, such eggs have shrunk in relation to the ZP presenting a large gap between the oocyte and surrounding zona. A large PVS would also occur if a larger portion of cytoplasm is extruded together with the haploid chromosomal set during PBI formation. This would result in a large PBI and as a consequence a large PVS.



Figure 71 Oocyte with an abnormally shaped ZP and with what appears to be a duplication of, or tears in, the ZP. The oocyte has a regular shape.



Figure 72 Oocyte with a large PVS. There is a large granular area in the cytoplasm.



Figure 73 Oocyte with a large PVS. Several fragments are present in the PVS.

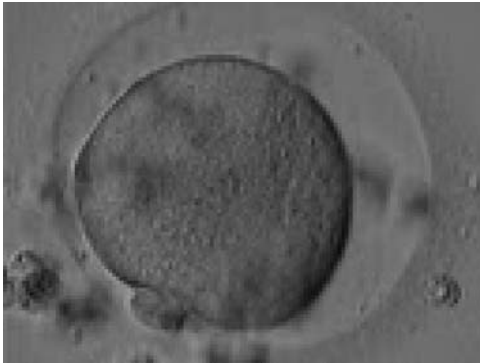


Figure 74 Oocyte with a large PVS and a granular cytoplasm.

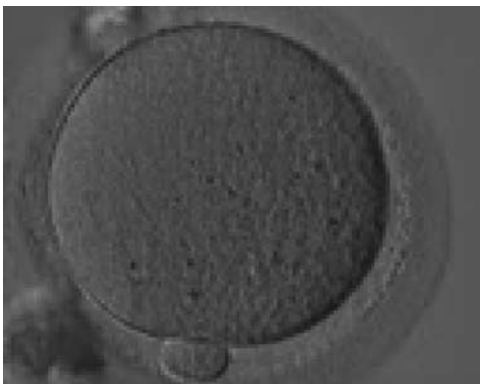


Figure 75 MII oocyte with a normal-sized PBI.

E.3 Polar body

Generally, PBI morphology can be seen as a reflection of postovulatory age of the oocytes since this by-product of meiosis fragments with time. Nevertheless, the impact of PBI morphology on outcome is still a matter of debate. Oocytes showing an intact PBI (Fig. 75) give rise to higher rates of implantation and pregnancy (Ebner *et al.*, 1999) probably due to an increase in blastocyst formation (Ebner *et al.*, 2002). Apparently, the benefit of selecting oocytes according to the morphology of PBI is diluted with increasing time between ovulation induction and ICSI, since studies with different schedules could not find a relationship between morphology of PBI and subsequent ICSI outcome (Ciotti *et al.*, 2004; De Santis *et al.*, 2005; Fancsovsits *et al.*, 2006).

However, the fact that a large PBI (Figs 76–78) has a very poor prognosis remains unchallenged (Fancsovsits *et al.*, 2006). When large PBI's are extruded, embryos with multinucleated blastomeres are a significantly more frequent consequence than for all other PBI

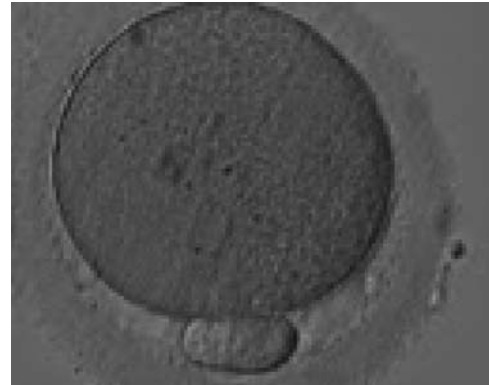


Figure 76 MII oocyte with a large PBI, 3–4 times larger than normal.



Figure 77 MII oocyte with a giant PBI, 5–6 times larger than normal.

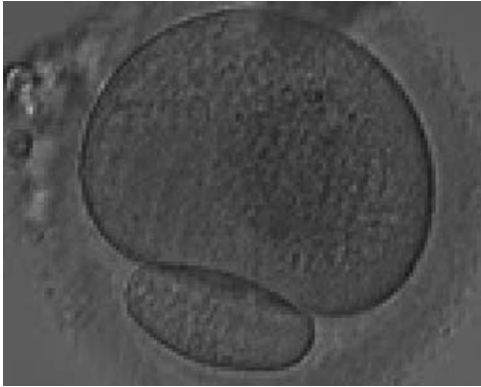


Figure 78 MII oocyte with a giant PBI.

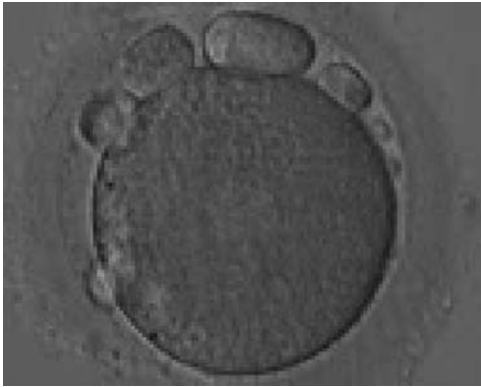


Figure 79 MII oocyte with large fragments and a large PBI in the PVS.

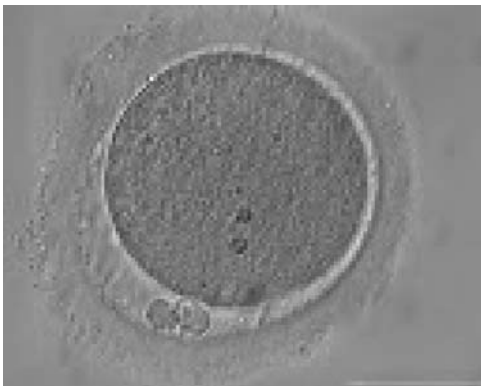


Figure 80 MII oocyte with a fragmented PBI (two pieces).



Figure 81 MII oocyte with a fragmented PBI (two pieces) (magnification $\times 1000$).

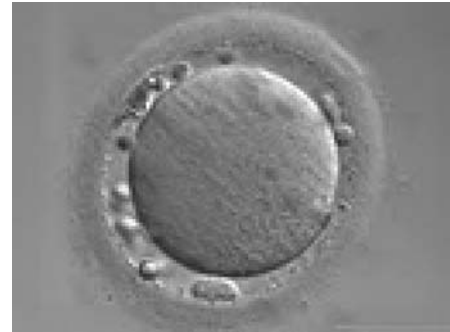


Figure 82 MII oocyte with a fragmented PBI and several cellular fragments within the PVS which are almost indistinguishable from PBI.

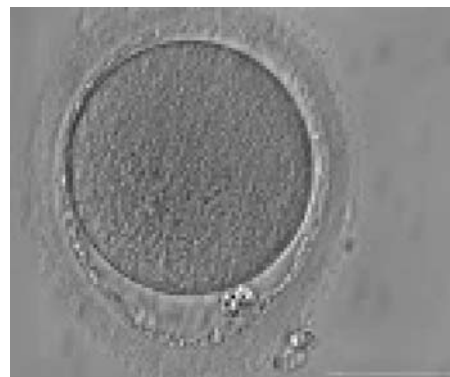


Figure 83 MII oocyte with a lobular/fragmented PBI and significant granulation in the ZP. The ZP has a dishomogeneous thickness and an irregular inner layer.



Figure 84 MII oocyte with a lobular/fragmented PBI and significant granulation in the PS. Two inclusion bodies can clearly be seen in the centre of the oocyte.

morphological categories (Fancsovičs *et al.*, 2006). It has been postulated that the extrusion of an abnormally large PBI is due to dislocation of the MS (Verlhac *et al.*, 2000).

Sometimes it is difficult to distinguish between heavily fragmented PBI's and debris within the PVS (Figs 79–82). Fertilization and cleavage rate as well as embryo quality have been found to be unaffected by the presence of coarse granules in the PVS (Figs 83 and 84); however, the rates of implantation and pregnancy seem to be influenced (Hassan-Ali *et al.*, 1998; Farhi *et al.*, 2002). Granularity in the PVS has been associated with over-maturity of oocytes (Miao *et al.*, 2009).

References

- Albertini DF, Combelles CM, Benecchi E, Carabatsos MJ. Cellular basis for paracrine regulation of ovarian follicle development. *Reproduction* 2001; **121**:647–653.
- Alpha Scientists in Reproductive medicine and ESHRE Special Interest Group of Embryology. The Istanbul consensus workshop on embryo assessment: proceedings of an expert meeting. *Hum Reprod* 2011; **26**:1270–1283.
- Balaban B, Urman B. Effect of oocyte morphology on embryo development and implantation. *Reprod Biomed Online* 2006; **12**:608–615.
- Balaban B, Urman B, Sertac A, Alatas C, Aksoy S, Mercan R. Oocyte morphology does not affect fertilization rate, embryo quality and implantation rate after intracytoplasmic sperm injection. *Hum Reprod* 1998; **13**:3431–3433.
- Balakier H, Bouman D, Sojkei A, Librach C, Squire JA. Morphological and cytogenetic analysis of human giant oocytes and giant embryos. *Hum Reprod* 2002; **17**:2394–2401.
- Baltz JM, Tartia AP. Cell volume regulation in oocytes and early embryos: connecting physiology to successful culture media. *Hum Reprod Update* 2009; **16**:166–176.
- Borini A, Lagalla C, Cattoli M, Sereni E, Sciajno R, Flamigni C, Cotichchio G. Predictive factors for embryo implantation potential. *Reprod Biomed Online* 2005; **10**:653–668.
- Ciotti PM, Notarangelo L, Morselli-Labate AM, Felletti V, Porcu E, Venturoli S. First polar body morphology before ICSI is not related to embryo quality or pregnancy rate. *Hum Reprod* 2004; **19**:2334–2339.
- Cohen Y, Malcov M, Schwartz T, Mey-Raz N, Carmon A, Cohen T, Lessing JB, Amit A, Azem F. Spindle imaging: a new marker for optimal timing of ICSI? *Hum Reprod* 2004; **19**:649–654.
- De Santis L, Cino I, Rabellotti R, Calzi F, Persico P, Borini A, Cotichchio G. Polar body morphology and spindle imaging as predictors of oocyte quality. *Reprod Biomed Online* 2005; **11**:36–42.
- De Sutter P, Dozortsev D, Qian C, Dhont M. Oocyte morphology does not correlate with fertilization rate and embryo quality after intracytoplasmic sperm injection. *Hum Reprod* 1996; **11**:595–597.
- Ebner T, Moser M, Yaman C, Feichtinger O, Hartl J, Tews G. Elective transfer of embryos selected on the basis of first polar body morphology is associated with increased rates of implantation and pregnancy. *Fertil Steril* 1999; **72**:599–603.
- Ebner T, Moser M, Sommergruber M, Yaman C, Pflieger U, Tews G. First polar body morphology and blastocyst formation rate in ICSI patients. *Hum Reprod* 2002; **17**:2415–2418.
- Ebner T, Moser M, Tews G. Is oocyte morphology prognostic of embryo developmental potential after ICSI? *Reprod Biomed Online* 2006; **12**:507–512.
- Ebner T, Shebl O, Moser M, Sommergruber M, Tews G. Developmental fate of ovoid oocytes. *Hum Reprod* 2008; **23**:62–66.
- Ebner T, Balaban B, Moser M, Shebl O, Urman B, Ata B, Tews G. Automatic user-independent zona pellucida imaging at the oocyte stage allows for the prediction of preimplantation development. *Fertil Steril* 2010; **94**:913–920.
- Esfandiari N, Ryan EAJ, Gotlieb L, Casper RF. Successful pregnancy following transfer of embryos from oocytes with abnormal zona pellucida and cytoplasm morphology. *Reprod Biomed Online* 2005; **11**:620–623.
- Esfandiari N, Burjaq H, Gotlieb L, Casper RF. Brown oocytes: implications for assisted reproductive technology. *Fertil Steril* 2006; **86**:1522–1525.
- Fancsovičs P, Tothne Z, Murber A, Takacs FZ, Papp Z, Urbancsek J. Correlation between first polar body morphology and further embryo development. *Acta Biol Hung* 2006; **57**:331–338.
- Farhi J, Nahum H, Weissman A, Zahalka N, Glezerman M, Levran D. Coarse granulation in the perivitelline space and IVF-ICSI outcome. *J Assist Reprod Genetics* 2002; **19**:545–549.
- Feuerstein P, Cadoret V, Dalbies-Tran R, Guerif F, Bidault R, Royere D. Gene expression in human cumulus cells: one approach to oocyte competence. *Hum Reprod* 2007; **22**:3069–3077.
- Gilchrist RB, Lane M, Thompson JG. Oocyte-secreted factors: regulators of cumulus cell function and oocyte quality. *Hum Reprod Update* 2008; **14**:159–177.
- Hassan-Ali H, Hisham-Saleh A, El-Gezeiry D, Baghdady I, Ismael I, Mandelbaum J. Perivitelline space granularity: a sign of human menopausal gonadotrophin overdose in intracytoplasmic sperm injection. *Hum Reprod* 1998; **13**:3425–3430.
- Laufer N, Tarlatzis BC, DeCherney AH, Masters JT, Haseltine FP, MacLusky N, Naftolin F. Asynchrony between human cumulus-corona cell complex and oocyte maturation after human menopausal gonadotropin treatment for *in vitro* fertilization. *Fertil Steril* 1984; **42**:366–372.
- Machtlinger R, Politch JA, Hornstein MD, Ginsburg ES, Racowsky C. A giant oocyte in a cohort of retrieved oocytes: does it have any effect on the *in vitro* fertilization cycle outcome? *Fertil Steril* 2011; **95**:573–576.
- Miao YL, Kikuchi K, Sun QY, Schatten H. Oocyte aging: cellular and molecular changes, developmental potential and reversal possibility. *Hum Reprod Update* 2009; **15**:573–585.
- Mikkelsen AL, Lindenberg S. Morphology of in-vitro matured oocytes: impact on fertility potential and embryo quality. *Hum Reprod* 2001; **16**:1714–1718.
- Montag M, Schimming T, Van der Ven H. Spindle imaging in human oocytes: the impact of the meiotic cycle. *Reprod Biomed Online* 2006; **12**:442–446.

- Montag M, Schimming T, Köster M, Zhou C, Dorn C, Rösing B, van der Ven H, Ven der Ven K. Oocyte zona birefringence intensity is associated with embryonic implantation potential in ICSI cycles. *Reprod Biomed Online* 2008;**16**:239–244.
- Montag M, Köster M, Van der Ven K, van der Ven H. Gamete competence assessment by polarizing optics in assisted reproduction. *Hum Reprod Update* 2011;**17**:654–666.
- Oldenbourg R. Polarized light microscopy of spindles. *Methods Cell Biol* 1999;**61**:175–208.
- Otoi T, Fujii M, Tanaka M, Ooka A, Suzuki T. Oocyte diameter in relation to meiotic competence and sperm penetration. *Theriogenology* 2000;**54**:534–542.
- Otsuki J, Nagai Y, Chiba K. Lipofuscin bodies in human oocytes as an indicator of oocyte quality. *J Assist Reprod Genet* 2007;**24**:263–270.
- Ouandaogo ZG, Haouzi D, Assou S, Dechaud H, Kadoch IJ, De Vos J, Hamamah S. Human cumulus cells molecular signature in relation to oocyte nuclear maturity stage. *PLoSOne* 2011;**6**:e27179.
- Paz G, Amit A, Yavetz H. Case report: pregnancy outcome following ICSI of oocytes with abnormal cytoplasm and zona pellucida. *Hum Reprod* 2004;**19**:586–589.
- Pelletier C, Keefe DL, Trimarchi JR. Noninvasive polarized light microscopy quantitatively distinguishes the multilaminar structure of the zona pellucida of living human eggs and embryos. *Fertil Steril* 2004;**81**:850–856.
- Petersen CG, Oliveira JBA, Mauri AL, Massaro FC, Baruffi RLR, Pontes A, Franco JG Jr. Relationship between visualization of meiotic spindle in human oocytes and ICSI outcomes: a meta-analysis. *Reprod Biomed Online* 2009;**18**:235–243.
- Rama Raju GA, Prakash GJ, Krishna KM, Madan K. Meiotic spindle and zona pellucida characteristics as predictors of embryonic development: a preliminary study using PolScope imaging. *Reprod Biomed Online* 2007;**14**:166–174.
- Rienzi L, Ubaldi F. Oocyte retrieval and selection. In: Gardner DK, Weissman A, Howles CM, Shoham Z (eds). *Textbook of Assisted Reproductive Technologies: Laboratory and Clinical Perspectives*, 3rd edn. London, UK: Informa Healthcare, 2009,5–101.
- Rienzi L, Ubaldi F, Martinez F, Iacobelli M, Minasi MG, Ferrero S, Tesarik J, Greco E. Relationship between meiotic spindle location with regard to the polar body position and oocyte developmental potential after ICSI. *Hum Reprod* 2003;**18**:1289–1293.
- Rienzi L, Ubaldi FM, Iacobelli M, Minasi MG, Romano S, Greco E. Meiotic spindle visualization in living human oocytes. *Reprod Biomed Online* 2005;**10**:192–198.
- Rienzi L, Ubaldi FM, Iacobelli M, Minasi MG, Romano S, Ferrero S, Sapienza F, Baroni E, Litwicka K, Greco E. Significance of metaphase II human oocyte morphology on ICSI outcome. *Fertil Steril* 2008;**90**:1692–1700.
- Rienzi L, Vajta G, Ubaldi F. Predictive value of oocyte morphology in human IVF: a systematic review of the literature. *Hum Reprod Update* 2011;**17**:34–45.
- Romão GS, Araújo MC, de Melo AS, de Albuquerque Salles Navarro PA, Ferriani RA, Dos Reis RM. Oocyte diameter as a predictor of fertilization and embryo quality in assisted reproduction cycles. *Fertil Steril* 2010;**93**:621–625.
- Rosenbusch B, Hancke K. Conjoined human oocytes observed during assisted reproduction: description of three cases and review of the literature. *Rom J Morphol Embryol* 2012;**53**:189–192.
- Rosenbusch B, Schneider M, Gläser B, Brucker C. Cytogenetic analysis of giant oocytes and zygotes to assess their relevance for the development of digynic triploidy. *Hum Reprod* 2002;**17**:2388–2393.
- Shen Y, Staf T, Mehnert C, Eichenlaub-Ritter U, Tinneberg HR. High magnitude of light retardation by the zona pellucida is associated with conception cycles. *Hum Reprod* 2005;**20**:1596–1606.
- Stanger JD, Stevenson K, Lakmaker A, Woolcott R. Pregnancy following fertilization of zona-free, coronal cell intact human ova. *Hum Reprod* 2001;**16**:164–167.
- Swain JE, Pool TB. ART failure: oocyte contributions to unsuccessful fertilization. *Hum Reprod Update* 2008;**14**:431–446.
- Tartia AP, Rudraraju N, Richards T, Hammer MA, Talbot P, Baltz JM. Cell volume regulation is initiated in mouse oocytes after ovulation. *Development* 2009;**136**:2247–2254.
- Ten J, Mendiola J, Vioque J, de Juan J, Bernabeu R. Donor oocyte dysmorphisms and their influence on fertilization and embryo quality. *Reprod Biomed Online* 2007;**14**:40–48.
- Van Blerkom J, Henry G. Oocyte dysmorphism and aneuploidy in meiotically mature human oocytes after ovarian stimulation. *Hum Reprod* 1992;**7**:379–390.
- Verlhac MH, Lefebvre C, Guillaud P, Rassinier P, Maro B. Assymmetric division in mouse oocytes: with or without MOS. *Curr Biol* 2000;**10**:1303–1306.
- Xia P. Intracytoplasmic sperm injection: correlation of oocyte grade based on polar body, perivitelline space and cytoplasmic inclusions with fertilization rate and embryo quality. *Hum Reprod* 1997;**12**:1750–1755.

The zygote

Loredana Papale, Agnese Fiorentino, Markus Montag, and
Giovanna Tomasi

Contents

Introduction

A. Fertilization assessment

- A.1 2PN
- A.2 1PN
- A.3 ≥ 3 PN

B. Pronuclear size

- B.1 Normal
- B.2 Small
- B.3 Differential in size

C. Pronuclear morphology

- C.1 Alignment parallel/tangential to plane of polar bodies
- C.2 Large angle between polar bodies
- C.3 Abutment/separation between PN
- C.4 Centrally/peripherally positioned PN
- C.5 Pronuclear membrane breakdown/syngamy

D. Nucleolar precursor bodies

- D.1 NPBs: aligned/scattered/differential in appearance between PN
- D.2 Numbers similar/numbers different between PN
- D.3 Similar size of NPBs/different size of NPB
- D.4 Ghost PN (absent NPB)/single NPB in one or more PN (bull's eye)

E. Cytoplasmic morphology assessment

- E.1 Normal/granular
- E.2 Small vacuoles/large vacuoles

Introduction

A series of dynamic and complex events are triggered following sperm–oocyte interaction that sequentially leads to fertilization and the formation of a zygote. These events include sperm penetration, sperm–oocyte fusion and oocyte activation, male and female pronucleus (PN) development and gradual migration of the pronuclei (PNs) to a central position in the oocyte.

Induced by the sperm penetration and subsequent calcium oscillations, the fertilized oocyte undergoes maternal-to-zygotic transition as a result of major changes in the molecular signals that control the arrest of meiotic development at the metaphase II stage of the second meiotic division (Ajduk *et al.*, 2011). In humans, the sperm centriole has the leading role in organizing the microtubules, which

direct the migration of PN and their rotation within the cytoplasm. In this way, PN position their axis toward the second polar body and achieve a proper orientation at syngamy by controlling the plane of the first mitotic division. During PN formation, nuclear precursor bodies (NPBs) become evident and start to migrate and merge into nucleoli in a time-dependent manner. The NPBs do not form a functionally active nucleolus at the zygote stage; however, they can be used as an indirect measure of the location and the grade of condensation of DNA within the PN. Nucleoli are the sites of synthesis of pre-rRNA and its availability is extremely important since newly synthesized rRNA is necessary for the translational processes when the embryonic genome becomes active (Gianaroli *et al.*, 2003). Asynchrony in the timing of any of the events associated with fertilization could compromise embryo development.

Once PN are aligned onto a polar axis, parental chromosomes then separate in preparation for mitosis. The human zygote's mitotic potential is paternally inherited with the spermatozoon delivering the centrosome (Palermo *et al.*, 1994; Sathananthan *et al.*, 1996).

A zygote's morphological characteristics are accepted to be an inherent indicator of both gamete quality and subsequent embryo implantation potential (Alpha Scientists in Reproductive medicine and ESHRE Special Interest Group of Embryology, 2011). Many studies have underlined the predictive value of zygote morphological assessment through correlations with chromosome constitution and the incidence of zygotic arrest (Gianaroli *et al.*, 2003; Balaban *et al.*, 2004; Edirisinghe *et al.*, 2005; Zamora *et al.*, 2011). Recent strategies in embryo selection include sequential morphology assessment where PN scoring has been shown to play an important role as an indicator of gamete constitution as well as a prognostic tool for embryo competence. Scoring of PN has also proved to be useful in countries where restrictive legislation mandates selection at the zygote stage for embryo transfer and consecutive elimination or cryopreservation of sibling zygotes (Senn *et al.*, 2006; Zollner *et al.*, 2005).

Although numerous studies have associated positive clinical results with the implementation of PN scoring, other reports have questioned the predictive value of PN scoring systems and see no benefits or improvement in the outcome (Nicoli *et al.*, 2010; Weitzman *et al.*, 2010). The Istanbul consensus workshop comprised a worldwide panel of experts who just recently evaluated the current practice of oocyte to embryo scoring and established common criteria for assessment (Alpha Scientists in Reproductive Medicine and ESHRE Special Interest Group of Embryology, 2011). Fertilization check is to be

performed at 17 ± 1 h post-insemination which may establish uniformity in the future and eliminate the variability in PN scoring regimens that have confounded comparative analyses. It must be noted, however, that the processes associated with fertilization by conventional insemination lags 1 h behind fertilization using ICSI (Nagy *et al.*, 1998). A more complete elucidation of events during the zygote stage, however, can be expected with the application of continuous monitoring through the introduction of time-lapse imaging instead of the traditional isolated observations using light microscopy (Montag *et al.*, 2011).

Normal fertilization is assessed by the presence of two centrally positioned, juxtaposed PNs with clearly defined membranes and two polar bodies. If an abnormal PN number is observed whether it be 1, or 3 or more, PNs, a low viable pregnancy is to be expected thus the transfer of these zygotes is to be avoided (Reichman *et al.*, 2010). Aberrant PN size and position have been correlated with developmental arrest and aneuploidy and are represented by PNs of unequal size ($>4 \mu\text{m}$), localized far apart or peripherally or with the presence of fragmented or additional micronuclei (Munné and Cohen, 1998; Sadowy *et al.*, 1998; Garello *et al.*, 1999; Nagy *et al.*, 2003; Scott *et al.*, 2007). Panel experts also agreed and strongly advised that the assessment and elimination of dysmorphic zygotes with smooth endoplasmic reticulum (SER) discs (see Chapter One) due to the association with severely adverse clinical outcomes (Otsuki *et al.*, 2004; Ebner *et al.*, 2008).

Correct alignment of PNs onto the polar axis is considered a fundamental feature for the completion of the first cleavage division and normal sequential development (Gardner, 1996, 1999, 2001; Edwards and Beard, 1997, 1999; Payne *et al.*, 1997; Garello *et al.*, 1999; Scott, 2001). Cell cycle-related dynamics of PN events have led many authors to investigate and correlate the presence, pattern and number of NPBs to embryo developmental potential. As shown for mitotic cells, the inequality in number, size or distribution of NPBs is correlated with abnormal development (Pedersen, 1998). Therefore, the panel experts from the consensus workshop established three categories for PN scoring that are based on the morphology of NPBs and PNs, namely: (i) *symmetrical*, (ii) *non-symmetrical* and (iii) *abnormal* (Alpha Scientists in Reproductive Medicine and ESHRE Special Interest Group of Embryology, 2011). Category 1 includes zygotes presenting with equal numbers and size of NPBs, either aligned at the junction between PNs or scattered in both PNs. Category 2, non-symmetrical, comprises all other patterns including peripherally localized PNs. Category 3, abnormal, includes single NPB ('bull's eye') or total absence of NPBs. The latter were found to be correlated with imprinting errors and delayed onset of functional NPBs and nucleoli formation in animal models (Svarcova *et al.*, 2009).

Reports on early cleavage checks have been demonstrated to be a beneficial tool in selecting embryos with high implantation potential and decreased chromosomal anomalies (Sakkas *et al.*, 1998; Lundin *et al.*, 2001). The consensus opinion on a second, Day 1 observation was to leave the choice to the operator's discretion, but if applied, is to be performed 26 ± 1 and 28 ± 1 h post-insemination for ICSI and IVF embryos, respectively.

Sequential morphology assessment through time-lapse cinematography will certainly shed light on the discrepancies in the literature with respect to PN scoring and an in-depth analysis and correlation with the clinical background behind the gametes forming the zygote will possibly reveal even more reliable prognostic tools to improve clinical outcomes.

A. Fertilization assessment

A.1 2PN

When assessments are performed 17 ± 1 h post-insemination, taking into consideration that pronuclear formation in IVF zygotes lags ~ 1 h behind ICSI zygotes, normally fertilized oocytes should be spherical and have two polar bodies and two PNs (Figs 85–87). PNs should be juxtaposed, approximately the same size, centrally positioned in the cytoplasm with two distinctly clear, visible membranes (Fig. 88). The presence of an equal number and size of NPBs aligned at the PN junction has been correlated with increased embryo competence (Tesarik and Greco, 1999; Tesarik *et al.*, 2000; Scott, 2003).



Figure 85 A zygote 16.5 h post-ICSI, having small-sized PNs with scattered NPBs and two visible polar bodies (400 \times magnification). The zona pellucida (ZP) appears regular; some debris is present in the perivitelline space (PVS). The cytoplasm is homogeneous and displays a clear cortical zone. It was transferred resulting in a clinical pregnancy followed by miscarriage.

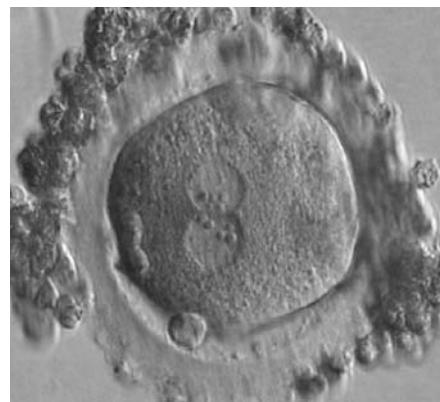


Figure 86 A slightly deformed zygote at 16.5 h after IVF with equal numbers of large-sized NPBs aligned at the PN junction (400 \times magnification). A great angle separates the two polar bodies. Some granulosa cells surround the ZP. It was transferred but failed to implant.



Figure 87 A zygote at 18.5 h generated by standard insemination using frozen/thawed ejaculated sperm (400× magnification). The two PNs are centrally located: one is slightly larger than the other. NPBs are of the same size, but different in number and are aggregated at adjacent borders of each PN. The ZP appears thick. It was transferred but failed to implant.



Figure 89 A single pronucleate oocyte displaying only one PN and a single polar body observed 16 h post-ICSI (200× magnification). The observation was repeated 17.5, 20 and 22 h post-ICSI and did not show significant variation in the PN size or position.



Figure 88 A zygote generated by ICSI with NPBs perfectly aligned at the junction of centrally located and juxtapsed PNs (600× magnification). Fragmented polar bodies are located in the longitudinal axis of the PNs. Category I (equivalent to ZI score; Scott, 2003) was assigned following assessment. Debris appears to be present in the PVS. The cytoplasm is light-coloured with a clear cortical zone. It was transferred and implanted.



Figure 90 A zygote observed 15 h post-IVF displaying a single, large-sized PN and two polar bodies (400× magnification).



Figure 91 A zygote 17 h post-IVF showing a single PN with NPBs of different size and two polar bodies (400× magnification).

A.2 IPN

The incidence of one pronucleates is around 1% after IVF or ICSI and may be parthenogenetic in origin as suggested by chromosomal analysis that shows a haploid set in approximately half of the studied oocytes (Plachot, 2000). In some cases, only one polar body is extruded into the perivitelline space (PVS) (Fig. 89).

The presence of IPN can also be a result of errors in the fertilization process with asynchrony in PN formation or PN fusion. In these cases, the resulting oocyte could have a diploid set of chromosomes, and two polar bodies are normally observed (Figs 90–93). The transfer of these oocytes could be considered, but the incidence of aneuploidy in the



Figure 92 A single, large PN and two polar bodies (partially overlapping) are present in this oocyte observed 16 h and 45 min post-IVF (400× magnification). Four large-sized NPBs are visible. The resulting embryo was transferred, but failed to implant.

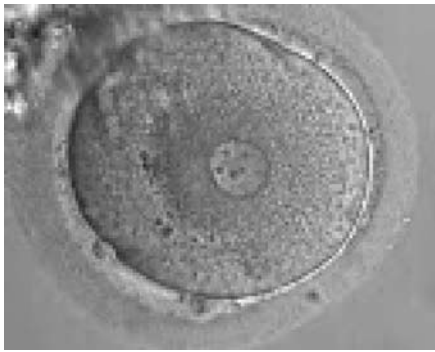


Figure 93 A zygote generated by ICSI showing a single PN and two polar bodies separated by some distance (600× magnification).



Figure 94 A zygote generated by ICSI displaying four PNs of approximately the same size and two of smaller size (150× magnification). Only one polar body is visible.

resulting embryos has been reported to be significantly higher compared with embryos derived from 2PN oocytes (Yan *et al.*, 2010).

A.3 ≥ 3 PN

The formation of triploid zygotes differs in origin, depending on whether they are generated by ICSI or IVF. Only 1% of oocytes after ICSI result in trippronuclear zygotes and are digynic due to failure in extrusion of the second polar body (Fig. 94). An exception is represented by giant oocytes (Fig. 95) that follow different patterns of extrusion due to their generally diploid condition (see Chapter One).

Diandry is the most probable cause of trippronucleates following IVF and occurs in ~5% of inseminated oocytes (Fig. 96). This condition arises from the entry of two spermatozoa into the cytoplasm owing to the incapacity of the oocyte to trigger protection against polyspermy. The second polar body is normally extruded and cleavage often occurs. In some cases, the presence of multiple PNs could be due to failed cytokinesis (Figs 94 and 97) or to penetration by a binucleate spermatozoon (Fig. 98).



Figure 95 A zygote displaying 3PNs with large-sized NPBs (400× magnification). One of the three PNs is slightly bigger than the others. The zygote was generated by ICSI performed on a giant oocyte.



Figure 96 A zygote displaying 3PNs of approximately the same size with large-sized NPBs, partly overlapped and aligned in the middle of the oocyte (400× magnification). It was generated by IVF and shows two polar bodies.



Figure 97 A zygote with 5PNs, halo cytoplasm, fragmented polar bodies, oval shape and dark ZP (400× magnification). It was warmed after vitrification.



Figure 98 A zygote displaying 3PNs after IVF with a small fragment adjacent to the PNs (200× magnification). There are two polar bodies in a large PVS and a thick ZP.

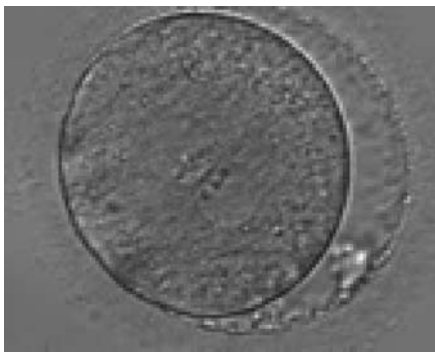


Figure 99 A zygote observed 18 h post-ICSI (400× magnification). The 2PNs are centrally located and juxtaposed in the cytoplasm (peripherally granular), of approximately the same size, and exhibit inequality in the number and size of NPBs. The PN on the right demonstrates fewer but larger nucleoli. Some debris appears to be present in the slightly increased PVS. Transferred on Day 3 (eight cells) along with two other embryos to a patient who delivered a healthy baby boy.

B. Pronuclear size

B.1 Normal

Some studies have demonstrated that the size of PN depends on gamete factors. Decondensation of the tightly compacted sperm chromatin is a crucial step in fertilization that includes the replacement of protamines with histones under the control of oocyte-decondensing factors. Therefore, the male PN size depends both on the sperm nuclear structure and on the oocyte's capacity of inducing decondensation by releasing appropriate levels of glutathione.

PNs normally appear to be similar in size, although the female PN that is often located towards the second polar body can be slightly smaller (Figs 99 and 100). However, PN formation and rotation is a dynamic process as demonstrated by time-lapse video recording, so positioning and morphology of PN are strictly time dependent (Fig. 101).

B.2 Small

The size of PN depends on the time of observation with an increase in size of close to 50% from abutment to 17 h post-ICSI (Payne et al., 1997). The presence of PN with a diameter smaller than normal (Figs 102–104) at the normal time of fertilization check could be an indicator of delayed fertilization possibly due to oocyte immaturity, or defects in the gametes. Nevertheless, implantation can occur as a result of transfer of these zygotes (Fig. 103).

B.3 Differential in size

Significant differences ($>4 \mu\text{m}$) between PN size (Figs 105–108), or the presence of micronuclei or fragmented PN (Figs 109 and 110) are considered to be abnormal and are associated with chromosomal abnormalities and major loss of developmental potential (Munné and Cohen, 1998; Scott et al., 2000; Nagy et al., 2003; Scott et al., 2007; Alpha Scientists in Reproductive medicine and ESHRE Special Interest Group of Embryology, 2011). Clinical studies have shown a high correlation between zygotes observed at 16–18 h post-insemination displaying large differences in PN size and their capability to maintain viability and development both *in vivo* and *in vitro* (Sadowy et al., 1998; Scott et al., 2000). Therefore, when performing embryo selection these embryos should be avoided for transfer.

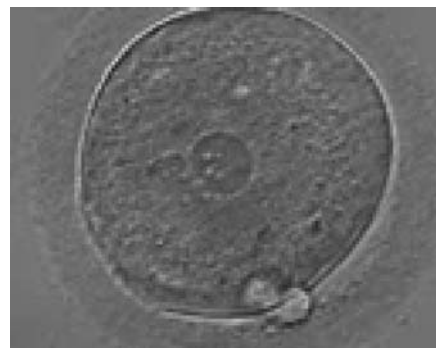


Figure 100 A zygote with equal numbers of large-sized NPBs scattered with respect to the PN junction (400× magnification). PN are juxtaposed and slightly eccentric. The two polar bodies are located in a plane that is parallel to the longitudinal axis of the PN.

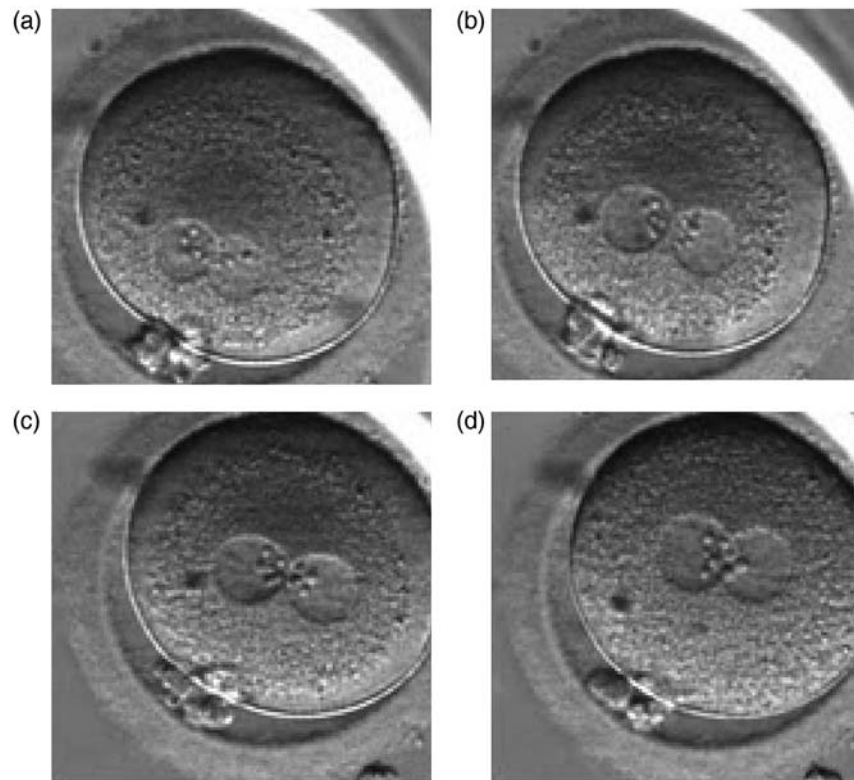


Figure 101 A zygote with changes in PN pattern, particularly with respect to the position in the cytoplasm and the NPBs' location over time at (a) 11.7, (b) 15.4, (c) 18.3 and (d) 28.3 h after ICSI (400 \times magnification).

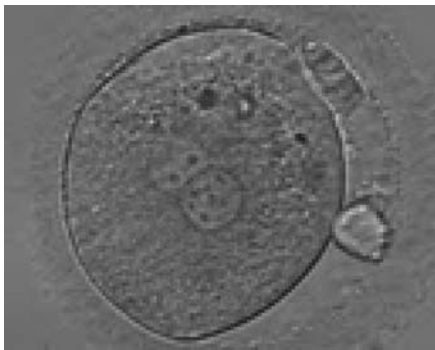


Figure 102 A zygote generated by ICSI and observed 18 h post-insemination (400 \times magnification). PNs are slightly smaller than normal and exhibit inequality in the number and the distribution of NPBs. Polar bodies are larger than the normal size.



Figure 103 A zygote generated by IVF using frozen/thawed ejaculated sperm and observed 16 h post-insemination (400 \times magnification). PNs are smaller than normal and are not exactly positioned in the centre of the oocyte. Small-sized NPBs are aligned at the PN junction. It was transferred and implanted.

C. Pronuclear morphology

C.1 Alignment parallel/tangential to the plane of the polar bodies

With the extrusion of the second polar body, following sperm entry and oocyte activation, the polar axis is established. Correct alignment

of PNs onto this axis is necessary for the formation of polar axes at syngamy and subsequent completion of the first cleavage division and normal development (Edwards and Beard, 1997; Payne *et al.*, 1997; Garellio *et al.*, 1999; Gardner, 2001; Scott, 2001). At apposition, the chromatin of both PNs begins to polarize and rotate to face each other with the male PN rotating onto the female PN and placing the



Figure 104 A zygote displaying two small PNs partly overlapping in this view (600× magnification). NPBs are large in size, equal in numbers and scattered in the two PNs. The ZP appears thickened and the PVS almost absent.



Figure 107 A zygote observed 18 h post-insemination displaying very unequal-sized PNs and inequality in number and alignment of NPBs (400× magnification). It was transferred on Day 3 (seven cells) along with two other embryos. The implantation result is therefore unknown. However, the patient delivered a healthy baby boy.



Figure 105 A zygote observed 18 h post-ICSI displaying very unequal-sized juxtaposed PNs, with the smaller PN being less visible (200× magnification). Two polar bodies and small-sized NPBs are scattered in both PNs.



Figure 108 A zygote generated by ICSI with one large and one normal-sized PN (200× magnification). The two polar bodies are at opposite sides of the oocyte.



Figure 106 A zygote displaying two polar bodies and unequal-sized juxtaposed PNs and inequality in number and alignment of small-sized NPBs (200× magnification).



Figure 109 A zygote after PB biopsy showing peripheral PNs that are very different in size with one larger and one smaller than the normal size (400× magnification). The ZP is oval in shape.

centrosome into the furrow between the two PNs (Van Blerkom *et al.*, 1997). In this way, the longitudinal axis of PNs is parallel to the plane of polar bodies (Figs 111–115). Further rotation brings the PNs aligned onto the polar axis; the position of the second polar body defines the plane of the first cleavage division (Figs 116–121). All these movements and rotations could cause the formation of the clear cortical zone known as the halo (Figs 114, 118 and 119).

C.2 Large angle between polar bodies

The failure of PNs to be juxtaposed and centrally positioned within the cytoplasm or having non-aligned polar bodies with respect to PNs at fertilization check could result in altered development, i.e. fertilization failure and abnormal cleavage of the embryo (Gianaroli *et al.*, 2003; Alpha Scientists in Reproductive medicine and ESHRE Special Interest Group of Embryology, 2011). Large angles between polar bodies (Figs 122–124) have been suggested to be predictors of poor embryo development (Gianaroli *et al.*, 2003). This effect could be due to sub-optimal orientation of PNs (Figs 125 and 126) generating



Figure 110 A zygote 18 h post-ICSI displaying very unequal-sized, juxtaposed PNs and inequality in number and alignment of NPBs (600 \times magnification). A vacuole-like structure is present in the cytoplasm. Fragments are visible in the PVS, not easily discernible from the polar bodies in this view.

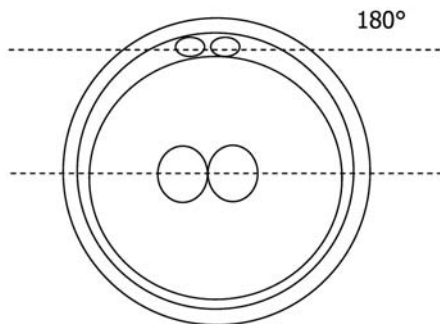


Figure 111 Diagram showing the plane through the polar bodies which is parallel to the contrasting plane through the longitudinal axis of the PNs.



Figure 112 A zygote generated by ICSI with different number of large-sized NPBs aligned at the PN junction (200 \times magnification). PNs are juxtaposed and centralized; polar bodies are located parallel to the longitudinal axis through the PNs.



Figure 113 An ICSI zygote with large-sized NPBs aligned at the PN junction (200 \times magnification). PNs are juxtaposed and centralized, fragmented polar bodies are located parallel to the longitudinal axis through the PNs ($\pm 30^\circ$).



Figure 114 An ICSI zygote displaying juxtaposed and centralized PNs. PN alignment is parallel to the plane of the polar bodies. The zygote displays inequality in number and alignment of NPBs. The latter are aligned in one PN and scattered in the other one with respect to the PN junction. A clear cortical zone with some inclusion bodies immediately below the area can be noted. It was replaced on Day 3 (eight cell cleavage embryo) but failed to implant.



Figure 115 A zygote with an equal number of large-sized NPBs aligned at the PN junction ($400\times$ magnification). PNs are juxtaposed and centralized and the polar bodies are located parallel to the longitudinal axis through the PNs. Observed 16 h after IVF.



Figure 118 An ICSI zygote with large-sized NPBs aligned at the PN junction ($400\times$ magnification). PNs are juxtaposed and centralized; polar bodies (the first polar body is fragmented, while the second is intact) are located tangential to the longitudinal axis through the PNs.

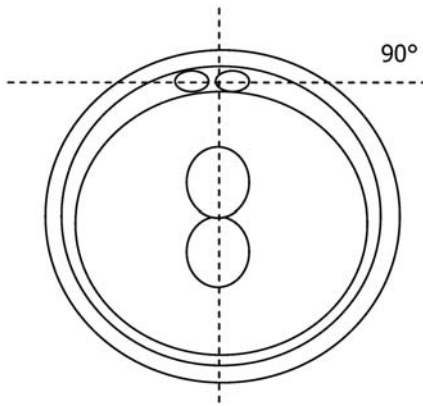


Figure 116 Diagram showing the plane through the polar bodies which is tangential to the contrasting plane through the longitudinal axis of the PNs.

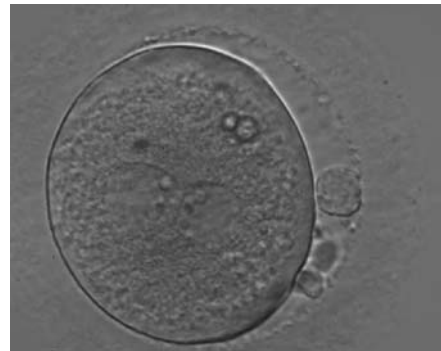


Figure 119 An ICSI zygote with large-sized NPBs aligned at the PN junction ($200\times$ magnification). PNs, juxtaposed and centralized, are tangential to the plane through the polar bodies. It was transferred on Day 3 (seven cells) along with two other embryos but failed to implant.

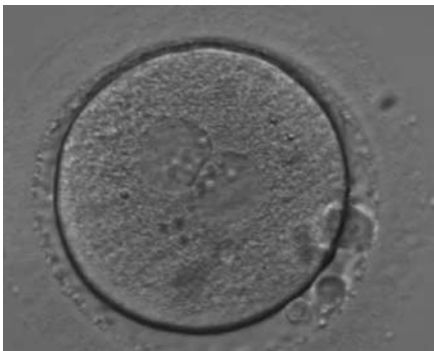


Figure 117 An ICSI zygote with large-sized NPBs aligned at the PN junction ($400\times$ magnification). PNs are juxtaposed and centralized; polar bodies (the first polar body is fragmented, the second is intact) are located tangential to the longitudinal axis through the PNs.

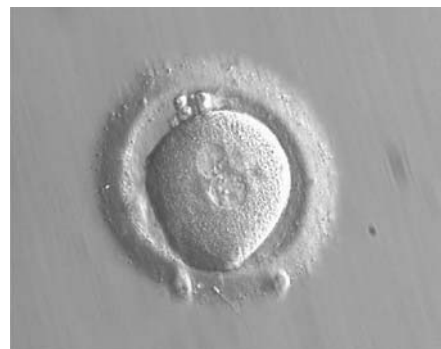


Figure 120 Zygote observed at 16.5 h post-IVF displaying unequal-sized juxtaposed and centralized PNs aligned tangentially to the plane through the polar bodies ($400\times$ magnification). NPBs are scattered in one PN and aligned in the other. The oocyte is irregular in shape and the PVS is enlarged. It failed to implant following transfer.



Figure 121 A deformed zygote with peripheral PNs and polar bodies aligned tangentially to the plane through the polar bodies observed 15 h post-IVF (400× magnification). Polar bodies are highly dysmorphic. Note the presence of small vacuoles in the cytoplasm.



Figure 122 An ICSI zygote displaying two PNs of approximately equal size, juxtaposed and clearly visible in the middle of the cytoplasm (400× magnification). Polar bodies are rotated $>30^\circ$ off the longitudinal axis through the PNs. A clear cortical area and coarse granularity of the cytoplasm can be observed. It was transferred but failed to implant.

a great degree of cytoplasmic turbulence, which could facilitate uneven cleavage or fragmentation (Garello *et al.*, 1999).

C.3 Abutment/separation between PNs

In human oocytes, the aster from the sperm centrosome organizes the microtubules, which control the abutment and apposition of PNs (Figs 127–131), and direct the formation of polar axes at syngamy by setting the plane of the first division. The subsequent movements and rotations favour the distribution of the mitochondria and chromatin alignment, which are essential for correct development.

Failed progression to apposition and syngamy (Figs 132–134) mostly depends on sperm centrosome activity. Observations of zygotes with separated PNs at fertilization check during subsequent development (Figs 135–136) demonstrate severe delay or arrest in development (Fig. 136) in almost 80% of cases (Gianaroli *et al.*, 2003). This condition



Figure 123 Zygote observed 18 h post-ICSI, with inequality in number and alignment of the NPBs (400× magnification). PNs are juxtaposed and centralized, NPBs are aligned in one of the two PNs and scattered in the other with respect to the PN junction. Both polar bodies are rotated $>30^\circ$ off the longitudinal or meridional axis with a large degree of separation between them. It is possible to observe a clear cortical zone and some dark inclusion bodies. It was transferred and failed to implant.



Figure 124 A zygote of irregular shape observed 18 h post-ICSI (400× magnification). The visible PNs show unequal distribution of the NPBs. PNs are juxtaposed and centralized and the polar bodies form a great angle with respect to the longitudinal axis through the PNs. It was transferred but failed to implant.

is most frequently associated with pathological spermatozoa, particularly from epididymal or testicular samples (Fig. 133).

C.4 Centrally/peripherally positioned PNs

The position of PNs has a relevant effect on the first cleavage plane that normally goes through the pronuclear axis (Scott, 2003). In the majority of zygotes with centrally positioned PNs (Fig. 137), the first cleavage occurs regularly, giving rise to normally developing embryos. Due to the dynamics of PN movements within the cytoplasm, their orientation on the polar axis varies depending on the progression of rotation (Figs 138 and 139) towards the final state which determines the first cleavage plane (Fig. 140).

In cases of peripherally positioned PNs (Figs 141 and 142), cleavage occurs according to the pronuclear axis and results frequently in



Figure 125 Zygote with large-sized NPBs scattered with respect to the PN junction (400× magnification). A clear cortical zone can be observed in the cytoplasm and the ZP is thick and very dense. Polar bodies form a great angle with respect to the longitudinal axis through the PNs. It was transferred but implantation outcome is unknown.



Figure 127 Irregularly shaped zygote showing two centrally located and juxtaposed PNs with equal numbers of large-sized NPBs aligned at the PN junction (200× magnification). Fragmented polar bodies are located parallel to the longitudinal axis through the PNs ($\pm 30^\circ$). A clear cortical area and coarse granularity of the cytoplasm can be observed. It was transferred on Day 3 along with two other embryos and the patient delivered two healthy baby girls and one healthy baby boy.

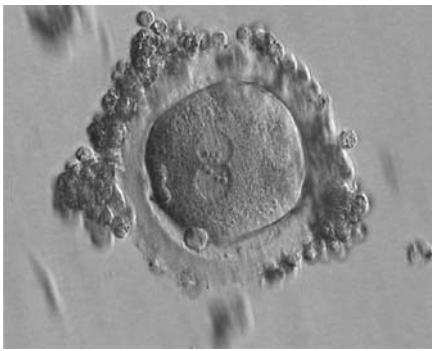


Figure 126 A zygote of irregular shape 16.5 h after IVF in which two PNs are clearly visible with NPBs aligned in both (400× magnification). Polar bodies form a right angle: one is aligned with the longitudinal axis through the PNs and the other is aligned with the meridional axis. It was transferred but failed to implant.

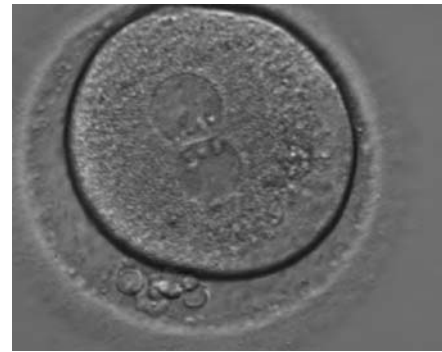


Figure 128 A zygote with two centrally located and juxtaposed PNs, an enlarged PVS and a significant amount of debris in the PVS (400× magnification). It was transferred but the result is unknown.

abnormal morphology (Fig. 143), cleavage (Fig. 144) and arrest of development (Fig. 145). Nevertheless implantation can occur (Fig. 146).

C.5 Pronuclear membrane breakdown/syngamy

Following sperm entry, both PNs migrate toward each other while replicating their own DNA. At juxtaposition, nuclear membranes break down a few hours prior to initiation of the first cleavage division (Figs 147 and 148). Syngamy occurs (Fig. 149) and the two sets of haploid genomes merge.

The astral centrosome containing two centrioles splits and relocates to opposite poles of a bipolar spindle to establish bipolarization that controls cell division. The centrioles take a pivotal position on spindle poles, while chromosomes organize on the equator of the metaphase plate. Anaphase and telophase ensue completing the first mitotic division.



Figure 129 A zygote with two centrally located and perfectly juxtaposed PNs in a granular cytoplasm with a clear cortical zone (400× magnification). NPBs are aligned, but are different in size. It was transferred but failed to implant.

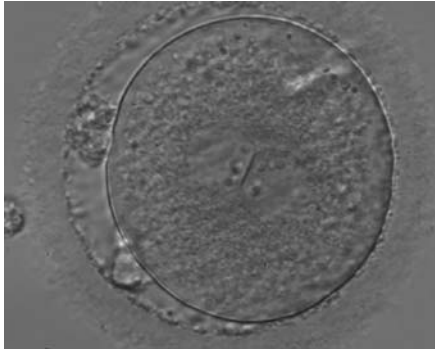


Figure 130 A zygote with two centrally located and perfectly juxtaposed PNs in a slightly granular cytoplasm with a clear cortical zone (400× magnification). There is debris in the PVS as well as fragmentation of one polar body (presumably the first polar body), which is significantly separated from the other polar body (presumably the second polar body). It was transferred but the outcome is unknown.



Figure 133 A zygote generated by ICSI using fresh epididymal sperm, observed 18 h post-insemination (400× magnification). PNs are not juxtaposed, different in size and NPBs are symmetrically distributed. It was transferred but failed to implant.



Figure 131 A zygote generated by IVF with a thick ZP (400× magnification). PNs are juxtaposed in the cytoplasm, which has a clear cortical zone. NPBs are small and aligned in one PN and scattered in the other. A refractile body is visible at the 11 o'clock position in this view.

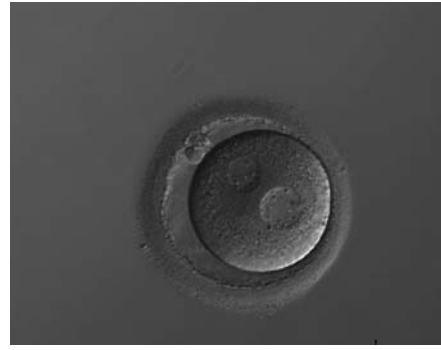


Figure 134 A zygote with widely separated and unequal-sized PNs, which show scattered small NPBs (150× magnification). The cytoplasm appears slightly granular and the PVS is enlarged. It was transferred but implantation outcome is unknown.

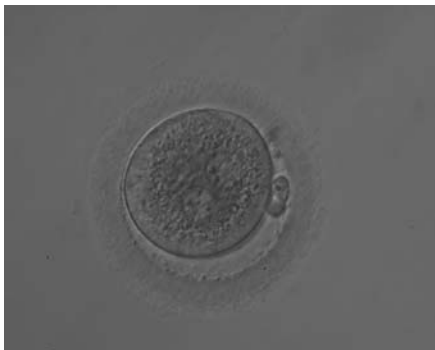


Figure 132 A zygote 18 h post-ICSI displaying two PNs that are not juxtaposed (200× magnification). NPBs are of different size, aligned in one PN and scattered in the other. The cytoplasm is very granular.



Figure 135 A zygote generated by ICSI and observed at 16, 17.5, 19 and 22 h after insemination (200× magnification). The two PNs are peripherally located, widely separated and have an unequal number of scattered NPBs. It was discarded.

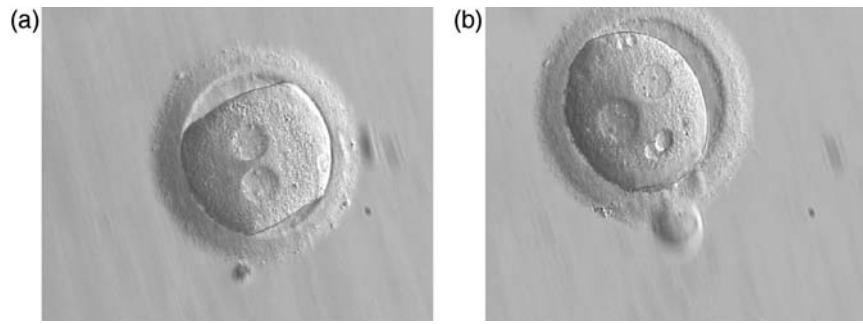


Figure 136 A zygote with an irregular shape, generated by ICSI and observed 18 h (a) and 20 h (b) post-ICSI (400× magnification). The polar body had been biopsied. PNs are widely separated and contain scattered small NPBs. The cytoplasm is normal in colour but displays two vacuole-like structures which are evident in (b). It failed to cleave during further development.



Figure 137 A zygote displaying centrally located, and in this view, partially overlapping PNs (400× magnification). The PN longitudinal axis is parallel to the polar bodies. NPBs are scattered in both PNs with respect to the PN junction but differ in number. It was transferred and implanted.

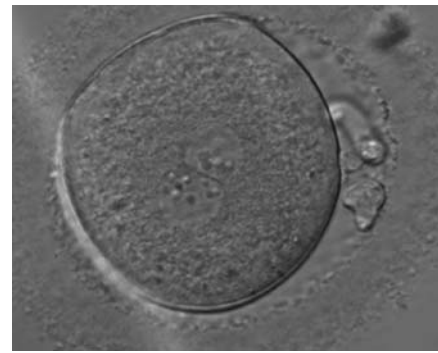


Figure 139 A zygote, generated by ICSI and observed 18 h post-insemination displaying centrally located PNs in which NPBs differ in number and size (400× magnification). The PN longitudinal axis is almost tangential to the plane through the polar bodies. NPBs are not symmetrically distributed, aligned in one PN and scattered in the other with respect to the PN junction. The ZP is thick and brush-like. It was transferred and failed to implant.



Figure 138 A zygote displaying centrally located PNs in which NPBs are symmetrically distributed and aligned with respect to the PN junction (400× magnification). A clear cortical zone, the halo, appears in the cytoplasm and there is a slightly enlarged PVS. It was transferred but implantation outcome is unknown.



Figure 140 A zygote with equal numbers of large-sized NPBs aligned at the PN junction (200× magnification). PNs are juxtaposed and centralized; polar bodies are aligned tangential to the longitudinal axis through the PNs.



Figure 141 An ICSI zygote displaying two perfectly juxtaposed PNs in a peripheral position in the cytoplasm, which is showing central granularity due to clustering of the organelles (400× magnification). NPBs are different in number and distribution. One polar body (presumably the first polar body) is fragmented and the other is intact. It was transferred but the outcome is unknown.



Figure 142 A zygote generated by IVF with normal-sized PNs slightly displaced to a peripheral position (400× magnification). NPBs are aligned and different in number. It was transferred but the outcome is unknown.

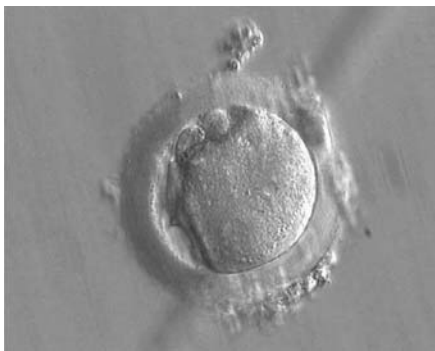


Figure 143 A deformed zygote at 16 h post-IVF displaying two PNs located peripherally in the cytoplasm (6–7 o'clock) that are parallel to the plane of the two large polar bodies (400× magnification).



Figure 144 A zygote observed 16 h post-IVF showing peripheral PNs partly overlapping in this view (400× magnification). NPBs are small in size and scattered in both PNs. The derived embryo was highly fragmented with uneven blastomeres and was discarded.

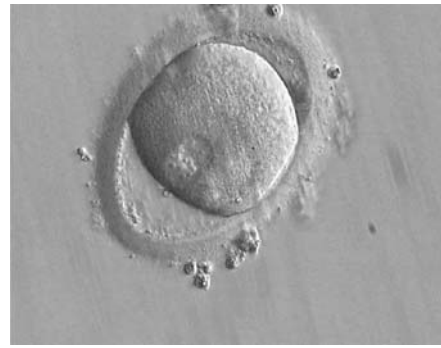


Figure 145 A zygote observed 16 h post-ICSI with peripherally positioned PNs (400× magnification). A large PVS is present inside a deformed, ovoid ZP. The oocyte has a clear cortical zone in the cytoplasm. It was not transferred because of arrested development.

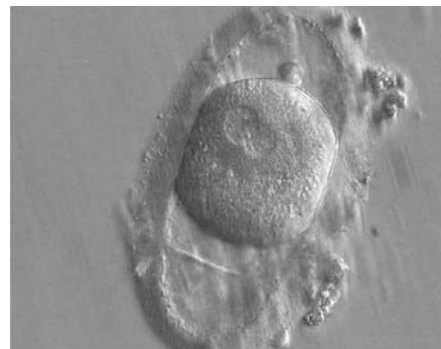


Figure 146 A zygote generated by ICSI displaying an ovoid ZP which demonstrates a duplication or tear in the layers (400× magnification). The fertilized oocyte is spherical and shows two PNs peripherally located and partly overlapping in this view. NPBs are small and scattered in both PNs. It was transferred and implanted.



Figure 147 A zygote entering syngamy observed at 18 h after ICSI (400× magnification). The PN membranes are becoming indistinct and have large-sized NPBs. The ZP appears 'brush-like' and there is a clear cortical region evident in the peripheral cytoplasm. Further development resulted in cleavage to 4 cell and arrest on Day 3.



Figure 148 A zygote which is entering syngamy and is displaying membrane breakdown particularly evident in the upper PN (400× magnification). The observation was performed 15 h after ICSI. One of the two PNs and its associated NPBs are now very indistinct. It was transferred but failed to implant.

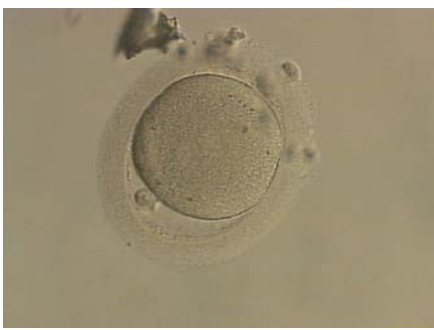


Figure 149 An ICSI zygote which has entered syngamy and is displaying pronuclear membrane breakdown (200× magnification). The NPBs are no longer distinct. It was transferred but the outcome is unknown.

In contrast to some animal species, membrane fusion of PNs (Fig. 150) is not a common process in human zygotes.

D. Nucleolar precursor bodies

D.1 NPBs: aligned/scattered/differential alignment between PNs

As PNs form after fertilization, there is polarized distribution in the chromatin into the furrow between them (Van Blerkom et al., 1997). As NPBs are attached to the chromatin, they should also polarize or align with it implying that, if there is correct chromatin polarization, the NPBs will appear polarized as well (Figs 151–154). Due to the dynamics of this event, some zygotes show symmetry in appearance of the PNs, but a delay in the alignment of the chromatin into



Figure 150 A zygote displaying PNs entering syngamy (400× magnification). The observation was performed 16 h after ICSI. The PN membranes are indistinct, particularly between the PNs where they have broken down, looking like PN membrane fusion. Large-sized NPBs are evident in the PNs. Polar bodies had been previously biopsied. It was transferred but failed to implant.



Figure 151 A zygote observed 18 h post-ICSI with equal numbers of NPBs aligned at the PN junction (200× magnification). It was transferred but the outcome is unknown.



Figure 152 A zygote observed 18 h post-ICSI with equal numbers of NPBs aligned at the PN junction (200× magnification). It shows a large PVS and an irregular ZP. The polar bodies are fragmented and overlapping in this view. It was transferred but the outcome is unknown.

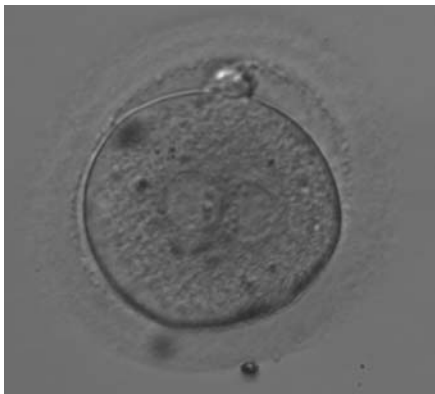


Figure 153 A zygote observed 18 h post-ICSI with NPBs aligned at the PN junction (200× magnification). NPBs differ in number and size between PNs. The polar bodies are overlapped in this view. It was discarded due to subsequent abnormal cleavage.

the furrow, or onto the mitotic plate (Figs 155–157). NPB and PN progression can occur even in highly dysmorphic zygotes (Fig. 158).

During the progression of the cell cycle, NPBs change in number, size and distribution (Fig. 101) and finally they disappear shortly before syngamy and initiation of the first cleavage division (Fig. 149). Recent investigations by time-lapse imaging have shown that NPBs are highly dynamic and that a characteristic NPB pattern may change within a short period of time (Montag *et al.*, 2011).

The potential use of the arrangement of NPBs in both PNs regarding size, number and symmetry was initially investigated as a major part of PN scoring in the late 90s (Scott and Smith, 1998). Several publications found a benefit of PN scoring and especially the distribution of NPBs with the outcome of assisted reproduction treatment (Tesarik



Figure 154 A zygote generated by ICSI, displaying two perfectly juxtaposed PNs within which the NPBs are aligned, have the same size and are similar in number (400× magnification). It was transferred but the outcome is unknown.

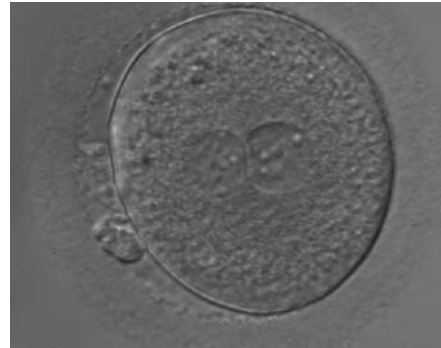


Figure 155 An ICSI zygote with large-sized NPBs scattered with respect to the PN junction (400× magnification). The cytoplasm appears granular. It was transferred but failed to implant.



Figure 156 An ICSI zygote with NPBs scattered with respect to the PN junction (400× magnification). Polar bodies are fragmented; there is debris in the PVS. It was transferred but implantation outcome is unknown.



Figure 157 An ICSI zygote displaying partially overlapping PNs in this view. NPBs are scattered in both PNs (400× magnification). It was transferred but the outcome is unknown.



Figure 158 A zygote generated by IVF at 16.40 h post-insemination (400× magnification). It shows small-sized NPBs scattered with respect to the PN junction and a lot of large cellular debris in the PVS. It was discarded.

and Greco, 1999; Scott et al., 2000; Balaban et al., 2001; Montag and van der Ven, 2001; Ebner et al., 2003; Senn et al., 2006). Others have reported no benefit (Payne et al., 2005; James et al., 2006; Nicoli et al., 2007; Brezinova et al., 2009).

NPBs' morphology is influenced by the patient's age and there is also a temporal difference in morphology between zygotes from IVF compared with ICSI. Therefore, comparative PN/NPB scoring should be performed according to strict guidelines considering timing, patient characteristics and insemination technique employed.

Many cell cycle control proteins are located in the nucleolus, and it has been shown in mitotic cells that asymmetry in number and pattern of NPBs is associated with abnormal cell cycles and ultimately with abnormal development (Pedersen, 1998). It is plausible that asymmetry between PNs in zygotes (Figs 159–162) can lead to abnormal development with an increase in fragmentation and abnormal cleavage, and

reduced viability (Scott, 2003). Nevertheless, implantation can occur (Figs 163 and 164).

Pronuclear scoring based on Scott's (2003) Z scores, which combines the assessment of PN orientation and NPB pattern, was



Figure 159 A zygote with inequality in numbers and alignment of NPBs. It was cryopreserved.

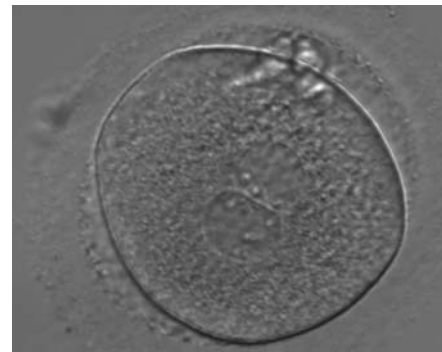


Figure 160 A zygote generated by ICSI with inequality in numbers and alignment of NPBs (400× magnification). NPBs are aligned in one PN and scattered in the other. Due to poor development, it was discarded.



Figure 161 A zygote generated by IVF with inequality in numbers and alignment of NPBs (600× magnification). It was discarded.



Figure 162 A zygote observed 16 h post-ICSI with small-sized NPBs scattered with respect to the PN junction in both PNs (400× magnification). It has a very thin ZP. It was transferred but failed to implant.

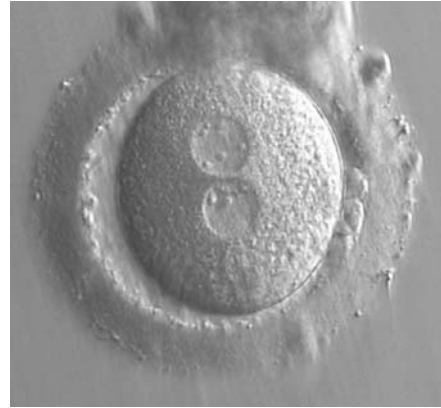


Figure 164 A zygote at 15 h post-IVF in which NPBs are scattered in one of the two PNs and aligned in the other (400× magnification). The ZP is thick and the PVS is enlarged. One of the two polar bodies is fragmented. It was transferred and implanted.

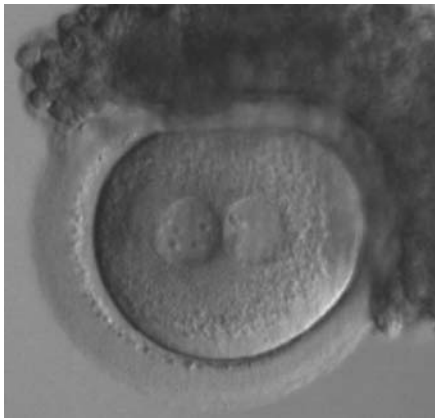


Figure 163 A zygote generated by ICSI with inequality in numbers and alignment of NPBs (200× magnification). Many granulosa cells are adherent to the ZP. It was transferred and implanted.



Figure 165 A zygote generated by ICSI with equal numbers of large-sized NPBs aligned at the PN junction (200× magnification). It was transferred but the outcome is unknown.

adopted by the consensus workshop (*Alpha Scientists in Reproductive medicine and ESHRE Special Interest Group of Embryology, 2011*) but modified into three categories:

- (i) symmetrical PNs (corresponding to Scott's Z1 and Z2)
- (ii) non-symmetrical PNs (other arrangements, peripheral PNs)
- (iii) abnormal PNs (PNs with none or one NPB, which are called respectively 'ghost' PNs and 'bulls-eye' PNs. Both have been associated with abnormal outcome in animal models.

D.2 Numbers similar/numbers different between PNs

Human cells generally have two to seven nucleoli per human nucleus with equal numbers in the two daughter cells after a mitotic division. Nucleoli appear and disappear depending on the cell cycle phase: they are more numerous at the G1 phase, then start to fuse, and at the S1

phase there are only one to two large nucleoli per nucleus. When asynchrony occurs, this appears to be the result of aberrant chromosomal function.

Transferring this model to the zygote, the ideal oocytes are those presenting with symmetry for number and size of NPBs that are aligned on the furrow between the 2PNs (Figs 165–167). Equality in number with non-alignment in both PNs is also indicative of synchronised development (Fig. 168). In contrast, any form of disparity in NPBs' size, number or pattern of alignment between the PNs, is associated with a poor outcome (Figs 169–172).

D.3 Similar size of NPBs/different size of NPBs

The dynamics of nucleoli formation associated with NPBs merging implies a time-related change in NPBs' size (Scott, 2003). A progressive increase in NPBs' size and a concomitant reduction in number



Figure 166 A zygote generated by ICSI with equal numbers of large-sized NPBs aligned at the PN junction (400× magnification). There is a halo in the cortical area; polar bodies are fragmented and the ZP appears brush-like. It was discarded due to subsequent abnormal development.



Figure 169 A zygote generated by ICSI showing different numbers of NPBs (400× magnification). The cytoplasm appears granular. It was transferred but failed to implant.

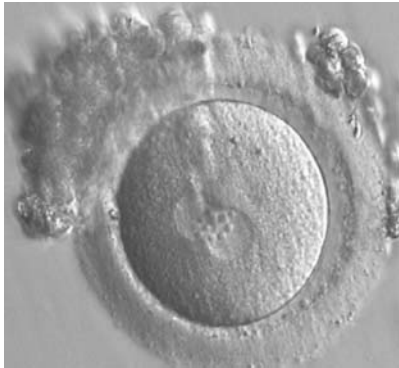


Figure 167 A zygote generated by IVF observed 17 h post-insemination (400× magnification). PNs have similar numbers of large-sized NPBs aligned at the PN junction. The PVS is slightly enlarged and the ZP is normal in size and surrounded by some granulosa cells. It was transferred but failed to implant.



Figure 170 A zygote observed 16.5 h post-ICSI, showing unequal number and size of NPBs: medium-sized and scattered in one PN, larger-sized and aligned in the other (400 × magnification). Polar bodies had been biopsied, and the slit opened mechanically in the ZP is evident at the 3 o'clock position. It was cryopreserved.

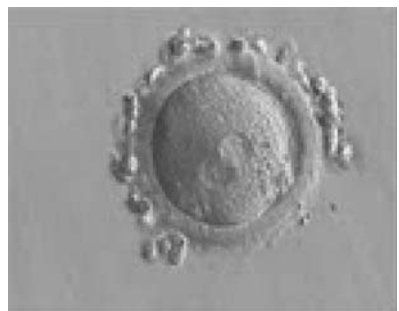


Figure 168 A zygote generated by IVF using frozen/thawed ejaculated sperm and observed 15 h post-insemination (400× magnification). Two PNs of approximately the same size are clearly visible in the cytoplasm. Peripheral granular cytoplasm can be seen. NPBs are scattered in both PNs. Both polar bodies are located at the 4 o'clock position. It was transferred and implanted.

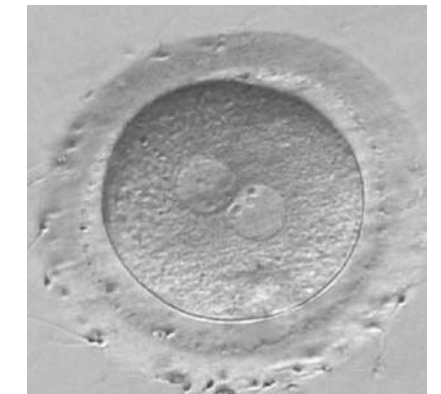


Figure 171 A zygote observed at 16 h post-IVF displaying different number and size of NPBs: small and scattered in one PN, large and aligned in the other (400 × magnification). It was discarded because of developmental arrest.

occur at the time of nucleoli alignment into the furrow between PNs (Figs 173–176).

The presence of small scattered and unequal-sized NPBs (Figs 177–179) could be indicative of functional defects in nucleoli with consequent decreased or ineffective synthesis of rRNA. The extent of malfunctioning possibly depends on the grade of asynchrony and on the number of affected nucleoli as demonstrated by the clinical outcome that may result in implantation (Fig. 180).

D.4 Ghost PNs (absent NPBs)/single NPB in one or more PNs (bull's eye)

Despite the difficulty of making comparative studies aimed at evaluating the relevance of PN scoring, the sequence of processes involved in fertilization underlines the importance and significance of NPBs and



Figure 172 A zygote generated by ICSI with a different number and size of scattered NPBs (600× magnification). It was discarded because of subsequent abnormal development.

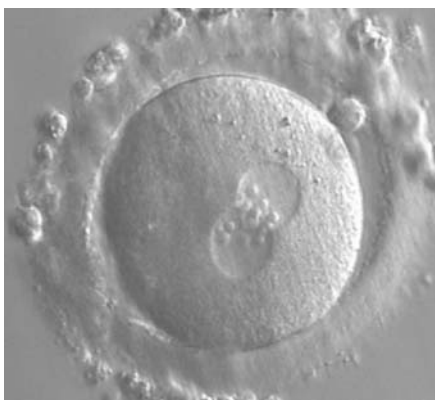


Figure 173 A zygote generated by ICSI showing equal number and size of NPBs, which are aligned at the PN junction (200× magnification). PNs are tangential to the plane of the polar bodies. It was transferred and resulted in a singleton pregnancy and delivery.

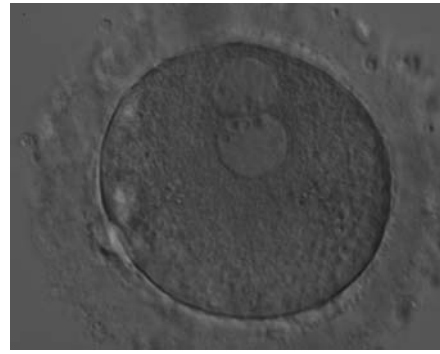


Figure 174 A zygote generated by ICSI with peripherally located PNs showing NPBs of similar size and number (200× magnification). Further development resulted in uneven cleavage and arrest on Day 3.



Figure 175 A zygote observed at 18 h after ICSI, with NPBs of equal size in both PNs and aligned at the PN junction (200× magnification). Polar bodies are intact and slightly larger than normal. The cytoplasm is granular with some inclusions. It was discarded due to subsequent abnormal development.

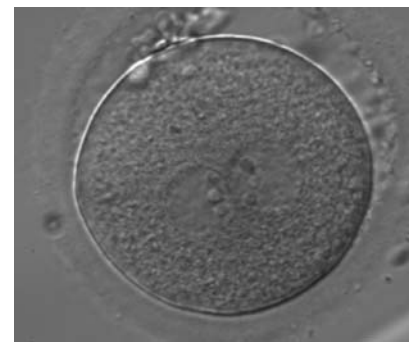


Figure 176 A zygote generated by ICSI showing equal number and size of NPBs, which are perfectly aligned at the PN junction (200× magnification). Polar bodies are highly fragmented. It was transferred but clinical outcome is unknown.



Figure 177 A zygote generated by ICSI displaying unequal number and size of NPBs between the PNs (400× magnification). It was transferred but clinical outcome is unknown.



Figure 178 A zygote generated by ICSI showing an unequal number of NPBs (400× magnification). The NPBs differ in size within each PN. It was transferred but clinical outcome is unknown.



Figure 179 A zygote generated by ICSI displaying unequal number and size of NPBs between the PNs (400× magnification). NPBs are mainly aligned at the PN junction. It was transferred but clinical outcome is unknown.

nucleoli in determining embryo viability. In light of these considerations, it is not surprising that the absence of nucleoli in PNs at the time of fertilization check, the so-called 'ghost' PNs (Figs 181–184), or the presence of a single NPB, known as 'bull's eye' PNs (Figs 185–189) has been reported to be associated with epigenetic defects and abnormal development in animals (Svarcova et al., 2009).

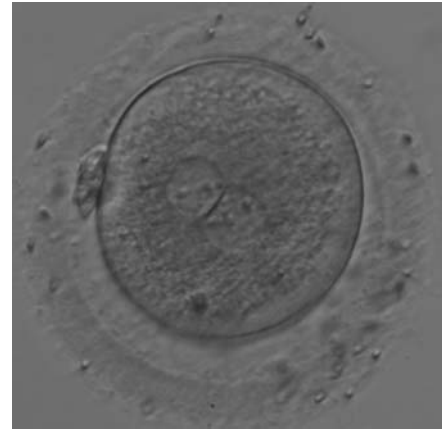


Figure 180 A zygote generated by IVF with large NPBs scattered with respect to the PN junction (200× magnification). NPBs display differences in sizes within each PN and are slightly larger in the PN on the right side. It was transferred and resulted in a singleton pregnancy with delivery.



Figure 181 One out of three sibling zygotes (see also Figs 182 and 183) generated by ICSI using frozen/thawed epididymal sperm observed 18 h post-insemination. All three zygotes clearly show two distinct PNs with well-defined membranes and without any NPBs. All three were transferred and two healthy baby boys were delivered.



Figure 182 The second out of three sibling zygotes (see also Figs 181 and 183) generated by ICSI using frozen/thawed epididymal sperm. All three zygotes showed refractile bodies in the cytoplasm.

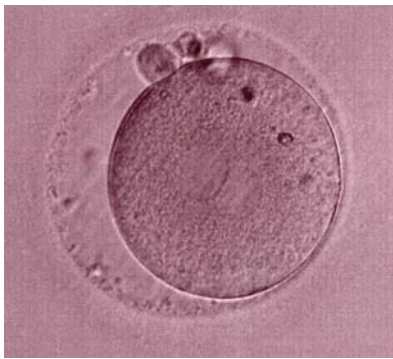


Figure 183 The third of three sibling zygotes (see also Figs 181 and 182) generated by ICSI using frozen/thawed epididymal sperm. Beside the absence of NPBs and the presence of refractile bodies, this zygote has a large perivitelline space.



Figure 184 A zygote generated by ICSI showing what looks like two distinct PNs with distinct membranes and the absence of NPBs in one of the PNs (400× magnification). One small vacuole is visible under the left PN. Two highly fragmented polar bodies are present at 9 o'clock. Despite the presence of 2 polar bodies after ICSI, it is possible that this is a 1PN zygote, and that the structure to the right is a vacuole (compare with Fig. 209). It was not transferred.



Figure 185 A zygote generated by ICSI showing two 'bull's eye' PNs, each having a single large NPB (200× magnification). The PNs are slightly separated and are not as yet juxtaposed. A clear cortical region is evident in the cytoplasm. It was discarded.



Figure 186 Oval-shaped zygote generated by ICSI, showing a single NPB in one of the two PNs ('bull's eye') and small, scattered NPBs in the other (200× magnification). The PVS is quite large and the polar bodies are highly fragmented. It was discarded.



Figure 187 Zygote generated by ICSI with one 'bull's eye' NPB in one PN and small, different-sized NPBs in the other (400× magnification). It was transferred but clinical outcome is unknown.



Figure 188 Zygote generated by ICSI displaying two centrally positioned PNs: in one PN there is a single large NPB ('bull's eye'), whereas the NPBs are smaller, different-sized and scattered in the other (600 \times magnification). It was discarded.



Figure 190 A zygote generated by IVF with frozen/thawed ejaculated sperm and observed at 16 h post-insemination showing normal cytoplasmic morphology (400 \times magnification). NPBs are obviously different in the two PNs. It was transferred but failed to implant.



Figure 189 A zygote generated by ICSI with one 'bull's eye' PN (400 \times magnification). The NPBs from each PN are aligned at the PN junction. It was transferred but clinical outcome is unknown.



Figure 191 A zygote generated by ICSI, which subsequently underwent polar body biopsy, shows normal cytoplasmic morphology (400 \times magnification). It was discarded due to aneuploidy.



Figure 192 A zygote generated by IVF with frozen/thawed ejaculated sperm and observed at 16 h post-insemination showing normal cytoplasmic morphology with an evident clear cortical zone, the halo, in the cytoplasm (400 \times magnification). NPBs are scattered and different-sized, polar bodies are fragmented. It was cryopreserved.

E. Cytoplasmic morphology assessment

E.1 Normal/granular

Homogeneous cytoplasm is expected in zygotes as for oocytes (Figs 190 and 191), but heterogeneous cytoplasm is of unknown developmental significance. Therefore, although some studies have reported that severe cytoplasmic anomalies in the zygote adversely affect the developmental and implantation potential of the resulting embryo (Kahraman *et al.*, 2000; Ebner *et al.*, 2003; Balaban and Urman, 2006), there is no clear evidence supporting these findings. Similarly, the presence of a peripheral cytoplasmic translucency in the fertilized oocyte (known as the 'halo'; Fig. 192) or of minor dysmorphisms such as debris in the PVS (Fig. 193) or presence of refractile bodies in the cytoplasm (Fig. 194) have not been proved to be of



Figure 193 A zygote generated by ICSI showing normal cytoplasmic morphology, a thin ZP and small debris in an enlarged PVS (400× magnification). It was transferred but clinical outcome is unknown.



Figure 194 A zygote generated by ICSI showing normal cytoplasmic morphology except for a refractile body visible at the 3 o'clock position in this view (400× magnification). It was transferred but clinical outcome is unknown.

prognostic value for implantation. Nevertheless, recording of these observations should be made as the accumulation of data could reveal some relevant links to developmental or implantation potential.

Normal cytoplasm is clearly distinguishable from granular cytoplasm, but to make comparative observations attention should be paid to the optical system and culture medium employed. The severity of granularity is generally based on the diameter and depth of the granular area that may occupy either the whole zygote (Fig. 195), or small (Figs 196–198) or large areas of the cytoplasm (Figs 199 and 200).

It has been reported that half of the oocytes with dysmorphic phenotypes such as organelle clustering are aneuploid, with hypohaploidy being the predominant abnormality (Van Blerkom and Henry, 1992). This severe cytoplasmic disorganization is associated with a lower intracytoplasmic pH and decreased ATP content (Van Blerkom *et al.*, 1997). These dysmorphic changes would be inherited in the zygote. Apparently, intracytoplasmic organelle clustering (Fig. 200) is a type of severe abnormality that is significantly repetitive in consecutive cycles and is a negative predictor of pregnancy and implantation



Figure 195 A zygote generated by ICSI displaying heterogeneous, granular cytoplasm (200× magnification). NPBs are large-sized and polar bodies are fragmented. It was discarded due to poor subsequent development.



Figure 196 A zygote generated by IVF using frozen/thawed ejaculated sperm and observed at 17 h post-insemination showing an irregular oolemma and dysmorphic granular cytoplasm (400× magnification). PBs are different in size and peripherally located. NPBs differ in size and number between PBs. It was transferred but failed to implant.



Figure 197 A zygote generated by ICSI with peripheral PNs (150× magnification). The oolemma is irregular and the cytoplasm is dysmorphic and granular. The ZP is thick and dark. It was discarded.



Figure 198 A zygote generated by ICSI displaying granular cytoplasm, especially in the area immediately adjacent to the clear cortical zone (400× magnification). There is an enlarged PVS and an ovoid ZP. NPBs differ in number and size. It was transferred but clinical outcome is unknown.



Figure 199 A zygote generated by ICSI with four PNPs (possibly a result of fragmentation of an originally normal-sized PN), displaying very granular cytoplasm and a clear cortical zone (600× magnification). It was discarded.



Figure 200 A zygote generated by ICSI using frozen/thawed ejaculated sperm (200× magnification). PNPs are peripherally located with a large inclusion positioned directly below the PNPs that is displaying a crater-like appearance as a consequence of severe organelle clustering. It was discarded.

rates, although the cleavage stage embryo quality, as observed by light microscopy, is apparently not affected (Meriano et al., 2001).

E.2 Small vacuoles/large vacuoles

The presence of a few small vacuoles (diameter of 5–10 μm) that are apparently fluid filled and transparent (Figs 201 and 202) have not been associated with detectable biological consequences, but some concern may arise when several vacuoles appear (Figs 203 and 204) or appear with other morphological anomalies (Fig. 205).

Large vacuoles (>14 μm in diameter) in fertilized oocytes (Figs 206–210) can interfere with cleavage planes, resulting in reduced blastocyst formation (Ebner et al., 2005). For this reason, they are normally not considered for transfer.

At the time of fertilization check and especially after conventional IVF, it is extremely important to carefully score the cytoplasm for the presence of SER discs (see Chapter One), which are associated with the risk of a deleterious clinical outcome (Otsuki et al., 2004).



Figure 201 An irregularly shaped zygote generated by ICSI showing centrally positioned PNPs and a medium-sized vacuole at the 8 o'clock position in the cytoplasm (400× magnification). It was transferred but clinical outcome is unknown.



Figure 202 A zygote generated by ICSI with centrally positioned different-sized PNPs, displaying two small vacuoles at the 9 o'clock position in the cytoplasm (400× magnification). It was transferred but clinical outcome is unknown.



Figure 203 A zygote generated by ICSI with an irregular oolemma and a large PVS with possibly highly fragmented polar bodies (150× magnification). Different sized overlapping PNs are peripherally positioned and several vacuoles of different sizes are present at the 2, 5 and 6 o'clock position in the cytoplasm. It was discarded.



Figure 204 A zygote generated by ICSI with slightly overlapping peripherally positioned PNs and a large PVS with one large and one fragmented polar body (150× magnification). Many small vacuoles are present throughout the cytoplasm. It was discarded.



Figure 205 Severely dysmorphic zygote generated by IVF showing small PNs and an irregularly shaped ZP and oolemma and lack of a PVS (600× magnification). There is a small vacuole present at 10 o'clock with refractile bodies immediately adjacent. It was discarded.



Figure 206 A zygote generated by ICSI showing peripherally positioned PNs and a very large vacuole at the 12 o'clock position in the cytoplasm (400× magnification). Polar bodies are fragmented and the ZP is of irregular thickness. It was discarded.



Figure 207 A zygote generated by ICSI showing cytoplasmic abnormalities (150× magnification). The PNs are juxtaposed and peripherally positioned with a large vacuole of irregular shape at the 6 o'clock position in the cytoplasm. The cytoplasm is granular and the ZP is thick and heterogeneous in appearance. It was discarded.



Figure 208 A zygote generated by ICSI showing severe cytoplasmic abnormalities (150× magnification). There is a large centralized vacuole with many small vacuoles surrounding it in a granular cytoplasm. It was discarded.



Figure 209 A zygote generated by ICSI showing peripherally located PNJs with the same number and size of NPBs perfectly aligned at the PN junction (400× magnification). There is a large vacuole immediately adjacent to the two PNJs that is almost the same size as the PNJs. It was discarded.



Figure 210 A zygote generated by ICSI showing centrally positioned PNJs and two large vacuoles immediately adjacent to each of the PNJs at the 3 and 9 o'clock positions in the cytoplasm (400× magnification). There are also refractile bodies present at the 6–7 o'clock positions and an area of clustering at 11 o'clock. It was discarded.

References

- Ajdk A, Ilozue T, Windsor S, Yu Y, Seres KB, Bompfrey RJ, Tom BD, Swann K, Thomas A, Graham C et al. Rhythmic actomyosin-driven contractions induced by sperm entry predict mammalian embryo viability. *Nat Commun* 2011;**2**:417.
- Alpha Scientists in Reproductive Medicine and ESHRE Special Interest Group of Embryology. The Istanbul consensus workshop on embryo assessment: proceedings of an expert meeting. *Hum Reprod* 2011; **26**:1270–1283.
- Balaban B, Urman B. Effect of oocyte morphology on embryo development and implantation. *Reprod BioMed Online* 2006; **12**:608–615.
- Balaban B, Urman B, Isiklar A, Alatas C, Aksoy S, Mercan R, Mumcu A, Nuhoglu A. The effect of pronuclear morphology on embryo quality parameters and blastocyst transfer outcome. *Hum Reprod* 2001; **16**:2357–2361.
- Balaban B, Yakin K, Urman b, Isiklar A, Tesarik J. Pronuclear morphology predicts embryo development and chromosome constitution. *Reprod Biomed Online* 2004;**8**:695–700.
- Brezinova J, Oborna I, Svobodova M, Fingerova H. Evaluation of day one embryo quality and IVF outcome—a comparison of two scoring systems. *Reprod Biol Endocrinol* 2009;**7**:9.
- Ebner T, Moser M, Sommergruber M, Gaiswinkler U, Wiesinger R, Puchner M, Tews G. Presence, but not type or degree of extension, of a cytoplasmic halo has a significant influence on preimplantation development and implantation behaviour. *Hum Reprod* 2003; **18**:2406–2412.
- Ebner T, Moser M, Sommergruber M, Gaiswinkler U, Shebl O, Jesacher K, Tews G. Occurrence and developmental consequences of vacuoles throughout preimplantation development. *Fertil Steril* 2005; **83**:1635–1640.
- Ebner T, Moser M, Shebl O, Sommergruber M, Tews G. Prognosis of oocytes showing aggregation of smooth endoplasmic reticulum. *Reprod Biomed Online* 2008;**16**:113–118.
- Edirisinghe WR, Jemmott R, Smith C, Allan J. Association of pronuclear Z score with rates of aneuploidy in in-vitro fertilised embryos. *Reprod Fertil Dev* 2005;**17**:529–534.
- Edwards RG, Beard HK. Oocyte polarity and cell determination in early mammalian embryos. *Mol Hum Reprod* 1997;**3**:863–905.
- Edwards RG, Beard HK. Hypothesis: sex determination and germline formation are committed at the pronuclear stage in mammalian embryos. *Mol Hum Reprod* 1999;**5**:595–606.
- Gardner RL. Can developmentally significant spatial patterning of the egg be discounted in mammals? *Hum Reprod Update* 1996;**2**:3–27.
- Gardner RL. Scrambled or bisected mouse eggs and the basis of patterning in mammals. *BioEssays* 1999;**21**:271–274.
- Gardner RL. Specification of embryonic axes begins before cleavage in normal mouse development. *Development* 2001;**128**:839–847.
- Garello C, Baker H, Rai J, Montgomery S, Wilson P, Kennedy CR, Hartshorne GM. Pronuclear orientation, polar body placement, and embryo quality after intracytoplasmic sperm injection and in vitro fertilization: further evidence for polarity in human oocytes? *Hum Reprod* 1999;**14**:2588–2595.
- Gianaroli L, Magli MC, Ferraretti AP, Fortini D, Grieco N. Pronuclear morphology and chromosomal abnormalities as scoring criteria for embryo selection. *Fertil Steril* 2003;**80**:341–349.
- James AN, Hennessy S, Reggio B, Wiemer K, Larsen F, Cohen J. The limited importance of pronuclear scoring of human zygotes. *Hum Reprod* 2006;**21**:1599–1604.
- Kahraman S, Yakin K, Dönmez E, Samli H, Bahçe M, Cengiz G, Sertyel S, Samli M, Imirzalioglu N. Relationship between granular cytoplasm of oocytes and pregnancy outcome following intracytoplasmic sperm injection. *Hum Reprod* 2000;**15**:2390–2393.
- Lundin K, Bergh C, Hardarson T. Early embryo cleavage is a strong indicator of embryo quality in human IVF. *Hum Reprod* 2001; **16**:2652–2657.
- Meriano JS, Alexis J, Visram-Zaver S, Cruz M, Casper RF. Tracking of oocyte dysmorphisms for ICSI patients may prove relevant to the outcome in subsequent patient cycles. *Hum Reprod* 2001; **16**:2118–2123.
- Montag M, van der Ven H. Evaluation of pronuclear morphology as the only selection criterion for further embryo culture and transfer: results of a prospective multicentre study. *Hum Reprod* 2001; **16**:2384–2389.
- Montag M, Liebenthron J, Köster M. Which morphological scoring system is relevant in human embryo development? *Placenta* 2011; **32**:S252–S256.

- Munné S, Cohen J. Chromosome abnormalities in human embryos. *Hum Reprod Update* 1998;**4**:842–855.
- Nagy ZP, Janssenswillen C, Janssens R, De Vos A, Staessen C, Van deVelde H, Van Steirteghem AC. Timing of oocyte activation, pronucleus formation and cleavage in humans after intracytoplasmic sperm injection (ICSI) with testicular spermatozoa and after ICSI or in-vitro fertilization on sibling oocytes with ejaculated spermatozoa. *Hum Reprod* 1998;**13**:1606–1612.
- Nagy ZP, Dozortsev D, Diamond M, Rienzi L, Ubaldi F, Abdelmassih R, Greco E. Pronuclear morphology evaluation with subsequent evaluation of embryo morphology significantly increases implantation rates. *Fertil Steril* 2003;**80**:67–74.
- Nicoli A, Valli B, Di Girolamo R, Di Tommaso B, Gallinelli A, La Sala GB. Limited importance of pre-embryo pronuclear morphology (zygote score) in assisted reproduction outcome in the absence of embryo cryopreservation. *Fertil Steril* 2007;**88**:1167–1173.
- Nicoli A, Capodanno F, Moscato L, Rondini I, Villani MT, Tuzio A, La Sala GB. Analysis of pronuclear zygote configurations in 459 clinical pregnancies obtained with assisted reproductive technique procedures. *Reprod Biol Endocrinol* 2010;**8**:77.
- Otsuki J, Okada A, Morimoto K, Nagai Y, Kubo H. The relationship between pregnancy outcome and smooth endoplasmic reticulum clusters in MII human oocytes. *Hum Reprod* 2004;**19**:1591–1597.
- Palermo G, Munné S, Cohen J. The human zygote inherits its mitotic potential from the male gamete. *Fertil Steril* 1994;**9**:1220–1225.
- Payne D, Flaherty SP, Barry MF, Matthews CD. Preliminary observations on polar body extrusion and pronuclear formation in human oocytes using time-lapse video cinematography. *Hum Reprod* 1997;**12**:532–541.
- Payne JF, Raburn DJ, Couchman GM, Price TM, Jamison MG, Walmer DK. Relationship between pre-embryo pronuclear morphology (zygote score) and standard day 2 or 3 embryo morphology with regard to assisted reproductive technique outcomes. *Fertil Steril* 2005;**84**:900–909.
- Pedersen T. Growth factors in the nucleolus? *J Cell Biol* 1998;**143**:279–281.
- Plachot M. Fertilization. *Hum Reprod* 2000;**15**(Suppl. 4):19–30.
- Reichman DE, Jackson KV, Racowsky C. Incidence and development of zygotes exhibiting abnormal pronuclear disposition after identification of two pronuclei at the fertilization check. *Fertil Steril* 2010;**94**:965–970.
- Sadowy S, Tomkin G, Munné S, Ferrara-Congedo T, Cohen J. Impaired development of zygotes with uneven pronuclear size. *Zygote* 1998;**6**:137–141.
- Sakkas D, Shoukir Y, Chardonens D, Bianchi PG, Campana A. Early cleavage of human embryos to the two-cell stage after intracytoplasmic sperm injection as an indicator of embryo viability. *Hum Reprod* 1998;**13**:182–187.
- Sathananthan AH, Ratnam SS, Ng SC, Tarin JJ, Gianaroli L, Trounson A. The sperm centriole: its inheritance, replication and perpetuation in early embryos. *Hum Reprod* 1996;**11**:345–356.
- Scott L. Oocyte and embryo polarity. *Semin Reprod Med* 2001;**18**:171–183.
- Scott L. Pronuclear scoring as a predictor of embryo development. *Reprod Biomed Online* 2003;**6**:201–214.
- Scott LA, Smith S. The successful use of pronuclear embryo transfers the day following oocyte retrieval. *Hum Reprod* 1998;**13**:1003–1013.
- Scott L, Alvero R, Leondires M, Miller B. The morphology of human pronuclear embryos is positively related to blastocyst development and implantation. *Hum Reprod* 2000;**15**:2394–2403.
- Scott L, Finn A, O'Leary T, McLellan S, Hill J. Morphologic parameters of early cleavage-stage embryos that correlate with fetal development and delivery: prospective and applied data for increased pregnancy rates. *Hum Reprod* 2007;**22**:230–240.
- Senn A, Urner F, Chanson A, Primi MP, Wirthner DW, Germond M. Morphological scoring of human pronuclear zygotes for prediction of pregnancy outcome. *Hum Reprod* 2006;**21**:234–239.
- Svarcova O, Dinnyes A, Polgar Z, Bodo S, Adorjan M, Meng Q, Maddox-Hyttel P. Nucleolar re-activation is delayed in mouse embryos cloned from two different cell lines. *Mol Reprod Dev* 2009;**76**:132–141.
- Tesarik J, Greco E. The probability of abnormal preimplantation development can be predicted by a single static observation on pronuclear stage morphology. *Hum Reprod* 1999;**14**:1318–1323.
- Tesarik J, Junca AM, Hazout A, Aubriot FX, Nathan C, Cohen-Bacrie P, Dumont-Hassan M. Embryos and high implantation potential after intracytoplasmic sperm injection can be recognized by a simple, non-invasive examination of pronuclear morphology. *Hum Reprod* 2000;**15**:1396–1399.
- Van Blerkom J, Henry G. Oocyte dysmorphism and aneuploidy in meiotically mature human oocytes after ovarian stimulation. *Hum Reprod* 1992;**7**:379–390.
- Van Blerkom J, Davis P, Merriam J, Sinclair J. Nuclear and cytoplasmic dynamics of sperm penetration, pronuclear formation and micro-tubule organization during fertilization and early preimplantation development in the human. *Hum Reprod Update* 1995;**1**:429–461.
- Van Blerkom J, Antczak M, Schrader R. The developmental potential of the human oocyte is related to the dissolved oxygen content of follicular fluid: association with vascular endothelial growth factor levels and perifollicular blood flow characteristics. *Hum Reprod* 1997;**12**:1047–1055.
- Weitzman VN, Schnee-Riesz J, Benadiva C, Nulsen J, Siano L, Maier D. Predictive value of embryo grading for embryos with known outcomes. *Fertil Steril* 2010;**93**:658–662.
- Yan J, Li Y, Shi Y, Feng HL, Gao S, Chenz Z. Assessment of sex chromosomes of human embryos arising from monpronucleus zygotes in in vitro fertilization and intracytoplasmic sperm injection cycles of Chinese women. *Gynecol Obstet Invest* 2010;**69**:20–23.
- Zamora RB, Sánchez RV, Pérez JG, Diaz RR, Quintana DB, Bethencourt JC. Human zygote morphological indicators of high rate of arrest at the first cleavage stage. *Zygote* 2011;**19**:339–344.
- Zollner U, Zollner KP, Steck T, Dietl J. Pronuclear scoring: time for international standardization. *J Reprod Med* 2003;**5**:365–369.

The cleavage stage embryo

Fernando J. Prados, Sophie Debrock, Josephine G. Lemmen,
and Inge Agerholm

Contents

- Introduction
- A. Cell numbers
- B. Fragmentation
- C. Blastomere size: 'stage specific' versus 'non-stage specific'
- D. Nucleation
- E. Cytoplasmic anomalies
- F. Spatial orientation
- G. Compaction

Introduction

A precise embryo quality evaluation is of paramount importance to sustain a successful *in vitro* fertilization (IVF) program. In most IVF clinics around the world, this quality assessment relies mainly on the morphological evaluation of cleavage stage embryos. Embryologists should be able to correlate the features observed at the optical microscope with the implantation potential of each particular embryo (Alikani *et al.*, 2000; Ebner *et al.*, 2003; Alpha Scientists in Reproductive Medicine and ESHRE Special Interest Group of Embryology, 2011). To achieve this goal, many scoring systems based on the morphological features of the dividing embryo have been developed (Giorgetti *et al.*, 1995; Veeck, 1999; Fisch *et al.*, 2001; de Placido *et al.*, 2002; Baczkowski *et al.*, 2004; reviewed by Rienzi *et al.*, 2005; Torelló *et al.*, 2005; Holte *et al.*, 2007). These embryo classification systems are based on the evaluation of the number of blastomeres, the degree of fragmentation, the symmetry of the blastomeres, the presence of multinucleation and the compaction status. It is very important that the features related to implantation potential are assessed accurately and similarly. The purpose of this chapter is to illustrate morphological aspects useful for the evaluation of the implantation potential of the embryos.

Cleavage stage embryos range from the 2-cell stage to the compacted morula composed of 8–16 cells. The number of blastomeres is used as the main characteristic with the highest predictive value (Van Royen *et al.*, 1999; Alikani *et al.*, 2000; Fisch *et al.*, 2001). Good quality embryos must exhibit appropriate kinetics and synchrony of division. In normal-developing embryos, cell division occurs every 18–20 h. Embryos dividing either too slow or too fast may have metabolic and/or chromosomal defects (Edwards *et al.*, 1980; Giorgetti *et al.*, 1995; Ziebe *et al.*, 1997; Van Royen *et al.*, 1999; Leese, 2002;

Munné, 2006; Magli *et al.*, 2007). Recent time-lapse studies indicate that not only the timing of cleavage, but also the time between each cell division is of importance. If all blastomeres divide in exact synchrony, only 2-, 4- or 8-cell embryos would be observed. However, it is frequent to observe 3-, 5-, 6-, 7- or 9-cell embryos, which is an indication of asynchronous development (Scott *et al.*, 2007; Lemmen *et al.*, 2008; Wong *et al.*, 2010; Meseguer *et al.*, 2011; reviewed by Kirkegaard *et al.*, 2012). Time of scoring with respect to the insemination event has to be precisely established for a correct evaluation of the kinetics of cell division (Scott *et al.*, 2007). However, it is also important to keep in mind that the environment in the specific laboratory, such as culture media and temperature, influences the kinetics of development.

Very frequently, the mitosis of embryos leads to externalization of parts of the cell cytoplasm, resulting in the presence of anuclear fragments surrounded by a plasma membrane (Antczak and van Blerkom, 1999). The size and distribution of fragments inside the space surrounded by the zona pellucida (ZP) are variable (Alikani *et al.*, 1999). The amount of fragments is widely used to predict the implantation potential of the embryos and fragmentation has been related to aneuploidy (Ebner *et al.*, 2001; Ziebe *et al.*, 2003; Munné, 2006). If fragmentation does not reach 10% of the total embryo volume it is agreed that it does not have an impact on the embryo's developmental potential (Van Royen *et al.*, 2001; Holte *et al.*, 2007).

Mitosis in blastomeres should produce two equally sized daughter cells. When the division is asymmetric, one of the blastomeres of the next generation will inherit less than half the amount of cytoplasm from the parent blastomere, leading to a defective lineage in the embryo. For example, 4- and 8-cell embryos with equal cell sizes have been shown to have lower multinucleation and aneuploidy rates and increased implantation rates (Hardarson *et al.*, 2001; Van Royen *et al.*, 2001; Hnida *et al.*, 2004; Scott *et al.*, 2007). After two cleavages, the zygote becomes a 4-cell embryo. The four cells of the embryo are normally arranged in a tetrahedron in the spherical space provided by the ZP. However, in some cases, the blastomeres are located close to a single, spatial plane produced by an incorrect orientation of the division axes. This can be associated with altered embryo polarity (Edwards and Hansis, 2005).

Each embryo blastomere should have a single nucleus. Multinucleation has been described to be associated with genetic disorders of the embryo (Kligman *et al.*, 1996; Hardarson *et al.*, 2001). It impairs cleavage rates and the implantation potential of human embryos

(Pelinck *et al.*, 1998; Van Royen *et al.*, 2003; Moriwaki *et al.*, 2004) and has been associated with an increased abortion rate (Meriano *et al.*, 2004). Multinucleation can be evaluated on Days 1, 2 and 3 of development. On Day 3, however, this characteristic is more difficult to evaluate due to the more complex structure of a Day 3 embryo (Van Royen *et al.*, 2003). Different morphological anomalies are often associated with each other, and uneven cleavage has been shown to be related to multinucleation (Hardarson *et al.*, 2001) and fragmentation (Hnida *et al.*, 2004).

A clear homogeneous cytoplasm is acknowledged as normal for cleavage stage embryos. The presence of anomalies such as an abundance of vacuoles and aggregation of organelles resulting in clear and granular cytoplasmic regions has to be considered in any embryo quality assessment (Veeck, 1999; Desai *et al.*, 2000; Ebner *et al.*, 2003).

After the embryo reaches the 8-cell stage, the blastomeres begin to show an increase in cell–cell adherence due to the spread of intercellular tight junctions. This is the start of compaction. The process of compaction advances during the next division until the boundaries between the cells are barely detectable (Veeck, 1999). If some of the blastomeres are excluded from this compaction process, the embryo may have a reduced potential for becoming a normal blastocyst (Tao *et al.*, 2002). In a proposed grading system compaction can be classified using the following criteria: the proportion of blastomeres undergoing compaction and the morphology of the compacted embryo (Tao *et al.*, 2002). The validity of this grading system remains to be confirmed.

This cleavage stage chapter seeks to illustrate the morphological aspects discussed in the Istanbul consensus workshop on embryo assessment (Alpha Scientists in Reproductive Medicine and ESHRE Special Interest Group of Embryology, 2011). The aim is to introduce a more accurate and widespread comprehension of the nomenclature applied to the characterization of cleavage stage embryos.

A. Cell numbers

The developmental stage of an embryo, defined as the number of blastomeres on Days 1, 2 or 3 after insemination is an essential predictive factor for subsequent implantation and pregnancy rates (1 cell to >10 cells; Figs 211–222). For assessment of embryo cleavage (numbers of blastomeres), the currently accepted observation schedule for optimal cleavage rates was defined at the Istanbul consensus workshop to be: Day 1 (26 ± 1 h post-ICSI, 28 ± 1 h post-IVF), 2-cells; Day 2 (44 ± 1 h), 4-cells and Day 3 (68 ± 1 h), 8-cells (Alpha Scientists in Reproductive Medicine and ESHRE Special Interest Group of Embryology, 2011). Early cleavage (Figs 211 and 212), i.e. the first mitosis occurring before 26 ± 1 h (ICSI) and 28 ± 1 h (IVF) respectively, has been shown to correlate with numbers of good quality embryos, blastocyst development and pregnancy rates (Lundin *et al.*, 2001; Fenwick *et al.*, 2002). A number of studies have shown that the transfer of 4-cell embryos on Day 2 of culture (Fig. 215) results in significantly higher implantation and pregnancy rates compared with the transfer of embryos with either lower (Figs 213 and 214) or higher (Fig. 216) cell numbers (Thurin *et al.*, 2005; Holte *et al.*, 2007; Scott *et al.*, 2007).

Correspondingly, several studies have shown that for Day 3 transfers, implantation and live birth rates are positively correlated with an increase in cell number on Day 3, with the 8-cell stage (having



Figure 211 A zygote undergoing first mitosis which has not been completed by 25 h post-insemination. The mitotic groove can be seen. This embryo should still be assessed as a 1-cell embryo.



Figure 212 The first embryo division nearing completion but the two daughter cells are still not separated. This should be assessed as a 2-cell embryo.

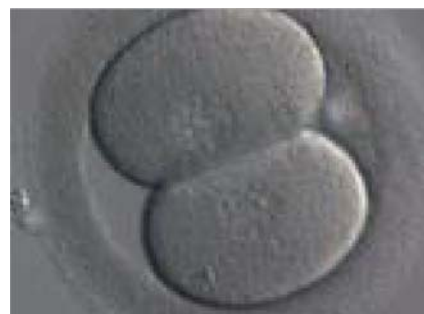


Figure 213 A 2-cell embryo with evenly sized blastomeres each containing one nucleus. Generated by ICSI but was not transferred.

been a 4-cell embryo on Day 2) having the highest rates (van Royen *et al.*, 1999; Racowsky *et al.*, 2011). The cleavage stage of the embryo at the time of transfer also seems to have a role in predicting early pregnancy loss. Hourvitz *et al.* (2006) found that five or



Figure 214 A 3-cell embryo with one larger blastomere and two smaller blastomeres, i.e. it has a stage-specific cell size (see Section C). The embryo was generated by ICSI but was not transferred.



Figure 217 A 6-cell embryo with four small and two larger blastomeres, i.e. it has a stage-specific cell size (see Section C). The embryo was generated by IVF and cryopreserved.



Figure 215 A 4-cell embryo with four evenly sized blastomeres each one containing one nucleus. Generated by ICSI. The embryo was transferred and implanted.



Figure 218 A 7-cell embryo in which four of the blastomeres show a single nucleus. The embryo was generated by ICSI, it was transferred and implanted.



Figure 216 A 5-cell embryo where one cell is slightly out of focus. There is a slight difference in cell size but not significant enough to be called an uneven sized embryo. It was generated by ICSI and cryopreserved.



Figure 219 An 8-cell embryo with evenly sized blastomeres with no visible nuclei. It was generated by ICSI and transferred but the outcome is unknown.

less blastomeres in the best embryo transferred on Day 3 was correlated with early pregnancy loss. A correlation between cell numbers at distinct observation time points and chromosomal errors has also

been reported. It was shown by Munné (2006) that Day 2 embryos with 4 cells had the lowest rate of chromosomal errors, while Magli et al. (2007) showed the same to be true for embryos with 7- to



Figure 220 A cryopreserved 9-cell embryo, warmed on Day 3. One blastomere is slightly larger and one blastomere is slightly smaller than the others. It was generated by ICSI and transferred but failed to implant.



Figure 221 A 10-cell embryo with visible nuclei in some blastomeres. It was generated by ICSI and cryopreserved.



Figure 222 An embryo with more than 10 cells on Day 4. This embryo has not compacted which is unusual at this late stage. Generated by ICSI and cryopreserved.

8 cells on Day 3 (Figs 218 and 219). The same pattern was observed by Finn *et al.* (2010) who described a higher rate of euploidy in embryos with seven to eight blastomeres on Day 3 compared with both six (Fig. 217) or less than six blastomeres and nine (Fig. 220) or more than nine (Figs 221 and 222) blastomeres.

B. Fragmentation

Small portions of cytoplasm enclosed by a cell membrane but usually not containing DNA are often formed during cell division. Fragmentation is therefore defined as the presence of anucleate



Figure 223 Day 2 4-cell embryo with <10% fragmentation and evenly sized blastomeres. It was generated by ICSI but not transferred.



Figure 224 Day 2 4-cell embryo with <10% scattered fragmentation and evenly sized blastomeres. It was generated by IVF but not transferred.



Figure 225 Day 2 4-cell embryo with <10% fragmentation and evenly sized blastomeres. Fragments are concentrated in one area of the perivitelline space (PVS). It was generated by ICSI and transferred but the outcome is unknown.



Figure 226 A 4-cell embryo with 10–15% scattered fragmentation, evenly sized blastomeres and a single nucleus per blastomere. It was generated by ICSI, transferred and implanted.



Figure 229 A 4-cell embryo with 15–20% concentrated fragmentation, evenly sized blastomeres and no visible nuclei. It was generated by ICSI, transferred and implanted.



Figure 227 A 4-cell embryo with 10–15% scattered fragmentation, evenly sized blastomeres and a single nucleus in some blastomeres. It was generated by IVF and cryopreserved.



Figure 230 A 4-cell embryo with 15–20% fragmentation, one of which is a large fragment and the others small and scattered. The blastomeres are evenly sized with no visible nuclei. It was generated by ICSI and cryopreserved.



Figure 228 A 4-cell embryo with 10–20% concentrated fragmentation, evenly sized blastomeres and no visible nuclei. It was generated by IVF, was transferred but failed to implant.



Figure 231 A 4-cell embryo with 15–20% scattered fragmentation, unevenly sized blastomeres and no visible nuclei. It was generated by IVF and cryopreserved.



Figure 232 An 8-cell embryo with around 15–20% scattered fragmentation, evenly sized blastomeres and visible nuclei in some blastomeres. It was generated by IVF but was not transferred.



Figure 234 An 8-cell embryo with 25% scattered fragmentation and evenly sized blastomeres. It was generated by ICSI and transferred but failed to implant.



Figures 233 Three views of the same embryo at different focal planes. It is a 4-cell embryo with 20–25% fragmentation which roughly corresponds to the size of one cell. Note the importance of assessing the embryo at different focal planes in order to establish the degree and type of fragmentation (scattered in this case). The blastomeres are evenly sized and have visible nuclei. It was generated by ICSI and cryopreserved.

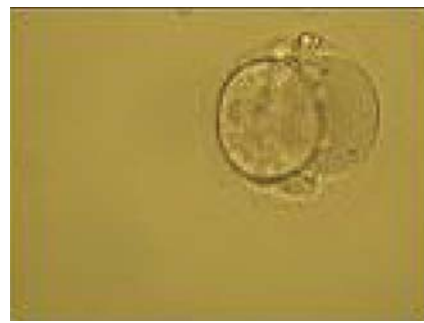


Figure 235 A 2-cell embryo with 20–25% fragmentation on Day 2 (slow development). The blastomeres are evenly sized but binucleated. It was generated by ICSI but was not transferred.



Figure 236 A 7-cell embryo with 30% fragmentation. Fragments are scattered in the PVS. It was generated by ICSI but was not transferred.



Figure 237 A 6-cell embryo with 30–40% fragmentation and unevenly sized blastomeres. Fragments are predominantly concentrated in one area. It was generated by ICSI but was not transferred.



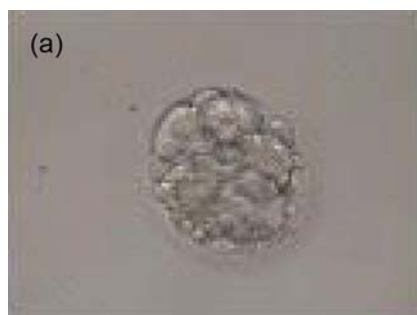
Figure 240 A 3-cell embryo with around 40% scattered fragmentation and unevenly sized blastomeres. It was generated by ICSI but was not transferred.



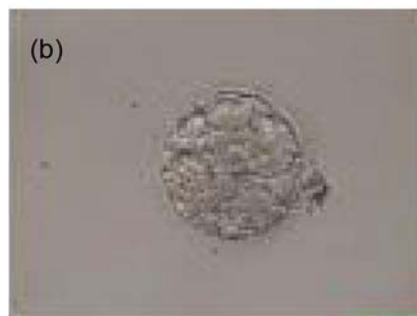
Figure 238 A 6-cell embryo with 30–40% concentrated fragmentation and a thick ZP. It was generated by ICSI but was not transferred.



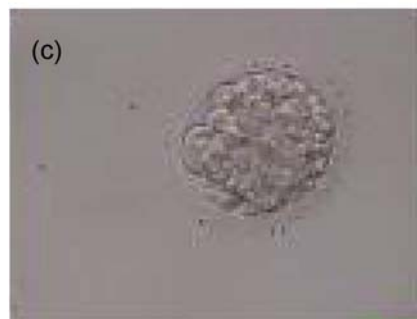
Figure 239 A 4-cell embryo with around 40% fragmentation which is scattered throughout the embryo. The blastomeres are unevenly sized. It was generated by ICSI but was not transferred.



(a)



(b)



(c)

Figures 241 (a–c) Three views of an embryo with >50% fragmentation. In one focal plane (a) three to four cells can be seen but in the other two focal planes only one to two cells can be seen (b and c). The embryo was generated by ICSI but was not transferred.

structures of blastomeric origin (Keltz *et al.*, 2006) and evaluation of the degree of fragmentation is included in almost every embryo scoring system. The degree of fragmentation is most often expressed as the percentage of the total cytoplasmic volume. The relative degree of fragmentation is defined as mild (<10%, Figs 223–225), moderate (10–25%, Figs 226–235) and severe (>25%, Figs 236–242).

It is often difficult to make the distinction between a large anucleate fragment and a small (nucleated) cell. Johansson *et al.* (2003) showed that portions of cytoplasm that were <45 μm in diameter on Day 2 and <40 μm in diameter on Day 3 did not contain DNA, and the authors suggested a standardization of defining fragments as all structures below these sizes.

It has been shown that a high degree of fragmentation correlates negatively with implantation and pregnancy rates (Racowsky *et al.*, 2000), while the presence of minor amounts of fragmentation has no negative or possibly even a positive impact (Alikani *et al.*, 1999). Two distinctly different types of fragmentation have been documented by time-lapse analysis in human embryos: definitive fragmentation, characterized as stable persistent fragments clearly detached from blastomeres and pseudo-fragmentation, characterized by a transient appearance during, or shortly after, cell cleavage, but not detected during later development (Van Blerkom *et al.*, 2001).

Increasing fragmentation also results in reduced blastocyst formation and can influence allocation of cells during differentiation (Hardy *et al.*, 2003). The spatial distribution of the fragments in the perivitelline space (PVS) can be differentiated into two patterns, i.e. scattered (Figs 224, 226, 227, 230–236, 239 and 240) or concentrated (Figs 223, 225, 228, 229, 237 and 238). The scattered appearance was found to be correlated with an increased incidence of chromosomal abnormality (Magli *et al.*, 2007). The higher the degree of fragmentation, the more difficult it is to differentiate between scattered and concentrated fragmentation (Figs 241 and 242). Fragmentation is considered to be an essential parameter to include in the evaluation of developing embryos, as embryos with very strong and persistent fragmentation are less likely to be viable.



Figure 242 A Day 3 embryo with >50% fragmentation. It was generated by IVF but was not transferred.

C. Blastomere size: ‘stage specific’ versus ‘non-stage specific’

It has been shown that a high degree of regularity in the blastomere size in embryos on Day 2 is related to increased pregnancy outcome following assisted reproduction treatments (Giorgetti *et al.*, 1995; Ziebe *et al.*, 1997; Hardarson *et al.*, 2001; Holte *et al.*, 2007). Uneven cleavage, i.e. a cell cleaving into two unequal sized cells, may result in an uneven distribution of cytoplasmic molecules, e.g. proteins and mRNAs, and has been shown to be correlated with a higher incidence of multinucleation and aneuploidy (Hardarson *et al.*, 2001; Magli *et al.*, 2001).

The relative blastomere size in the embryo is dependent on both the cleavage stage and the regularity of each cleavage division (Diagrams 1 and 2). The blastomeres of 2-, 4- and 8-cell embryos should be equal (stage-specific embryos, Figs 243–245) rather than unequal in size (non-stage-specific embryos, Figs 246–252). In contrast, blastomeres of embryos with cell numbers other than 2, 4 and 8 should have different sizes as there is an asynchrony in the division of one or more blastomeres (Figs 253–256). A 3-cell embryo should preferably have one large and two small blastomeres (Fig. 253); a 5-cell embryo, three large and two smaller blastomeres (Fig. 254); a 6-cell embryo, two large and four smaller blastomeres (Fig. 255) and a 7-cell embryo, one large and six smaller blastomeres (Fig. 256). These embryos are thereby also considered to be stage specific. However, a 4-cell embryo with one or two blastomeres much larger than the others (Figs 248–251), a 3-cell embryo with all blastomeres even in size (Fig. 257), a 5-cell embryo with two large and three smaller blastomeres (Figs 258 and 259) or one small and four larger blastomeres (Fig. 260), a 6-cell embryo with all blastomeres even in size (Fig. 261) or extremely

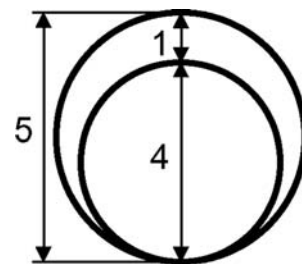


Diagram 1 A diagram illustrating the expected cell size of a cleavage stage embryo: a human 2-cell embryo should contain two equal blastomeres of the size of the 2-cell stage and are thereby stage specific. Unequal blastomeres at the 2-cell stage (>25% difference in the diameter size of the smallest cell, i.e. less than a 1:4 proportion) are not 2-cell stage specific. The same rule can be applied to 4- and 8-cell embryos. The numbers show proportions of diameter size.

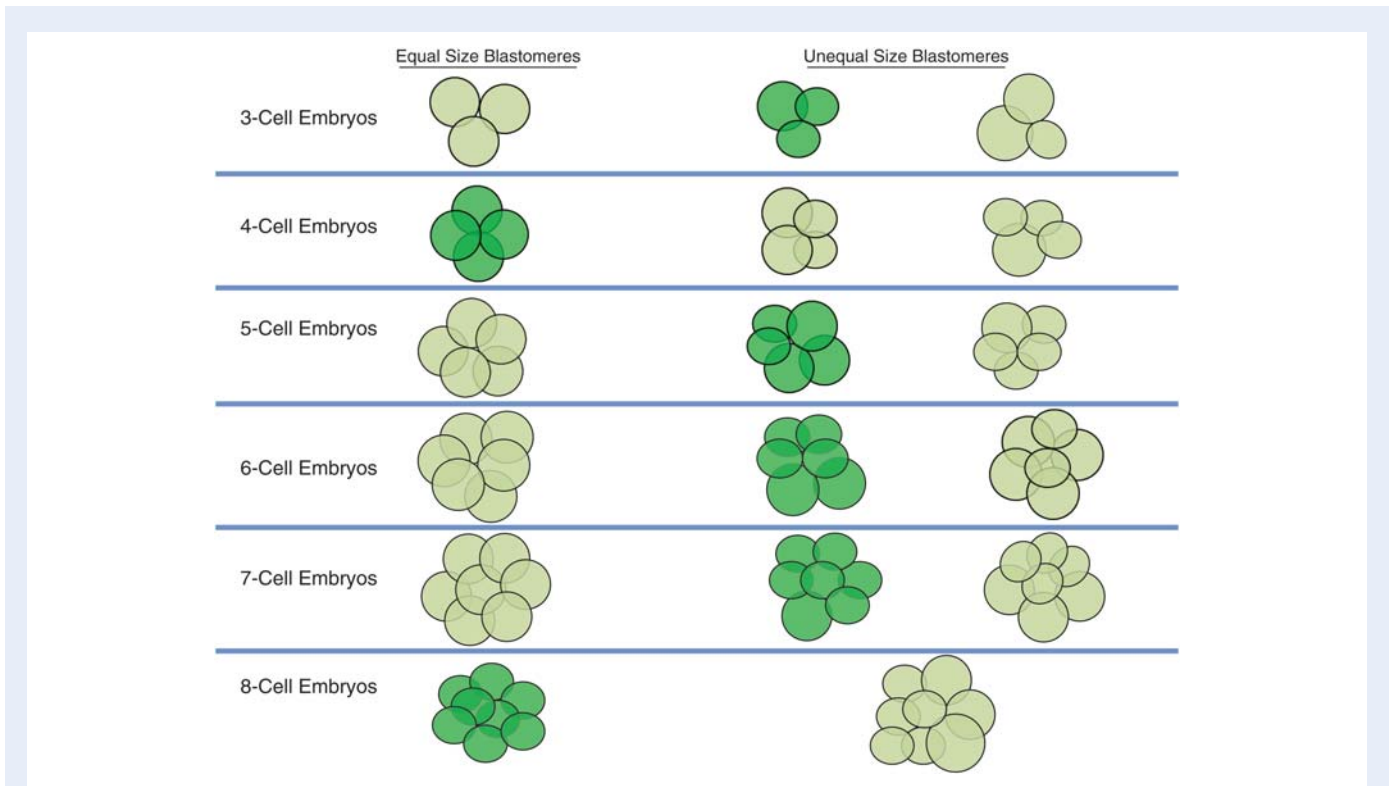


Diagram 2 A diagram illustrating the concept of stage-specific versus non-stage-specific cleavage patterns. The dark green color indicates stage-specific cleavage stage embryos, whereas the light green color indicates non-stage-specific cleavage stage embryos.



Figure 243 A 2-cell embryo with evenly sized blastomeres and no fragmentation on Day 2. The blastomeres are stage-specific cell size. The embryo was transferred but did not result in a pregnancy.



Figure 244 A 4-cell embryo with evenly sized blastomeres and no fragmentation on Day 2. The blastomeres are stage-specific cell size. Notice the clover shape arrangement of the blastomeres. It was transferred and implanted.



Figure 245 An 8-cell embryo with evenly sized blastomeres and no fragmentation on Day 3. The blastomeres are stage-specific cell size. It was transferred and resulted in a pregnancy.



Figure 248 A 4-cell embryo with unevenly sized blastomeres on Day 2, with the cell to the right being 25% smaller than the cell to the left. The blastomeres are therefore not stage-specific cell size. The embryo was transferred and implanted.

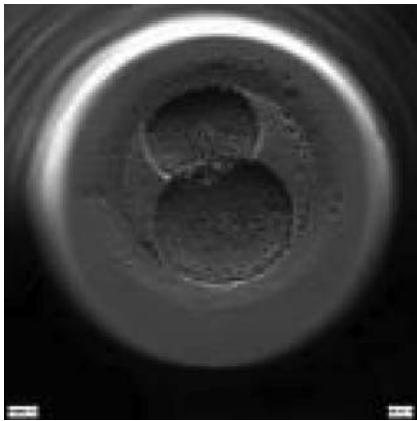


Figure 246 A 2-cell embryo with unevenly sized blastomeres on Day 2. The blastomeres are not stage-specific cell size.



Figure 249 A 4-cell embryo with unevenly sized blastomeres on Day 2. One blastomere is indistinct in this view. The blastomeres are not stage-specific cell size.



Figure 247 A 2-cell embryo with unevenly sized blastomeres and up to 10% fragmentation on Day 2. The blastomeres are not stage-specific cell size.



Figure 250 A 4-cell embryo with unevenly sized and irregular blastomeres with two blastomeres being larger than the other two. The blastomeres are not stage-specific cell size. Note that the ZP of this embryo is elongated.



Figure 251 A 4-cell embryo with unevenly sized blastomeres. The blastomeres are not stage-specific cell size.



Figure 254 A 5-cell embryo with three large and two small blastomeres. The blastomeres are stage-specific cell size.



Figure 252 An 8-cell embryo with unevenly sized blastomeres. The blastomeres are not stage-specific cell size. The embryo was transferred but did not result in a pregnancy.



Figure 255 A 6-cell embryo with two large and four small blastomeres. The blastomeres are stage-specific cell size.



Figure 253 A 3-cell embryo with one large and two small blastomeres on Day 2. The blastomeres are stage-specific cell size. The embryo was transferred but failed to implant.



Figure 256 A 7-cell embryo with one large and six small blastomeres. The blastomeres are stage-specific cell size.



Figure 257 A 3-cell embryo with three blastomeres of the same size at 26 h after insemination. The blastomeres are not stage-specific cell size.



Figure 260 A 5-cell embryo with four large and one small blastomeres instead of three large and two small blastomeres; therefore, not stage-specific cell size.



Figure 258 A 5-cell embryo with two large and three small blastomeres instead of three large and two small blastomeres; therefore, not stage-specific cell size.



Figure 261 A thawed 6-cell embryo with six blastomeres of the same size rather than two large and four smaller blastomeres; therefore, not stage-specific cell size.



Figure 259 A 5-cell embryo with two large and three small blastomeres instead of three large and two small blastomeres therefore not stage-specific cell size.

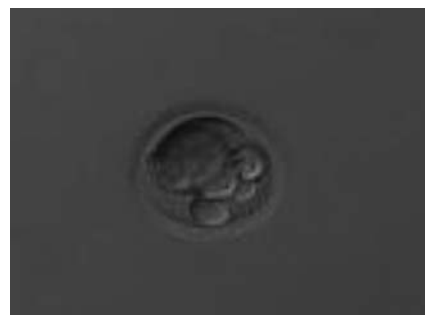


Figure 262 A 6-cell embryo with two very large and four very small blastomeres. The extreme size difference between the large and small blastomeres makes this embryo not stage specific.



Figure 263 A 7-cell embryo with three large and four small blastomeres instead of one large and six small blastomeres; therefore, not stage-specific cell size. One blastomere shows multinucleation.

different in size (Fig. 262) and a 7-cell embryo with three large and four smaller blastomeres (Fig. 263) would not be considered to have normal blastomere sizes in relation to cell numbers and are therefore not considered to be stage specific (for further clarification see Diagrams 1 and 2).

D. Nucleation

The nucleation status is defined as the presence or absence of nuclei in the blastomeres of the cleavage stage embryo. Ideally, the nucleation status of each blastomere in the embryo should be evaluated as a single nucleus per blastomere (Figs 264–266), no nuclei visible or multinucleation (Figs 267–270).

The most studied nucleation status is multinucleation, which is defined as the presence of more than one nucleus in at least one blastomere of the embryo (Jackson et al., 1998; Van Royen et al., 2003). Multinucleation can be evaluated both in the early cleaved Day 1 ($26\text{--}28 \pm 1$ h post-insemination), Day 2 (44 ± 1 h post-insemination) and Day 3 (68 ± 1 h post-insemination) cleavage stage embryos, although the assessment of a Day 3 embryo may be more complicated due to the smaller cell size and the larger number of cells (Van Royen et al., 2003). Embryo quality has been shown to correlate with multinucleation, and 4-cell embryos on Day 2 and 8-cell embryos on Day 3 show reduced multinucleation compared with the other cell stages observed on these days (Van Royen et al., 2003; Ziebe et al., 2003).

Multinucleation is predictive of a decreased implantation potential (Jackson et al., 1998; Pelinck et al., 1998; Van Royen et al., 2003; Moriwaki et al., 2004) and multinucleated embryos are associated with an increased level of chromosome abnormalities (Pickering et al., 1995; Hardarson et al., 2001; Agerholm et al., 2008) as well as an increased risk of spontaneous abortion (Scott et al., 2007). Multinucleation is more frequent in blastomeres originating from embryos with uneven cleavage compared with embryos with evenly cleaved blastomeres (Hardarson et al., 2001).

Multinucleation can also be divided into binucleation (two nuclei per cell, Figs 268 and 269) or multi/micronucleation (more than two nuclei per cell, Fig. 270). These appearances probably have different origins (Meriano et al., 2004). Multinucleated embryos are usually excluded from transfer. However, it has been shown that binucleated



Figure 264 A 4-cell embryo with equally sized, mononucleated blastomeres arranged in a clover shape on Day 2 post-injection. There is a single nucleus clearly visible in each blastomere.



Figure 265 A 4-cell embryo with equally sized, mononucleated blastomeres arranged in a tetrahedron shape on Day 2 post-injection.



Figure 266 A 4-cell embryo with equally sized, mononucleated blastomeres arranged in a tetrahedron shape on Day 2 post-injection. There is a single nucleus clearly visible in each blastomere.

cells on Day 1 can cleave into chromosomally normal cells (Staessen and Van Steirteghem, 1998). On the other hand, severe multinucleation is probably not compatible with normal cell cleavage.

Multinucleation evaluation should be included in any embryo assessment protocol to select the highest quality embryo for transfer, and although these embryos do give rise to live births, they should be

excluded from selection for embryo transfer if an alternative embryo is available.

The absence or presence of a single nucleus per blastomere has been shown to be a predictor of embryo implantation potential (Moriwaki *et al.*, 2004; Saldeen and Sundström, 2005). Visualization of four mononucleated blastomeres in a 4-cell embryo (Figs 265 and 266) predicted a higher implantation rate than in cases where zero (Fig. 266) to



Figure 267 A 4-cell embryo with blastomeres of unequal size and with one binucleated blastomere. The embryo was transferred but failed to implant.



Figure 268 A 4-cell embryo with one binucleated blastomere.



Figure 269 A 2-cell embryo with two binucleated blastomeres and 25–30% fragmentation.



Figure 270 A 2-cell embryo with blastomeres of unequal size with several (four) nuclei in one blastomere.

three mononucleated blastomeres (Fig. 268) were seen (Saldeen and Sundström, 2005). However, other studies have found that grading embryo nuclear score on Day 2 had no additive value for the prediction of implantation rate above that predicted by Day 3 embryo morphology (Bar-Yoseph *et al.*, 2011).

E. Cytoplasmic anomalies

The cytoplasm of cleaving embryos is normally pale, and clear or finely granular in appearance (Hartshorne, 2000). Cytoplasmic anomalies, such as cytoplasmic granularity, cytoplasmic pitting and the presence of vacuoles, occur occasionally and can also be scored in the morphological assessment of Days 2 and 3 embryos. However, a possible predictive value of these features to embryo quality or implantation potential is unclear.

Cytoplasmic pitting (Figs 271 and 272) is characterized by the presence of numerous small pits with an approximate diameter of 1.5 μm on the surface of the cytoplasm (Biggers and Racowsky, 2002). Although cytoplasmic pitting in Day 3 embryos seems to be associated with improved blastocyst formation, the appearance of cytoplasmic granularity has no prognostic value to embryo quality (Rienzi *et al.*, 2003) or to pregnancy (Desai *et al.*, 2000). Other studies have shown that culture conditions may induce cytoplasmic pitting (Biggers and Racowsky, 2002; Ebner *et al.*, 2005b) which in extreme cases may result in an increased risk of early loss of gestational sacs (Ebner *et al.*, 2005b).

The cytoplasm of blastomeres may be excessively darkened with centralized granularity associated with a cortical halo, as cytoplasmic organelles retract toward the center of the blastomere (Fig. 273). It was suggested that these embryos have reduced implantation potential or are destined for degeneration (Veeck, 1999). Similarly, embryos with alternating areas of granularity and clear zones within the blastomeres are even more likely to degenerate (Fig. 274).

Cytoplasmic vacuolization is probably the most common cytoplasmic dysmorphism in human oocytes/embryos. Vacuoles vary in size and in number (Figs 275–280). They are membrane-bound cytoplasmic inclusions filled with fluid that are virtually identical with the perivitelline fluid (Van Blerkom, 1990). Whereas vacuoles have been well studied and described in human oocytes, very little is known about their incidence

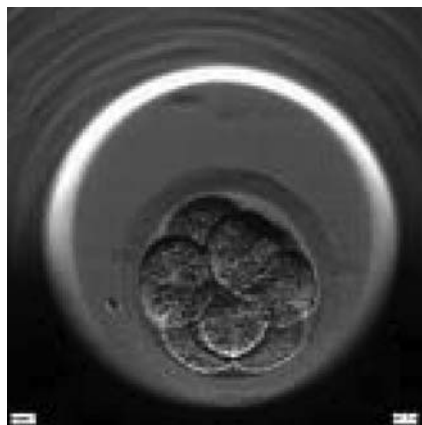


Figure 271 An 8-cell embryo with equally sized blastomeres showing cytoplasmic pitting. Numerous small pits are present on the surface of the cytoplasm.



Figure 272 An 8-cell embryo with equally sized blastomeres showing cytoplasmic pitting. Numerous small pits are homogeneously distributed in the cytoplasm. The 5 blastomeres in focus are arranged in one spatial plane.



Figure 273 A 2-cell embryo with a clear halo in both blastomeres, characterized by centralized granularity associated with an absence of organelles in the peripheral cortex.



Figure 274 A 4-cell embryo on Day 2 with an abnormal distribution of organelles leading to differential granular and smooth zones inside each cell.



Figure 275 An 8-cell embryo with one blastomere showing a small vacuole (arrow).

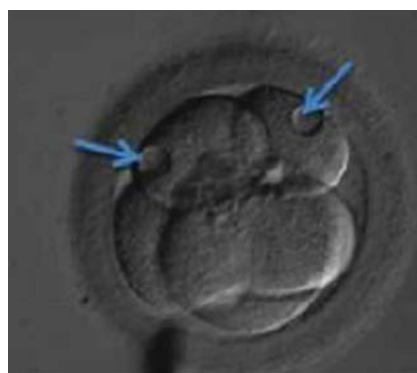


Figure 276 A 5-cell embryo with two small and three large blastomeres. There is a small vacuole in each of the two smaller blastomeres.

and role in developing embryos. Beside vacuoles visible at the time of oocyte collection and those created artificially by ICSI, vacuoles may also arise at the compaction stage (Ebner et al., 2005a). *De novo*



Figure 277 An embryo with abundant small vacuoles.



Figure 278 A 2-cell embryo with large vacuoles in both blastomeres and 15% concentrated fragmentation.



Figure 279 A 3-cell embryo with a large vacuole in the blastomere in the first plane in this view. A smaller vacuole is present in another blastomere. High fragmentation, about 40%, concentrated in one area.

formation of vacuoles on Day 4 is related to developmental arrest with a detrimental effect on blastocyst formation (Ebner *et al.*, 2005a). It is believed that the occurrence of a few, small vacuoles (Figs 275 and

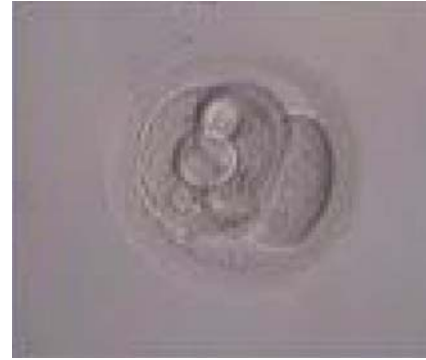


Figure 280 A 3-cell embryo with different sized blastomeres showing both large and small vacuoles.

276) is not of importance (Alpha Scientists in Reproductive Medicine and ESHRE Special Interest Group of Embryology, 2011), but in cases of extensive vacuolization (Figs 277–280) it may be detrimental, mainly to spatial development, and the assessment should be added to the selection score.

F. Spatial distribution of cells

Human oocytes are polarized from their earliest stages of formation and consist of an animal and vegetal pole (Antczak and Van Blerkom, 1997, 1999; Edwards and Beard, 1997). This animal and vegetal gradient is distributed differently to specific 4-cell blastomeres via the combination of meridional and equatorial cleavage divisions (Gulyas, 1975). The first cleavage occurs meridionally and results in two nearly identical daughter blastomeres each inheriting similar polarities of animal and vegetal cytoplasm. In the second cleavage, one cell divides meridionally while the other cell divides equatorially which results in four cells with different polarity (Diagram 3). The two daughter cells resulting from the meridional cleavage have inherited full polarity, while the two daughter cells from the equatorial cleavage differ in polarity with one cell containing mostly animal cytoplasm and the other cell containing mostly vegetal cytoplasm (Gulyas, 1975; Edwards and Hansis, 2005). These cleavages lead to a typical pyramidal or tetrahedral arrangement of three blastomeres with animal cytoplasm associating with the polar body; and one blastomere, inheriting only vegetal cytoplasm, located distant to the polar body (Figs 281 and 282; Edwards and Hansis, 2005). Other ways of meridional or equatorial cleavage divisions may lead to a different distribution of animal and vegetal poles in the daughter cells and may result in non-tetrahedral or 'clover' shaped 4-cell stage embryos (Figs 283–285). The clover shape can be maintained in the following division (Fig. 286).

Another feature sometimes seen is ovoid embryos, originating from ovoid oocytes (Figs 287–290). In these embryos, the spatial distribution of blastomeres is necessarily abnormal.

In summary, the cleavage planes are thought to determine various aspects of later development. Elucidation of the fundamental aspects of the genetic regulation of the cleavage divisions may play an important role in understanding their impact on the developmental capacity and the implantation potential of an embryo *in vitro* (Edwards, 2005).

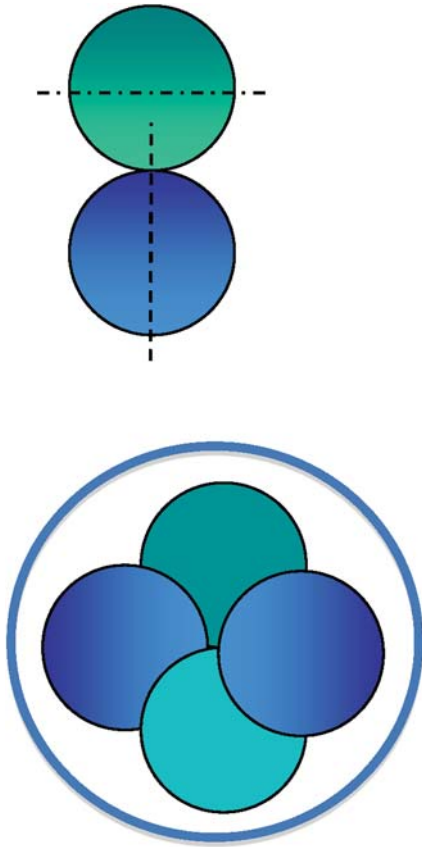


Diagram 3 Diagram showing the dividing planes of the second mitotic cleavage, where one cell cleaves equatorially and one cell cleaves meridionally, giving rise to four daughter cells with different polarity.

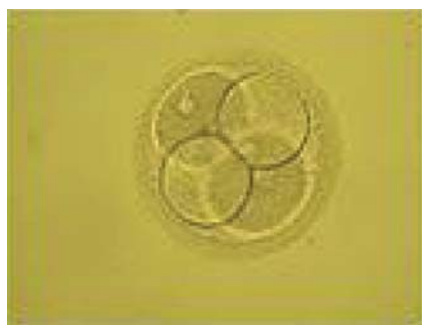


Figure 281 A 4-cell embryo with a typical pyramidal or tetrahedral structure. The embryo was generated by IVF and was transferred and implanted.



Figure 282 A 4-cell embryo with a typical pyramidal or tetrahedral structure. The embryo was generated by IVF and was transferred but failed to implant.



Figure 283 A 4-cell embryo with a non-tetrahedral or clover structure. It was generated by ICSI and was cryopreserved.

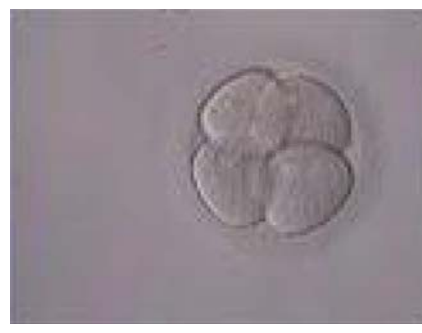


Figure 284 A 4-cell embryo generated by ICSI with a non-tetrahedral or clover structure. It was transferred but failed to implant.



Figure 285 A clover-shaped 4-cell embryo with an expanded ZP. The relative size of the blastomeres with respect to the ZP is smaller than usual in this embryo.



Figure 288 A 7-cell, ovoid embryo showing blastomeres predominantly arranged in the one spatial plane. The ZP is septate.



Figure 286 A double clover-shaped 8-cell embryo. The clover shape of the 4-cell embryo was maintained in the subsequent division.



Figure 289 An ovoid embryo showing eight blastomeres arranged in one spatial plane.



Figure 287 An ovoid embryo showing four blastomeres arranged in a clover shape.



Figure 290 An ovoid embryo showing seven blastomeres arranged in one spatial plane. The ZP has an irregular shape.

G. Compaction

The human embryo appears as an indistinguishable mass of cells on Day 4 of development, the morula. A good quality morula is

composed of 16–32 blastomeres and all of the blastomeres should be included in the compaction process (Tao et al., 2002).

The increase in cell-to-cell adherence should begin at the 8-cell stage and then progress rapidly with time (Figs 291–293). The cell ad-



Figure 291 An 8-cell embryo that shows no signs of compaction. Cells are evenly sized and barely touching.



Figure 294 A clover shaped 4-cell embryo showing signs of very early compaction. A single nucleus is clearly visible in each cell.



Figure 292 An 8-cell embryo showing signs of initial compaction. The cells are tightening their contact.

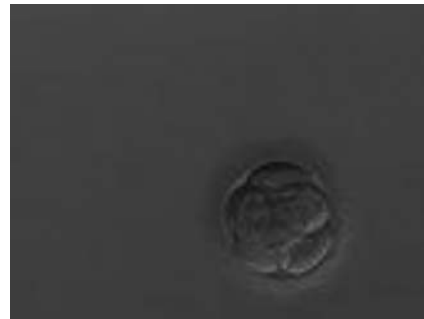


Figure 295 A 7-cell embryo showing signs of early compaction. This embryo was transferred but failed to implant.



Figure 293 An 8-cell embryo showing signs of moderate compaction. Individual blastomeres are becoming difficult to identify.



Figure 296 An embryo with more than 12 blastomeres showing no signs of compaction. With this number of cells it is very unusual that the embryo has not yet initiated compaction.



Figure 297 A morula of good quality. All blastomeres have been included in the compaction process and individual cells are no longer evident.



Figure 298 A fair quality morula. Some cell boundaries are still visible and a few small cells (or fragments) are not completely incorporated into the compaction process.



Figure 299 A fair quality morula. Cell boundaries are still visible and an occasional cell is not completely incorporated into the compaction process.



Figure 300 A poor quality morula with several cells and fragments excluded from the main mass of compacted cells.

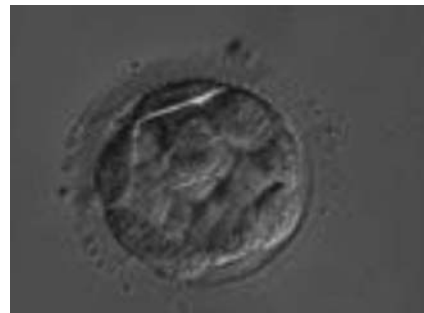


Figure 301 Embryo showing early cavitation with an initial blastocoele cavity beginning to appear.



Figure 302 Embryo showing early cavitation. An initial blastocoele cavity is beginning to appear. The ZP is broken after blastomere biopsy.

hesion protein E-cadherin changes in distribution from the cytoplasm to the cell membrane. Cell junctions between cells, in particular tight junctions, begin to spread (Alikani, 2005). This process has been linked to activation of the embryonic genome (Desai *et al.*, 2000) and is

therefore considered to be a good sign of the developmental capacity of the embryo. Culture media composition and other environmental conditions can also play a role in the kinetics of an early compaction event.

Compaction can be observed in embryos before the 8-cell stage (Figs 294 and 295), while embryos with more than 10 blastomeres that do not show signs of compaction are uncommon (Fig. 296). A study by Skiadas *et al.* (2006) showed that early compacted embryos had an increased implantation potential; however, this was only true for good quality embryos (<10% fragmentation).

The Istanbul consensus has established that for a Day 4 embryo to be considered of good quality, all cells must be included in the morula (Fig. 297), while those embryos in which some cells or fragments are excluded from the compaction process (Figs 298–300) have a decreased probability of implantation.

The outer cells of compacted embryos have probably lost their totipotency as they are bound to form the trophectoderm (Cauffman *et al.*, 2009). The next phase of development is the beginning of cavitation that leads to the formation of the blastocyst (Figs 301 and 302).

References

- Alikani M. Epithelial cadherin distribution in abnormal human pre-implantation embryos. *Hum Reprod* 2005;**20**:3369–3375.
- Alikani M, Cohen J, Tomkin G, Garrisi GJ, Mack C, Scott RT. Human embryo fragmentation *in vitro* and its implications for pregnancy and implantation. *Fertil Steril* 1999;**71**:836–842.
- Alikani M, Calderon G, Tomkin G, Garrisi J, Kokot M, Cohen J. Cleavage anomalies in early human embryos and survival after prolonged culture *in-vitro*. *Hum Reprod* 2000;**15**:2634–2643.
- Agerholm IE, Hnida C, Crüger DG, Berg C, Bruun-Petersen G, Kølvrå S, Ziebe S. Nuclei size in relation to nuclear status and aneuploidy rate for 13 chromosomes in donated four cells embryos. *J Assist Reprod Genet* 2008;**25**:95–102.
- Alpha Scientists in Reproductive medicine and ESHRE Special Interest Group of Embryology. The Istanbul consensus workshop on embryo assessment: proceedings of an expert meeting. *Hum Reprod* 2011;**26**:1270–1283.
- Antczak M, Van Blerkom J. Oocyte influence on early development: the regulatory proteins leptin and STAT 3 are polarized in mouse and human oocytes and differentially distributed within the cells of the preimplantation stage embryo. *Mol Hum Reprod* 1997;**3**:1067–1086.
- Antczak M, Van Blerkom J. Temporal and spatial aspects of fragmentation in early human embryos: possible effects on developmental competence and association with the differential elimination of regulatory proteins from polarized domains. *Hum Reprod* 1999;**14**:429–447.
- Baczkowski T, Kurzawa R, Głabowski W. Methods of embryo scoring in *in vitro* fertilization. *Reprod Biol* 2004;**4**:5–22.
- Bar-Yoseph H, Levy A, Sonin Y, Alboteanu S, Livitas E, Lunenfeld E, Har-Vardi I. Morphological embryo assessment: reevaluation. *Fertil Steril* 2011;**95**:1624–1628.
- Biggers JD, Racowksy C. The development of fertilized human ova to the blastocyst stage in KSOM^{AA} medium: is a two-step protocol necessary? *Reprod Biomed Online* 2002;**5**:133–140.
- Cauffman G, De Rycke M, Sermon K, Liebaers I, Van de Velde H. Markers that define stemness in ESC are unable to identify the totipotent cells in human preimplantation embryos. *Hum Reprod* 2009;**24**:63–70.
- De Placido G, Wilding M, Strina I, Alviggi E, Alviggi C, Mollo A, Varicchio M.T, Tolino A, Schiattarella C, Dale B. High outcome predictability after IVF using a combined score for zygote and embryo morphology and growth rate. *Hum Reprod* 2002;**17**:2402–2409.
- Desai NN, Goldstein J, Rowland DY, Goldfarb JM. Morphological evaluation of human embryos and derivation of an embryo quality scoring system specific for day 3 embryos: a preliminary study. *Hum Reprod* 2000;**15**:2190–2196.
- Ebner T, Yaman C, Moser M, Sommergruber M, Polz W, Tews G. Embryo fragmentation *in vitro* and its impact on treatment and pregnancy outcome. *Fertil Steril* 2001;**76**:281–285.
- Ebner T, Moser M, Sommergruber M, Tews G. Selection based on morphological assessment of oocytes and embryos at different stages of preimplantation development: a review. *Hum Reprod Update* 2003;**9**:251–262.
- Ebner T, Moser M, Sommergruber M, Gaiswinkler U, Shebl O, Jesacher K, Tews G. Occurrence and developmental consequences of vacuoles throughout preimplantation development. *Fertil Steril* 2005a;**83**:1635–1640.
- Ebner T, Tews G, Sommergruber M, Moser M. Cytoplasmic pitting has a negative influence on implantation outcome. *J Assist Reprod Genet* 2005b;**22**:239–244.
- Edwards RG. Genetics of polarity in mammalian embryos. *Reprod Biomed Online* 2005;**11**:104–114.
- Edwards RG, Beard HK. Oocyte polarity and cell determination in early mammalian embryos. *Mol Hum Reprod* 1997;**3**:863–905.
- Edwards RG, Hansas C. Initial differentiation of blastomeres in 4-cell human embryos and its significance for early embryogenesis and implantation. *Reprod Biomed Online* 2005;**11**:206–218.
- Edwards RG, Steptoe PC, Purdy JM. Establishing full-term human pregnancies using cleaving embryos grown *in vitro*. *Br J Obstet Gynaecol* 1980;**87**:737–756.
- Fenwick J, Platteau P, Murdoch AP, Herbert M. Time from insemination to first cleavage predicts developmental competence of human preimplantation embryos *in vitro*. *Hum Reprod* 2002;**17**:407–412.
- Finn A, Scott L, O'leary T, Davies D, Hill J. Sequential embryo scoring as a predictor of aneuploidy in poor-prognosis patients. *Reprod Biomed Online* 2010;**21**:381–390.
- Fisch JD, Rodriguez H, Ross R, Overby G, Sher G. The Graduated Embryo Score (GES) predicts blastocyst formation and pregnancy rate from cleavage-stage embryos. *Hum Reprod* 2001;**16**:1970–1975.
- Giorgetti C, Terriou P, Auquier P, Hans E, Spach JL, Salzmann J, Roulier R. Embryo score to predict implantation after *in-vitro* fertilization: based on 957 single embryo transfers. *Hum Reprod* 1995;**10**:2427–2431.
- Gulyas BJ. A reexamination of cleavage patterns in eutherian mammalian eggs: rotation of blastomere pairs during second cleavage of the rabbit. *J Exp Zool* 1975;**193**:235–248.
- Hardarson T, Hanson C, Sjögren A, Lundin K. Human embryos with unevenly sized blastomeres have lower pregnancy and implantation rates: indications for aneuploidy and multinucleation. *Hum Reprod* 2001;**16**:313–318.
- Hardy K, Stark J, Winston RML. Maintenance of the inner cell mass in human blastocysts from fragmented embryos. *Biol Reprod* 2003;**68**:1165–1169.
- Hartshorne F. The embryo. *Hum Reprod* 2000;**15**:31–41.
- Hnida C, Engenheiro E, Ziebe S. Computer-controlled, multilevel, morphometric analysis of blastomere size as biomarker of fragmentation and multinuclearity in human embryos. *Hum Reprod* 2004;**19**:288–293.
- Holte J, Berglund L, Milton K, Garello C, Gennarelli G, Revelli A, Bergh T. Construction of an evidence-based integrated morphology cleavage embryo score for implantation potential of embryos scored and transferred on day 2 after oocyte retrieval. *Hum Reprod* 2007;**22**:548–557.
- Hourvitz A, Lerner-Geva L, Elizur SE, Baum M, Levron J, David B, Meirou D, Yaron R, Dor J. Role of embryo quality in predicting early

- pregnancy loss following assisted reproductive technology. *Reprod Biomed Online* 2006;**13**:504–509.
- Jackson KV, Ginsburg ES, Hornstein MD, Rein MS, Clarke RN. Multinucleation in normally fertilized embryos is associated with an accelerated ovulation induction response and lower implantation and pregnancy rates in *in vitro* fertilization-embryo transfer cycles. *Fertil Steril* 1998;**70**:60–66.
- Johansson M, Hardarson T, Lundin K. There is a cut off limit in diameter between a blastomere and a small anucleate fragment. *J Assist Reprod Genet* 2003;**20**:309–313.
- Keltz MD, Shorupski JC, Bradlye K, Stein D. Predictors of embryo fragmentation and outcome after fragment removal in *in vitro* fertilization. *Fertil Steril* 2006;**86**:321–324.
- Kirkegaard K, Agerholm I, Ingerslev HJ. Time-lapse monitoring as a tool for clinical embryo assessment. *Hum Reprod* 2012;**27**:1277–1285.
- Kligman I, Benadiva C, Alikani M, Munne S. The presence of multinucleated blastomeres in human embryos is correlated with chromosomal abnormalities. *Hum Reprod* 1996;**11**:1492–1498.
- Leese HJ. Quiet please, do not disturb: a hypothesis of embryo metabolism and viability. *Bioessays* 2002;**24**:845–849.
- Lemmen JG, Agerholm I, Ziebe S. Kinetic markers of human embryo quality using time-lapse recordings of IVF/ICSI-fertilized oocytes. *Reprod Biomed Online* 2008;**17**:385–391.
- Lundin K, Bergh C, Hardarson T. Early embryo cleavage is a strong indicator of embryo quality in human IVF. *Hum Reprod* 2001;**16**:2652–2657.
- Magli MC, Gianaroli L, Ferraretti AP. Chromosomal abnormalities in embryos. *Mol Cell Endocrinol* 2001;**183**:29–34.
- Magli MC, Gianaroli L, Ferraretti AP, Lappi M, Ruberti A, Farfalli V. Embryo morphology and development are dependent on the chromosomal complement. *Fertil Steril* 2007;**87**:534–540.
- Meriano J, Clark C, Cadesky K, Laskin CA. Binucleated and multinucleated blastomeres in embryos derived from human assisted reproduction cycles. *Reprod BioMed Online* 2004;**9**:511–520.
- Meseguer M, Herrero J, Tejera A, Hilligsoe KM, Ramsing NB, Remohi J. The use of morphokinetics as a predictor of embryo implantation. *Hum Reprod* 2011;**26**:2658–2671.
- Moriwaki T, Suganuma N, Hayakawa M, Hibi H, Katsumata Y, Oguchi H, Furuhashi M. Embryo evaluation by analysing blastomere nuclei. *Hum Reprod* 2004;**19**:152–156.
- Munné S. Chromosome abnormalities and their relationship to morphology and development of human embryos. *Reprod Biomed Online* 2006;**12**:234–253.
- Pelinc M, De Vos M, Dekens M, Van der Elst J, De Sutter P, Dhont M. Embryos cultured *in vitro* with multinucleated blastomeres have poor implantation potential in human *in-vitro* fertilization and intracytoplasmic sperm injection. *Hum Reprod* 1998;**13**:960–963.
- Pickering SJ, Taylor A, Johnson MH, Braude PR. Diagnosing and preventing inherited disease: an analysis of multinucleated blastomere formation in human embryos. *Hum Reprod* 1995;**10**:1912–1922.
- Racowsky C, Jackson KV, Cekleniak NA, Fox JH, Hornstein MD, Ginsburg ES. The number of eight-cell embryos is a key determinant for selecting day 3 or day 5 transfer. *Fertil Steril* 2000;**73**:558–564.
- Racowsky C, Stern JE, Gibbons WE, Behr B, Pomeroy KO, Biggers JD. National collection of embryo morphology data into Society for Assisted Reproductive Technology Clinic Outcomes Reporting System: associations among day 3 cell number, fragmentation and blastomere asymmetry, and live birth rate. *Fertil Steril* 2011;**95**:1985–1989.
- Rienzi L, Ubaldi F, Minasi MG, Iacobelli M, Martinez F, Tesarik J, Greco E. Blastomere cytoplasmic granularity is unrelated to developmental potential of day 3 human embryos. *J Assist Reprod Genet* 2003;**20**:314–317.
- Rienzi L, Ubaldi F, Iacobelli M, Romano S, Minasi M, Ferrero S, Sapienza F, Baroni E, Greco E. Significance of morphological attributes of the early embryo. *Reprod Biomed Online* 2005;**10**:669–681.
- Saldeen P, Sundström P. Nuclear status of four cell preembryos predicts implantation potential in IVF treatment cycles. *Fertil Steril* 2005;**84**:584–589.
- Scott L, Finn A, O'Leary T, McLellan S, Hill J. Morphologic parameters of early cleavage-stage embryos that correlate with fetal development and delivery: prospective and applied data for increased pregnancy rates. *Hum Reprod* 2007;**22**:230–240.
- Skiadas CC, Jackson KV, Racowsky C. Early compaction on day 3 may be associated with increased implantation potential. *Fertil Steril* 2006;**86**:1386–1391.
- Staessen C, Van Steirteghem A. The genetic constitution of multinuclear blastomeres and their derivative daughter blastomeres. *Hum Reprod* 1998;**13**:1625–1631.
- Tao J, Tamis R, Fink K, Williams B, Nelson-White T, Craig R. The neglected morula/compact stage embryo transfer. *Hum Reprod* 2002;**17**:1513–1528.
- Thurin A, Hardarson T, Hausken J, Jablonowska B, Lundin K, Pinborg A, Bergh C. Predictors of ongoing implantation in IVF in a good prognosis group of patients. *Hum Reprod* 2005;**20**:1876–1880.
- Torelló MJ, Ardoy M, Calderón G, Cuadros J, Herrero R, Moreno JM, Ortiz A, Prados F, Rodríguez L, Ten J. *Criterios ASEBIR de valoración morfológica de Oocitos, Embriones tempranos y Blastocistos*. ASEBIR Congress, Zaragoza, 2005.
- Van Blerkom J. Occurrence and developmental consequences of aberrant cellular organization in meiotically mature human oocytes after exogenous ovarian hyperstimulation. *J Electron Microsc Techn* 1990;**16**:324–346.
- Van Blerkom J, Davis P, Alexander S. A microscopic and biochemical study of fragmentation phenotypes in stage-appropriate human embryos. *Hum Reprod* 2001;**16**:719–729.
- Van Royen E, Mangelschots K, De Neubourg D, Valkenburg M, Van de Meerssche M, Ryckaert G, Eestermans W, Gerris J. Characterization of a top quality embryo, a step towards single-embryo transfer. *Hum Reprod* 1999;**14**:2345–2349.
- Van Royen E, Mangelschots K, De Neubourg D, Laureys I, Ryckaert G, Gerris J. Calculating the implantation potential of day 3 embryos in women younger than 38 years of age: a new model. *Hum Reprod* 2001;**16**:326–332.
- Van Royen E, Mangelschots K, Vercruyssen M, De Neubourg D, Valkenburg M, Ryckaert G, Gerris J. Multinucleation in cleavage stage embryos. *Hum Reprod* 2003;**18**:1062–1069.
- Vecek LL. Preembryo grading and degree of cytoplasmic fragmentation. In: *An Atlas of Human Gametes and Conceptuses: An Illustrated Reference for Assisted Reproductive Technology*. New York, USA: Parthenon Publishing, 1999, 46–51.
- Wong CC, Loewke KE, Bossert NL, Behr B, De Jonge CJ, Baer TM, Reijo Pera RA. Non-invasive imaging of human embryos before embryonic genome activation predicts development to the blastocyst stage. *Nat Biotechnol* 2010;**28**:1115–1121.
- Ziebe S, Petersen K, Lindenberg S, Andersen AG, Gabrielsen A, Andersen AN. Embryo morphology or cleavage stage: how to select the best embryos for transfer after *in-vitro* fertilization. *Hum Reprod* 1997;**12**:1545–1549.
- Ziebe S, Lundin K, Loft A, Bergh C, Nyboe Andersen A, Selleskog U, Nielsen D, Grøndahl C, Kim H, Arce JC, for the CEMAS II and III Study Group. FISH analysis for chromosomes 13, 16, 18, 21, 22, X and Y in all blastomeres of IVF pre-embryos from 144 randomly selected donated human oocytes and impact on pre-embryo morphology. *Hum Reprod* 2003;**18**:2575–2581.

The blastocyst

Thorir Hardarson, Lisbet Van Landuyt, and Gayle Jones

Contents

Introduction

- A. Degree of expansion
- B. ICM morphology
- C. TE morphology
- D. Cellular degeneration in blastocysts
- E. Cytoplasmic strings/bridges between ICM and TE
- F. Other morphological features
 - F.1 Vacuoles/vacuolation
 - F.2 More than one point of natural hatching

Introduction

Despite the fact that the first IVF pregnancy ever reported was from a blastocyst (Edwards and Brody, 1995), the transfer of cleavage stage embryos has dominated IVF for decades. This was mainly due to difficulties in successfully culturing embryos to the blastocyst stage as the culture media used were not complex and did not completely support normal development. In the early 1990s, knowledge of the metabolic requirements of the developing embryo increased and both co-culture techniques and sequential media were introduced. This dramatically increased the proportion of embryos developing to the blastocyst stage and therefore the application of blastocyst transfer in clinical IVF. The main objective of blastocyst culture was to increase the success rate of IVF because of better embryo selection after genomic activation and/or better endometrial synchronicity. Blastocyst culture has also been used as a tool to select the most viable embryos in a cohort with a consequent reduction in the number of embryos transferred and the corresponding reduction in the incidence of multiple gestations.

As the popularity of blastocyst culture increased, so did the need for a morphological scoring system. The blastocyst grading system introduced by Gardner and Schoolcraft in 1999 was quickly adopted by the majority of IVF laboratories. Although the system does not cover all aspects of blastocyst morphology, especially aberrant morphology, it has been very useful in classifying the degree of blastocyst expansion as well as the morphological appearance of the inner cell mass (ICM) and the trophoblast (TE) cells. The Istanbul consensus document (Alpha Scientists in Reproductive Medicine and ESHRE Special Interest Group of Embryology, 2011) is mainly based on the Gardner and Schoolcraft system with some exceptions. The Gardner and Schoolcraft scoring system was an early attempt to describe blastocyst quality. The degree of expansion (i.e. Grades 1–6)

was thought to reflect both the number of cells present and the blastocyst's ability to form a cohesive barrier of cells (TE) through tight junctions which enables the blastocyst to utilize energy to regulate their osmotic environment. This morphological differentiation was thought to represent the developmental capability of the blastocyst. As the blastocyst expanded, a more detailed morphological 'picture' could be obtained allowing for distinction between the ICM and TE cells (i.e. Grades 3–6). According to the grading system, the ICM and the TE cells could be assigned three grades depending on the number of cells present and the cohesiveness of the cell populations.

The blastocyst grading in this Atlas is based on the Gardner and Schoolcraft system with only minor changes using numerical grades for ICM and TE instead of letters, enabling mathematical computations, e.g. mean values. However, their system did not include a number of important morphological parameters often observed in the IVF laboratory. Albeit of unknown importance, some of these parameters were briefly introduced in the Istanbul consensus document, i.e. the formation of cytoplasmic strings often linking together different cells and cell types. Cellular and/or non-cellular structures within the perivitelline space (PVS) and/or the blastocyst cavity have also been described. In addition to these parameters we have also included additional morphological features commonly seen when observing human blastocysts as described further in the following text and sub-headings.

A. Degree of expansion

A defining moment in embryonic development is when fluid starts to accumulate between cells at the morulae stage of development. As the fluid's volume increases, a cavity appears gradually forming the blastocoel. This normally happens between Days 4 and 5 in human embryos *in vitro* and marks a new 'era' in the embryo's life, the blastocyst stage. As the fluid inside the newly formed blastocyst increases, so does the number of cells, and the combination of these two features causes a progressive enlargement of the blastocyst and its cavity with a consequent progressive thinning of the zona pellucida (ZP). Finally, the blastocyst breaks free of the ZP through a process called hatching. The number of cells that comprise a blastocyst can vary considerably as shown in one study to range between 24 and 322 cells (Hardarson *et al.*, 2003), which is often reflected in the blastocyst's morphology. The physiological events that underlie this transformation of a 'cellular mass' at the compaction stage to a highly structured blastocyst are not fully understood. However, cells that either by chance or fate are located in the outer part of the embryo start to flatten out, making contact with neighboring cells through tight junctions. In this way a

barrier is created between the outside and the inside of the embryo, a prerequisite for blastocyst formation. Blastocyst formation is initiated through an initial secretion between the morula cells and this small cavity is then maintained and increased by actions of the membrane channels Na/K-ATPase that raise the salt concentration within the embryo, attracting water through osmosis (Watson *et al.*, 2004). This increased water pressure gradually increases the size of the cavity which continues throughout the blastocyst stages.

The Istanbul consensus document (Alpha Scientists in Reproductive Medicine and ESHRE Special Interest Group of Embryology, 2011) uses a simplified system of only four groups combining the first two and the last two groups of the Gardner and Schoolcraft (1999) grading system into two single groups which may be a limitation for the possibility to assess blastocysts. In this Atlas we have adopted the grading system that divides the grade of expansion into six categories and the ICM (Section B) and TE cell (Section C) grading into three categories similar to Gardner and Schoolcraft (1999) but have used the numerical scoring system suggested by the Istanbul consensus document: Grade 1 blastocysts are those in which the blastocoel cavity is less than half of the volume of the embryo (Figs 303–308); Grade 2 blastocysts are those in which the blastocoel cavity is half,

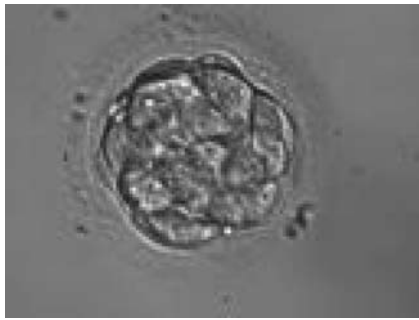


Figure 303 A very early blastocyst with a small cavity appearing centrally. The blastocyst was transferred but the outcome is unknown.



Figure 304 An early blastocyst with a cavity occupying <50% of the volume of the embryo. Note the early formation of the outer TE cells that are beginning to be flattened against the zona pellucida (ZP). The blastocyst was transferred and resulted in an ectopic pregnancy.



Figure 305 A very early blastocyst with a small cavity appearing centrally and can be seen most obviously at the 12 o'clock position in this view. Note the cellular debris that is not incorporated into the early blastocyst formation that has been sequestered to the peritelline space (PVS).



Figure 306 An early blastocyst with a cavity occupying <50% of the volume of the embryo. Note the flattened squamous-like trophoblast (TE) cells lining the left half of the cavity in this view. The blastocyst was transferred but failed to implant.



Figure 307 An early blastocyst with a cavity occupying almost 50% of the volume of the embryo. Note the large flattened TE cells lining the initial blastocoel cavity and the single spermatozoon embedded in the ZP at the 11 o'clock position in this view. The blastocyst was transferred but the outcome is unknown.

or more than half, of the volume of the embryo (Figs 309–314); Grade 3 blastocysts are those in which the blastocoel cavity completely fills the embryo (Figs 315–320); Grade 4 blastocysts in which the



Figure 308 An early blastocyst with a cavity beginning to be formed centrally. Note the early formation of the flattened TE cells which at this stage are large, with two cells stretching to line the cavity from the 9 o'clock to the 3 o'clock position in this view. The blastocyst was transferred but failed to implant.



Figure 309 An early blastocyst with the cavity clearly visible and occupying half the volume of the embryo. The blastocyst was transferred but the outcome is unknown.



Figure 310 An early blastocyst with the cavity occupying >50% of the volume of the embryo. The overall volume of the blastocyst remains unchanged with no thinning of the ZP. The large cellular debris does not take part in the blastocyst formation.

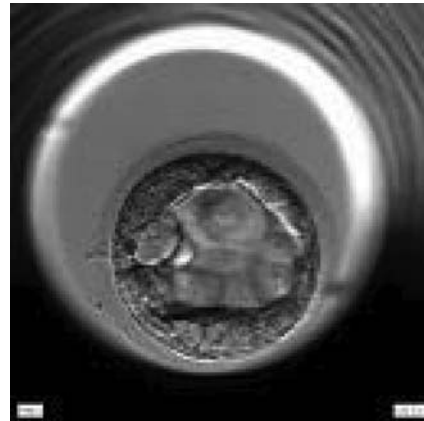


Figure 311 An early blastocyst with the cavity occupying >50% of the volume of the embryo. The TE cells are very large at this stage.



Figure 312 An early blastocyst with the cavity occupying >50% of the volume of the embryo. The overall volume of the blastocyst remains unchanged with no thinning of the ZP. The early ICM can be seen on the left half of the blastocyst in this view. The blastocyst was transferred and implanted.



Figure 313 An early blastocyst with the cavity occupying >50% of the volume of the embryo. The overall volume of the blastocyst remains unchanged with no thinning of the ZP. The early ICM can be seen at the base of the blastocyst in this view. The blastocyst was transferred but failed to implant.



Figure 314 An early blastocyst with the cavity occupying $>50\%$ of the volume of the embryo. The overall volume of the blastocyst remains unchanged with no thinning of the ZP. The early ICM can be seen at the 12 o'clock position in this view. The blastocyst was transferred and resulted in a biochemical pregnancy.



Figure 315 Blastocyst (Grade 3:2:1) showing a cavity occupying the total volume of the embryo. The ICM can be seen at the 3 o'clock position in this view and is loosely made up of only a few cells. The blastocyst was transferred but the outcome is unknown.



Figure 316 Blastocyst (Grade 3:1:1) showing a very large, mushroom-shaped ICM at the 10 o'clock position in this view. The ICM is made up of many cells that are tightly compacted. The blastocyst was transferred and resulted in the delivery of a healthy girl.



Figure 317 Blastocyst (Grade 3:1:1) showing a compact ICM at the base of the blastocyst in this view. The blastocyst was transferred and resulted in the delivery of a healthy boy.

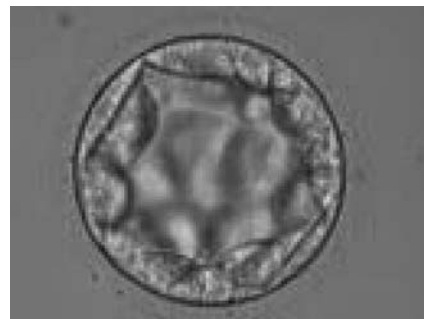


Figure 318 Blastocyst (Grade 3:3:2) with no clearly identifiable ICM and TE cells that in places are quite large and stretch over great distances to reach the next cell.



Figure 319 Blastocyst (Grade 3:1:1) with a dense ICM clearly visible at the 10 o'clock position in this view. The TE cells are variable in size but form a cohesive epithelium. The blastocyst was transferred but the outcome is unknown.

blastocyst cavity is now greater than the original volume of the embryo and the ZP is thinned (Figs 321–326); Grade 5 blastocysts or hatching blastocysts in which the blastocoel cavity is greater than the original volume of the embryo and the TE is herniating through a natural



Figure 320 Blastocyst (Grade 3:1:1) with a dense, almost triangular, ICM clearly visible at the base of the blastocyst in this view. The blastocyst was transferred but failed to implant.



Figure 323 Expanded blastocyst (Grade 4:1:1) showing a large ICM at the base of the blastocyst in this view. The ICM is made up of many cells that are tightly compacted. The blastocyst volume is now larger than the original volume of the embryo causing the ZP to thin. The blastocyst was transferred but the outcome is unknown.



Figure 321 Good quality expanded blastocyst (Grade 4:1:1) with a large mushroom-shaped ICM. The blastocyst is now a greater volume than the original volume of the embryo and the ZP is thinned. There appears to be cytoplasmic strings extending from the ICM to the TE. The blastocyst was transferred and implanted.



Figure 324 Expanded blastocyst (Grade 4:1:1) showing a large ICM at the 4 o'clock position in this view. The ICM is made up of many cells and is very compact. The blastocoel cavity is now larger than the original volume of the embryo and the ZP is very thin. The blastocyst was transferred but the outcome is unknown.



Figure 322 Expanded blastocyst (Grade 4:1:1) with an ICM clearly visible at the 4 o'clock position in this view. There are very many evenly sized cells making up a cohesive TE that surround the enlarged blastocoel cavity. The ZP is very thin. The blastocyst was transferred but the outcome is unknown.

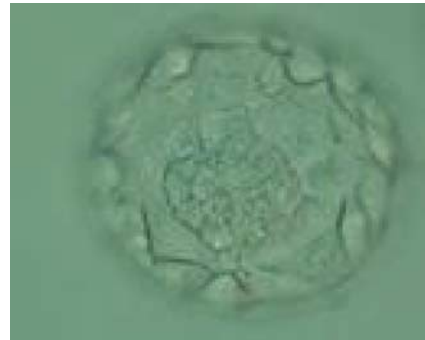


Figure 325 Expanded blastocyst (Grade 4:1:1) showing a large ICM at the base of the blastocyst in this view. There are very many TE cells forming a cohesive epithelium that lines the enlarged blastocoel cavity. The ZP is very thin. The blastocyst was transferred but failed to implant.

breach in the ZP (Figs 327–332) and Grade 6 blastocysts or hatched blastocysts are those in which the blastocyst has completely escaped from a natural breach in the ZP (Figs 333–338). The latter



Figure 326 Expanded blastocyst (Grade 4:1:1) showing a compact ICM at the 4 o'clock position in this view. The blastocyst is now larger in volume than the original volume of the embryo causing the ZP to thin. The blastocyst was transferred but failed to implant.



Figure 327 Hatching blastocyst (Grade 5:2:1) showing a small triangular ICM being drawn out along with the herniating TE cells at the 1 o'clock position in this view. There are very many TE cells of similar size lining the blastocoel cavity and the ZP is thinned. The blastocyst was transferred but the outcome is unknown.

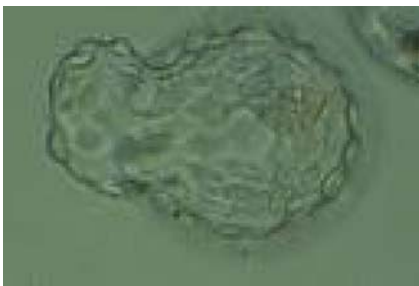


Figure 328 Hatching blastocyst (Grade 5:1:1) showing a large, compact ICM at the 1 o'clock position in this view. Approximately 25% of the blastocyst has herniated from a breach in the thinned ZP at the 8–10 o'clock positions in this view. The blastocyst was transferred but the outcome is unknown.

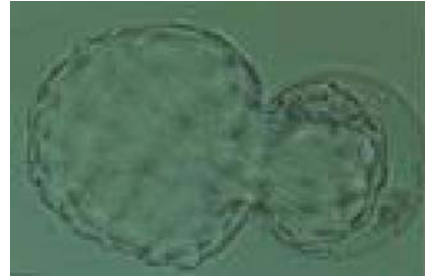


Figure 329 Hatching blastocyst (Grade 5:1:1) showing a large, compact, crescent-shaped ICM retained within the ZP at the 12 o'clock position in this view. There are very many TE cells and almost 75% of the blastocyst has herniated out through a breach in the ZP at the 8–10 o'clock positions in this view. The blastocyst was transferred but the outcome is unknown.



Figure 330 Hatching blastocyst (Grade 5:1:1) showing a large, compact ICM at the 2 o'clock position in this view. There are many TE cells of equivalent size lining the blastocoel cavity and several TE cells are herniating through a breach in the thinned ZP at the 8 o'clock position in this view. The blastocyst was transferred and implanted.



Figure 331 Hatching blastocyst (Grade 5:1:1) showing a large, compact ICM at the base of the blastocyst toward the 5 o'clock position and slightly out of focus in this view. There are very many TE cells of equivalent size making up a cohesive epithelium. Several TE cells have herniated out through a breach in the ZP at the 11 o'clock position in this view. The blastocyst was transferred and implanted.

two grades should be distinguished from blastocysts that are hatching or have hatched from an artificial breach in the ZP created by an assisted hatching procedure or following embryo biopsy whereby the breach in the ZP is quite large, permitting the blastocyst to escape earlier and well before complete expansion of the blastocoel cavity. The artificially hatched blastocyst could therefore contain far fewer cells than those that undergo natural hatching.

It is not uncommon to observe blastocysts that have collapsed or are in the process of collapsing (Figs 339–341). In this instance it is difficult to accurately grade the blastocysts and the consensus document (Alpha Scientists in Reproductive Medicine and ESHRE Special Interest Group of Embryology, 2011) suggests that 1–2 h is allowed to elapse before the blastocyst is re-assessed as regular cycles of expansion and collapse are normal and can be observed even without intervention as has been recorded using continuous time-lapse recording within the incubator.



Figure 332 Hatching blastocyst (Grade 5:1:1) showing a large, compact and slightly granular ICM toward the 3 o'clock position in this view. There are very many TE cells of varying sizes making up a cohesive epithelium with several cells herniating out through a breach in the ZP at the 9 o'clock position in this view. The blastocyst was transferred but the outcome is unknown.



Figure 333 Hatched blastocyst (Grade 6:1:1) that is now completely free of the ZP. There is a large, compact ICM slightly out of focus at the base of the blastocyst toward the 4 o'clock position in this view. The blastocyst is now more than twice the size of the original expanded blastocyst. The blastocyst was transferred but failed to implant.



Figure 334 Hatched blastocyst (Grade 6:1:1) that is now completely free of the ZP showing a compact ICM at the 6 o'clock position in this view. The ICM appears to be connected or anchored to the TE by a broad triangular bridge. The TE cells vary in size but form a cohesive epithelium. The blastocyst is now more than twice the size of the original expanded blastocyst. The blastocyst was transferred but the outcome is unknown.

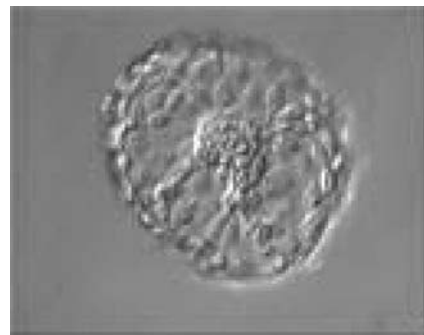


Figure 335 Hatched blastocyst (Grade 6:1:1) that is now completely free of the ZP. The ICM positioned centrally at the base of the blastocyst appears to be connected or anchored to the TE by several bridges. There are very many TE cells of similar size forming a cohesive epithelium. The blastocyst is now more than twice the size of the original expanded blastocyst.

The timing and grade of blastocyst expansion has been shown by several investigators to be an important predictor of implantation (Dokras et al., 1993; Gardner et al., 2000; Shapiro et al., 2008; Ahlström et al., 2011). It must, however, be remembered that embryologists have traditionally chosen to transfer the most developed blastocyst with the highest grade of expansion when available for transfer. No randomized, controlled trial comparing transfer of good quality blastocysts of a lower grade when they are present within a cohort that includes blastocysts with higher grades has been undertaken. Furthermore, recent evidence suggests that human female embryos undergo X chromosome inactivation from the 8-cell cleavage stage to the blastocyst stage of development which takes some time, therefore meaning that female blastocysts may be less expanded than their male sibling blastocysts but may be just as viable (van den Berg et al., 2009).



Figure 336 Hatched blastocyst (Grade 6:1:1) that is now completely free of the ZP which can be seen in the same view. Some cellular debris remains behind in the empty ZP. The ICM is large and compact at the base of the blastocyst and there are many TE cells making up a cohesive epithelium. In this view, it is possible to clearly see the increase in diameter of the blastocyst from the diameter of the original embryo which was accommodated within the ZP.

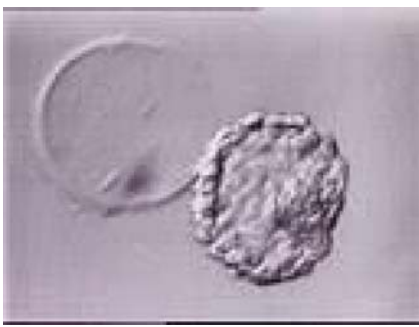


Figure 337 Hatched blastocyst (Grade 6:1:1) that is now completely free of the ZP which can be seen in the same view. The breach in the ZP is large. The ICM and TE both have many cells and the blastocyst has collapsed slightly and appears more dense. The blastocyst was transferred but the outcome is unknown.

B. ICM morphology

Once the blastocyst has reached an expansion grade of 3 or more, a clear distinction can be made between the two newly formed cell populations. The outer cells of the blastocyst, forming the blastocyst structure itself are called the TE cells and the cells located inside the blastocoel, often forming a cell clump at one pole of the blastocyst, are called the ICM cells. The destiny of the ICM is to become the embryo proper and its associated extra-embryonic structures. Morphologically, the ICM can range from being very large with tightly packed cells to almost non-existent with loosely bound cells. Accordingly, the ICM has been categorized into three morphological categories (Gardner and Schoolcraft, 1999; Alpha Scientists in Reproductive Medicine and ESHRE Special Interest Group of Embryology, 2011).



Figure 338 Hatched blastocyst (Grade 6:1:1) that is now just free of the ZP which can also be seen in the low magnification view. The ICM is slightly out of focus in this view and is made up of many cells. The TE is similarly made up of many cells forming a cohesive epithelium. There is some cellular debris discarded in the ZP. The blastocyst was transferred but the outcome is unknown.



Figure 339 Collapsed blastocyst, which judging from the thickness of the ZP, is at least a Grade 3. The ICM and TE however cannot be accurately assessed. The blastocyst was transferred but the outcome is unknown.



Figure 340 Collapsed blastocyst, which judging from the thickness of the ZP, is at least a Grade 3. In this view the ICM is clearly discernible at the 3 o'clock position and appears to be of Grade 1 quality. Similarly what can be seen of the TE cells appears to be Grade 1 in quality. There is some extraembryonic cellular debris in the PVS. The blastocyst was transferred but failed to implant.



Figure 341 Collapsed hatching blastocyst (Grade 5) with the hatching site clearly visible as a breach in the ZP at the 11 o'clock position in this view. There is extraembryonic cellular debris both within the blastocoel cavity and external to the blastocyst in the PVS. Both the ICM and TE cannot be properly evaluated. The blastocyst was transferred but failed to implant.



Figure 343 Expanded blastocyst (Grade 4:1:1) showing a large ICM at the base of the blastocyst in this view. The ICM is made up of many cells that are tightly compacted. The blastocyst was transferred but the outcome is unknown.



Figure 342 Expanded blastocyst (Grade 4:1:1) showing a large ICM at the 4 o'clock position in this view. The ICM is made up of many cells and is very compact. The blastocyst was transferred but the outcome is unknown.



Figure 344 Blastocyst (Grade 3:1:1) showing a very large, mushroom-shaped ICM at the 10 o'clock position in this view. The ICM is made up of many cells that are tightly compacted. The blastocyst was transferred and resulted in the delivery of a healthy girl.

The best ICM category (1) contains many cells that are tightly packed together (Figs 342–345), the middle ICM category (2) is composed of several cells that are loosely grouped (Figs 346–349) and the worst category (3) describes an ICM that contains very few cells that are loosely bound (Figs 350–353). The number of cells composing the ICM can vary as well as the morphology of the cells within the ICM. Several studies have shown a positive correlation between the morphological appearance of the ICM to clinical outcome, the hypothesis being that the larger the ICM the better the chances of a successful implantation (Balaban et al., 2000; Richter et al., 2001).

The shape of the ICM has been observed to be quite variable in appearance. It has been reported that the optimal shape of the ICM with respect to implantation potential is more oval in shape rather than the rounder or more elongated forms (Richter et al., 2001). The shape of the ICM could in this instance reflect the number of cells involved. This Atlas identifies some further variability in shape and has classified the ICM into mushroom shaped (Figs 354–356), stellate shaped (Figs 357–359) and crescent shaped (Figs 360–362),



Figure 345 Hatching blastocyst (Grade 5:1:1) showing a large ICM at the base of the blastocyst in this view. The ICM is made up of many cells that are tightly compacted. The blastocyst was transferred but the outcome is unknown.



Figure 346 Blastocyst (Grade 3:2:1) showing a compact ICM at the 11 o'clock position in this view. The ICM is small relative to the diameter of the blastocyst and probably made up of few cells. The blastocyst was transferred but failed to implant.



Figure 349 Hatching blastocyst (Grade 5:2:1) showing a compact ICM toward the 1 o'clock position in this view. The ICM is very small and made up of few cells relative to the size of the blastocyst. There are a few small, dark degenerative foci in the TE cells. The blastocyst was transferred but failed to implant.

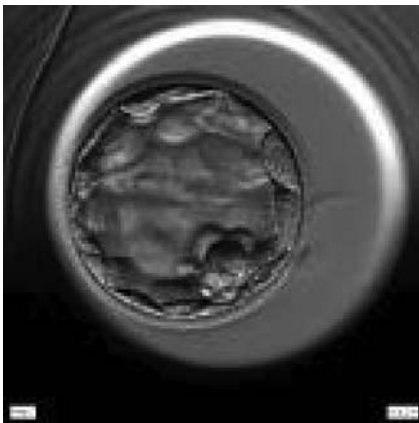


Figure 347 Blastocyst (Grade 3:2:1) showing a compact ICM at the 5 o'clock position in this view. The ICM is very small and made up of only a few cells. The blastocyst was transferred but the outcome is unknown.

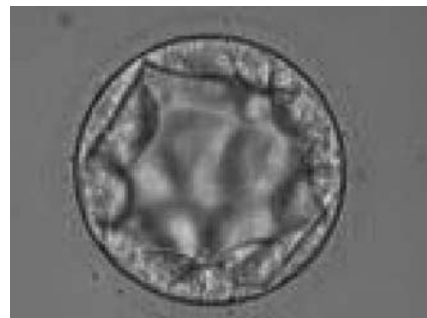


Figure 350 Blastocyst (Grade 3:3:2) with no clearly identifiable ICM and with TE cells that in places are quite large and stretch over great distances to reach the next cell.

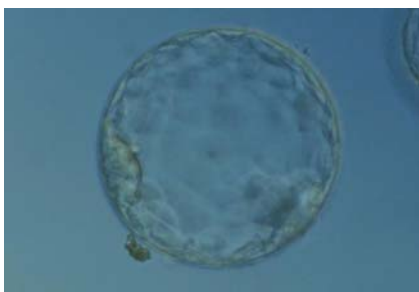


Figure 348 Hatching blastocyst (Grade 5:2:1) showing a compact ICM at the 8 o'clock position in this view. The ICM is small and flattened and made up of few cells relative to the size of the blastocyst. The blastocyst was transferred but the outcome is unknown.



Figure 351 Blastocyst (Grade 3:3:3) with no clearly identifiable ICM and sparse TE that does not form a cohesive epithelium.



Figure 352 Expanded blastocyst (Grade 4:3:3) with no clearly identifiable ICM. TE is made up of a few, sparse cells that do not form a cohesive epithelium.



Figure 355 Expanded blastocyst (Grade 4:2:1) with a small, mushroom-shaped compact ICM. There is some cellular debris present in the space between the ZP and the TE at the 10–12 o'clock positions. The blastocyst was transferred but the outcome is unknown.

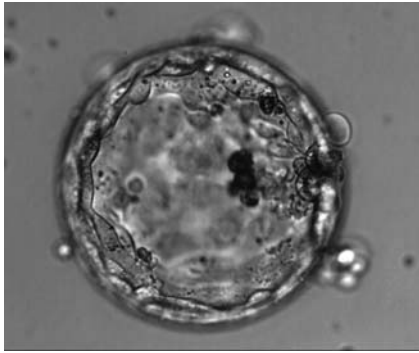


Figure 353 Hatching blastocyst (Grade 4:3:1) with no clearly identifiable ICM but a TE that is made up of many cells forming a cohesive epithelium. Dark, degenerate cells are present toward the 3 o'clock position in this view.



Figure 356 Blastocyst (Grade 3:1:1) showing a very large, mushroom-shaped ICM at the 10 o'clock position in this view and made up of many cells that are tightly compacted. The blastocyst was transferred and resulted in the delivery of a healthy girl.



Figure 354 Good quality expanded blastocyst (Grade 4:1:1) with a large mushroom-shaped ICM. There appears to be cytoplasmic strings extending from the ICM to the TE. The blastocyst was transferred and implanted.



Figure 357 Expanded blastocyst (Grade 4:1:1) with a large stellate ICM flattened at the base of the blastocyst in this view. The blastocyst was transferred and implanted.



Figure 358 Hatching blastocyst (Grade 5:1:2) with a large stellate ICM present at the base of the blastocyst in this view. The ICM seems to be connected to the TE cells with short triangular cytoplasmic strings or bridges. The blastocyst was transferred but failed to implant.



Figure 359 Expanded blastocyst (Grade 4:1:1) with a large stellate ICM present at the base of the blastocyst in this view. The blastocyst was transferred and implanted.



Figure 360 Hatching blastocyst (Grade 5:1:1) with a compact crescent-shaped ICM flattened to the TE at the 9 o'clock position in this view. There is a large amount of TE herniating from a breach in the ZP at the 3 o'clock position and a second smaller site of herniation at the 6 o'clock position. The blastocyst developed following ICSI and so the breach in the ZP at the 6 o'clock position may be a result of the injection site. This blastocyst did not result in a pregnancy following transfer.



Figure 361 Hatching blastocyst (Grade 5:1:1) showing a large crescent-shaped ICM at the 12 o'clock position in this view. The blastocyst was transferred and implanted.



Figure 362 Blastocyst (Grade 3:1:1) with a crescent-shaped ICM at the 10 o'clock position in this view. The blastocyst was transferred but the outcome is unknown.

the significance of the shape variations to implantation potential being unknown.

An occasional observation is the presence of two separate ICMs within the blastocyst. Chida (2000) reported the incidence of a double ICM as 3.1% for *in vitro* cultured mouse blastocysts and the majority of these developed after hatching into trophoblastic outgrowth formation with a double ICM. They found that the frequency of a double ICM was significantly higher in *in vitro* fertilized blastocysts than that for *in vivo* fertilized blastocysts (0.6%). Therefore, it was hypothesized that the *in vitro* fertilization conditions could influence the incidence of double ICMs and as a consequence the incidence of monozygotic twinning.

Meintjes *et al.* (2001) reported a human IVF monozygotic pregnancy resulting from a blastocyst with two distinct ICMs. In fact, it was a triplet pregnancy obtained after transfer of two Day 5 blastocysts. The monozygotic pregnancy was found to be dichorionic diamniotic, indicating the splitting of the TE as well. Payne *et al.* (2007) presented at the ESHRE congress in 2007 a time-lapse recording of frozen–thawed human embryos cultured to the blastocyst stage. Out of 26 blastocysts, two had a double ICM already evident at the early blastocyst stage. Remarkably, the second ICM seemed to be developed after ectopic adhesion of ICM cells to the opposing TE cells following early collapse of the blastocoel cavity. This Atlas illustrates two incidences where the ICM appears to be duplicated (Figs 363 and 364).

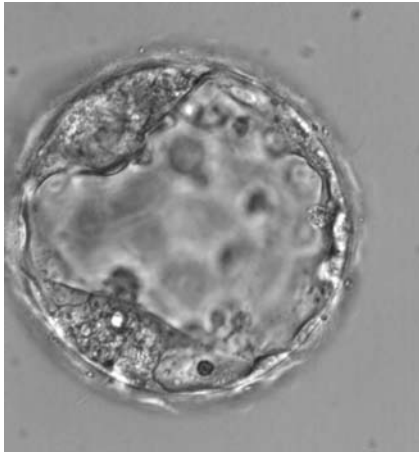


Figure 363 Expanded blastocyst (Grade 4:1:1) with two distinct ICMs at the 7 and 11 o'clock positions in this view. Both ICMs are of reasonable size and compact.



Figure 364 Hatching blastocyst (Grade 5:1:1) with two separate ICMs that appear to be connected to each other at the 2 o'clock position in this view. One ICM appears to be smaller than the other and is beginning to herniate through a breach in the ZP at the 4 o'clock position along with several TE cells. The blastocyst was transferred and failed to implant.

C. TE morphology

The TE cells can be clearly distinguished from the ICM cells as the blastocyst begins to expand (i.e. expansion Grade 3 or higher). The role of the TE cells in the early stages of blastocyst development is not entirely clear but their role in creating the fluid filled blastocoel may be a key parameter in ICM determination. The role of the TE cells, however, is better understood during and after implantation as they play a key role in apposition, adhesion and invasion of the endometrium, thus allowing the blastocyst to embed in the uterus. The TE cells also produce several molecular factors that aid in the implantation process (Aplin, 2000). Without properly functional TE cells, the embryo would remain within the ZP as these cells are actively involved in breaking free of the ZP (Sathananthan et al., 2003). The ultimate fate of the TE cells is to become the fetal extra-embryonic membranes as well as the placenta.

The TE cells have traditionally been scored in a similar manner to the ICM, i.e. by their number and cohesiveness according to three different grades (1–3). The best TE category (1) contains many cells that form a cohesive epithelium (Figs 365–368), the middle TE category



Figure 365 Expanded blastocyst (Grade 4:1:1) with many evenly sized cells making up a cohesive TE surrounding the enlarged blastocoel cavity. The ICM is clearly visible at the 4 o'clock position in this view. The blastocyst was transferred but the outcome is unknown.



Figure 366 Early hatching blastocyst (Grade 5:1:1) with many cells making up a cohesive epithelium. The ICM is not clearly visible in this view. The blastocyst was transferred but failed to implant.

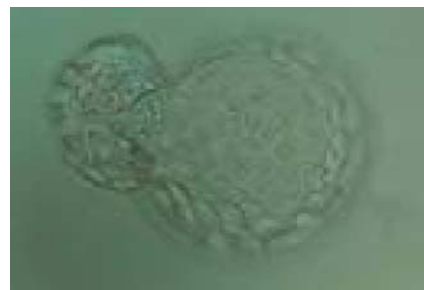


Figure 367 Hatching blastocyst (Grade 5:1:1) with many cells making up a cohesive TE. The ICM is herniating through a breach in the ZP at the 10 o'clock position in this view. The blastocyst was transferred but failed to implant.

(2) is composed of few cells forming a loose epithelium (Figs 369–372) and the worst category (3) describes a TE that contains very few, large cells that struggle to form a cohesive epithelium (Figs 373–376). The grading of the TE cells has been demonstrated in some reports to have an association with implantation (Zaninovic *et al.*, 2001; Ahlström *et al.*, 2011), whereas other publications have

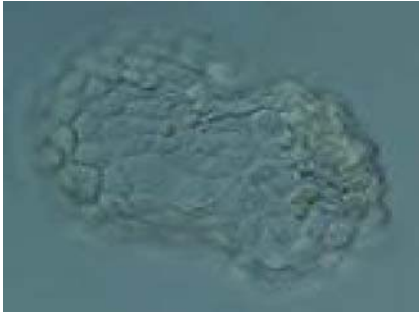


Figure 368 Hatching blastocyst (Grade 5:1:1) with many cells, some of variable size, making up a cohesive epithelium. The blastocyst was transferred but failed to implant.

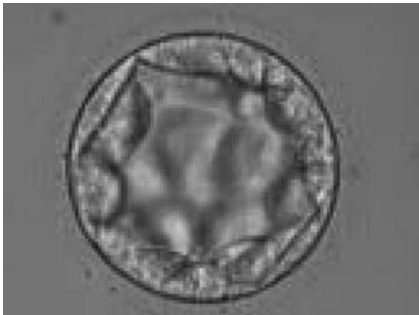


Figure 369 Blastocyst (Grade 3:3:2) with TE cells that in places are quite large and stretch over great distances to reach the next cell. No ICM can be identified.



Figure 370 Hatching blastocyst (Grade 5.1:2) with few TE cells that form a loosely cohesive epithelium, and with a mushroom-shaped ICM at the 12 o'clock position in this view. The blastocyst was transferred but failed to implant.



Figure 371 Hatching blastocyst (Grade 5.1:2). The TE cells vary in size with some cells quite large forming a loosely cohesive epithelium. A stellate ICM can be seen at the 8 o'clock position in this view. The blastocyst was transferred and failed to implant.



Figure 372 Expanded blastocyst (Grade 4:1:2). The TE cells vary in size with some cells quite large being particularly evident at the edge of the blastocyst where the cells stretch over some distance to reach their nearest neighbors. The blastocyst was transferred but the outcome is unknown.



Figure 373 Early hatching blastocyst (Grade 5:1:3) with a very sparse TE that does not form a cohesive epithelium. The ICM is visible at the 10 o'clock position in this view.



Figure 374 Blastocyst (Grade 3:3:3) with sparse TE that does not form a cohesive epithelium. The ICM is not clearly identifiable.



Figure 375 Expanded blastocyst (Grade 4:3:3) with sparse TE that does not form a cohesive epithelium. The ICM is hardly distinguishable despite the expansion of the blastocoel cavity.

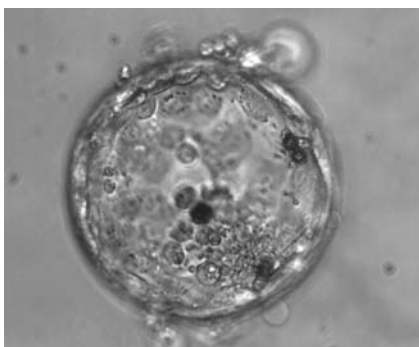


Figure 376 Hatching blastocyst (Grade 5:3:3). The TE varies in size and does not form a cohesive epithelium. Several loosely cohesive ICM cells can be seen at the 5 o'clock position in this view. There are several dark degenerate foci within the blastocyst.

found no relationship between TE grade and viability (Richter *et al.*, 2001).

Fong *et al.* (2001) reported the detailed ultrastructural appearance of TE cells from naturally hatched and enzymatically hatched blastocysts. There was no difference in the ultrastructural appearance of the TE cells following exposure to enzyme: outer tight and adherent junctions, desmosomes, gap junctions, microvilli on the free surfaces, oval-to-tubular mitochondria with well-developed cristae typical of blastocysts, rough endoplasmic reticulum, Golgi complexes, occasional centrioles associated with microtubules, lysosomes, multivesicular bodies and spherical lipid globules present in many cells. Dark granules can be observed in many TE cells at the light microscopic level which are likely to be the lipid globules (Figs 377–379).

D. Cellular degeneration in blastocysts

Cell death can occur by necrosis or apoptosis, two processes with different morphological features and significance. Necrosis involves swelling of cells and membrane rupture that follows irreversible damage (Wyllie, 1980). Cell death generally occurs by apoptosis, characterized



Figure 377 Expanded blastocyst (Grade 4:1:1). Note several dark granules within the majority of the TE cells. The ICM has several fragments. The blastocyst was transferred but failed to implant.



Figure 378 Hatching blastocyst (Grade 5:1:1) showing the herniating TE cells at high magnification. Many of the TE cells contain several dark granules. The blastocyst was transferred but the outcome is unknown.



Figure 379 Hatching blastocyst (Grade 5:1:1) showing many of the TE cells contain dark granules. Several fragments are associated with a centrally positioned, compact ICM. The blastocyst was transferred and implanted.



Figure 380 Blastocyst (Grade 3:1:1) with a compact ICM at the base of the blastocyst that is associated with several granular cellular fragments and two darker foci of cell degeneration. The TE cells appear to be healthy and form a cohesive epithelium. The blastocyst was transferred but failed to implant.

by cellular shrinkage and involves aggregation of nuclear chromatin, condensation of the cytoplasm and indentation of nuclear and cytoplasmic membranes (Figs 380–382). The nucleus becomes fragmented, the cell forms blebs and fragments into apoptotic bodies (Hardy 1997; 1999).

Hardy *et al.* (1989) showed by differential labelling of TE and ICM nuclei in supernumerary human blastocysts that the percentage of cell death was similar in both ICM and TE cells and increased with culturing blastocysts up to Day 7. The dead cell index was <10% for Days 5 and 6 good quality blastocysts but was increased up to 27.0 and 38.5% for Day 6 morphologically abnormal and polyspermic blastocysts, respectively. Dead cells within the blastocyst can be dissolved by the process of phagocytosis.

Isolated foci of degeneration should be distinguished from total degenerative change within the blastocyst as described and classified as BG3 blastocysts by Dokras *et al.* (1993; Fig. 382). These blastocysts are irredeemable, continue to degenerate further and have no potential to implant and develop to term.

Arrested cells that have arisen at any time throughout preimplantation development are often excluded from the formation of the blastocyst and are sequestered to the PVS and can be observed

between the further developing blastocyst and the ZP (Figs 383–385). Occasionally these cells, or more likely cells that have arrested much later in development, are present internally during blastocyst



Figure 381 Hatched blastocyst (Grade 6:1:1) showing many cells in the TE making a cohesive epithelium. Many of the TE cells contain dark granules. The ICM is not clearly seen in this view and there are several degenerative foci (dark cells) associated with the ICM and polar TE. The blastocyst was transferred and implanted.



Figure 382 Poor quality, degenerating, early blastocyst in which the majority of cells are showing dark, degenerative changes.



Figure 383 Blastocyst (Grade 3:1:2) with a large, mushroom-shaped ICM toward the 1 o'clock position in this view. From the 6 o'clock to the 3 o'clock position there is a significant amount of cellular debris, both large and small, between the mural TE and the ZP.

formation and rather than being sequestered to the PVS are sequestered to the blastocoel cavity (Figs 386–388) and take no further part in development. It has been demonstrated that excluded cells have poor gap junction communication with the embryo (Hardy et al., 1996). It was hypothesized that the presence of isolated cells in the blastocyst at a time when phagocytosis is possible indicates the absence of cell surface markers that promote their ingestion by neighboring cells (Hardy, 1997).

Kovacic et al. (2004) studied the developmental capacity of morphologically suboptimal blastocysts, classified into different categories. It was found that live birth rates after transfer of poor quality blastocysts was decreased in the following order of categories compared with the live birth rate in a control group of good quality blastocysts (45.2%): blastocysts with cytoplasmic fragments and necrotic TE (32.8%), blastocysts with a maximum of 20% excluded blastomeres (16.7%), necrotic TE and ICM (7.7%) and finally very small blastocysts with >20% excluded cells (1.2%).



Figure 384 Hatching blastocyst that has collapsed into a dense mass of cells making it impossible to evaluate the ICM and TE cells. Several cells not participating in blastocyst formation can be seen in the PVS.



Figure 385 An early blastocyst with a large blastocoel cavity. Note the large cellular debris sequestered into the PVS which does not take part in the blastocyst formation.



Figure 386 Early blastocyst (Grade 2) in which the ICM is not yet clearly discernible. Many of the TE cells contain dark granules. In addition there is a large number of small fragments which can be best seen between the 8 and 9 o'clock positions in this view. The blastocyst was transferred but the outcome is unknown.

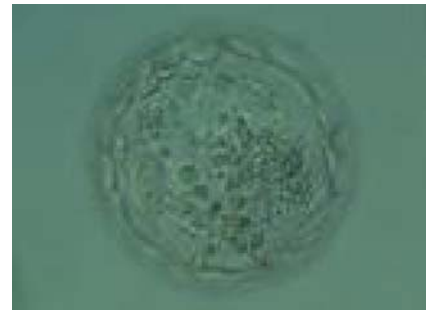


Figure 387 Expanded blastocyst (Grade 4:1:1) in which the ICM is not clear in this view. The TE cells vary in size but form a cohesive epithelium. There are several small- to medium-sized fragments present inside the blastocoel cavity, some of which are quite dark. The blastocyst was transferred but failed to implant.



Figure 388 Hatching blastocyst (Grade 5:1:1) in which a large, compact ICM can be seen at the 7 o'clock position and the herniating TE can be seen at the 12 o'clock position in this view. Several large fragments can be observed inside the blastocoel cavity. The blastocyst failed to implant after transfer.

E. Cytoplasmic strings/bridges between ICM and TE

TE cells proliferate in the early blastocyst but once the blastocyst is expanding, the mitotic activity of the mural TE cells (separated from the ICM by the blastocoel) declines. This means that by the time the embryo implants, cell division occurs only at the polar region in both the polar TE cells and ICM (Copp, 1978). Cell numbers increase in the ICM but this is not the case for the polar TE due to migration of polar TE cells to the mural TE region, which is mitotically inactive (Copp 1979). Studies of the ultrastructure of blastocysts have demonstrated that some TE cells at the polar-mural junction extend cell projections to the surface of the ICM cells (Figs 389–391; Ducibella *et al.*, 1975). In the work of Salas-Vidal and Lomeli (2004), these cytoplasmic extensions or filopodia in mouse blastocysts were extensively characterized. They contain filamentous actin and can be classified into short and long filopodia. The short filopodia extend both from the ICM and the mural TE into the blastocoel cavity and are found abundantly. The



Figure 389 Good quality expanded blastocyst (Grade 4:1:1) with a large mushroom-shaped ICM and a well organized TE. There appears to be cytoplasmic strings extending from the ICM to the TE. The blastocyst was transferred and implanted.



Figure 390 Hatching blastocyst (Grade 5:1:2) with a large stellate ICM that seems to be connected to the TE cells with short triangular cytoplasmic strings or bridges. The blastocyst was transferred but failed to implant.



Figure 391 Hatched blastocyst (Grade 6:1:1) that is now completely free of the ZP showing a compact ICM that appears to be connected or anchored to the TE by a broad triangular bridge. The blastocyst was transferred but the outcome is unknown.

long, thin filopodia traverse the blastocoel from the mural TE to a central ICM cell and were found in 40% of *in vivo* produced mouse blastocysts. However, they were observed in almost all *in vitro* cultured blastocysts, indicating a possible defect associated with *in vitro* culture. Normally, these long extensions appear in the early blastocyst and are withdrawn in the expanded blastocyst once the polar TE cells have migrated to the mural TE. When these extensions are still present during expansion, this could be an indication of poor embryo development, breakdown of polarization or poor media conditions (Scott, 2000). With digital imaging video, Salas-Vidal and Lomeli (2004) observed vesicle-like bulges moving along the long filopodia, suggesting cellular activity. Immunolocalization of the FGFR2 and ErbB3 receptors also suggest signal transduction activity within these filopodia indicating a direct communication between the mural TE and the ICM cells.

F. Other morphological features

F.1 Vacuoles/vacuolation

Vacuoles can arise during *in vitro* culture of human embryos at any stage of development (Ebner *et al.*, 2005). Those first detected on Day 4 of development have the most severe impact on blastocyst development (Ebner *et al.*, 2005). Vacuoles appearing in early development cannot often be detected within the blastocyst or can be detected only in excluded cells (Ebner *et al.*, 2005). Vacuoles when found within the blastocyst appear more often in the TE than in the ICM (Figs 392–394; Ebner *et al.*, 2005). These vacuoles should be distinguished from degenerative changes or vacuolation described and classified as BG3 blastocysts by Dokras *et al.*, 1993.

F.2 More than one point of natural hatching

A rare finding in blastocyst assessment is the occurrence of two or more sites of hatching (Figs 395–397; 2%; Fong *et al.*, 2001). It has been suggested that this might arise in ICSI-generated blastocysts due to incomplete closure of the zona breach created by the micro-injection pipette (Fong *et al.*, 1997). Hatching at more than one point in the ZP, particularly when one of the holes is very small could result in trapping of the blastocyst within the ZP as the pressure



Figure 392 Expanded blastocyst (Grade 4:3:2) in which a large vacuole can be seen at the 6 o'clock position between TE cells. The blastocyst was transferred but the outcome is unknown.



Figure 393 Hatching blastocyst (Grade 5:1:1) showing a compact ICM at the 6 o'clock position which is associated with several cellular fragments. The TE is made up of many cells that form a cohesive epithelium but there are two medium-sized vacuoles within TE cells abutting the ICM toward the 9 o'clock position. The blastocyst was transferred but failed to implant.



Figure 394 Early blastocyst (Grade 2) with large vacuolization of the TE distinct from the blastocoel cavity at the 10 o'clock position in this view. The blastocyst was transferred but the outcome is unknown.



Figure 395 Early hatching blastocyst (Grade 5:1:1) which is beginning to hatch naturally from two different small breaches in the ZP. The ICM is large and compact and the TE cells are many and form a cohesive epithelium. The blastocyst was transferred but the outcome is unknown.

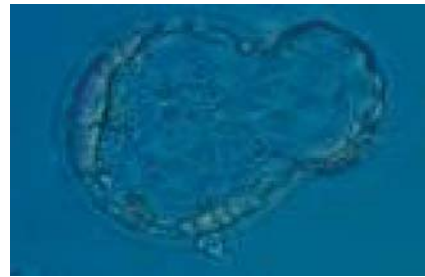


Figure 396 Hatching blastocyst (Grade 5:1:1) with a large amount of TE herniating from a breach in the ZP at the 3 o'clock position and a second smaller site of herniation at the 6 o'clock position. The blastocyst developed following ICSI and so the breach in the ZP at the 6 o'clock position may be a result of the injection site. This blastocyst did not result in a pregnancy following transfer.

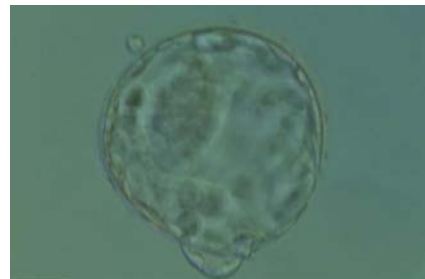


Figure 397 Hatching blastocyst (Grade 5:1:1) with two distinct points of natural hatching, one at the 11 o'clock and one at the 6 o'clock position. The ICM is large and compact and the TE cells are many and form a cohesive epithelium. There is a significant difference in the diameter of the two breaches in the ZP. The blastocyst developed following standard insemination and so the smaller diameter breach is not a result of sperm injection. The blastocyst was transferred but failed to implant.

within the blastocoel cavity would be dissipated and not concentrated on one hatching site.

References

- Ahlström A, Westin C, Reiser E, Wikland M, Hardarson T. Trophoctoderm morphology: an important parameter for predicting pregnancy and birth after single blastocyst transfer. *Hum Reprod* 2011; **26**:3289–3296.
- Alpha Scientists in Reproductive Medicine and ESHRE Special Interest Group of Embryology. The Istanbul consensus workshop on embryo assessment: proceedings of an expert meeting. *Hum Reprod* 2011; **26**:1270–1283.
- Aplin JD. The cell biological basis of implantation. *Baillieres Best Pract Res Clin Obstet Gynaecol* 2000; **14**:757–764.
- Balaban B, Urman B, Sertac A, Alatas C, Aksoy S, Mercan R. Blastocyst quality affects the success of blastocyst-stage embryo transfer. *Fertil Steril* 2000; **74**:282–287.
- Chida S. Monozygous double inner cell masses in mouse blastocysts following fertilization *in vitro* and *in vivo*. *J In Vitro Fert Embryo Transf* 2000; **7**:177–179.
- Copp AJ. Interaction between inner cell mass and trophoctoderm of the mouse blastocyst. I. A study of cellular proliferation. *J Embryol Exp Morphol* 1978; **48**:109–125.
- Copp AJ. Interaction between inner cell mass and trophoctoderm of the mouse blastocyst. II. The fate of the polar trophoctoderm. *J Embryol Exp Morphol* 1979; **51**:109–120.
- Dokras A, Sargent IL, Barlow DH. Human blastocyst grading: an indicator of developmental potential? *Hum Reprod* 1993; **8**:2119–2127.
- Ducibella T, Albertini DF, Anderson E, Biggers JD. The preimplantation mammalian embryo: characterization of intercellular junctions and their appearance during development. *Dev Biol* 1975; **45**:231–250.
- Ebner T, Moser M, Sommergruber M, Gaiswinkler U, Shebl O, Jesacher K, Tews G. Occurrence and developmental consequences of vacuoles throughout preimplantation development. *Fertil Steril* 2005; **83**:1635–1640.
- Edwards RG, Brody SA. History and ethics of assisted human conception. In: Brody SA (ed.). *Principles and Practice of Assisted Human Reproduction*. Philadelphia, USA: WB Saunders, 1995, 17–47.
- Fong CY, Bongso A, Ng SC, Anandakumar C, Trounson A, Ratnam S. Ongoing normal pregnancy after transfer of zona-free blastocysts: implications for embryo transfer in the human. *Hum Reprod* 1997; **12**:557–560.
- Fong CY, Bongso A, Sathananthan H, Ho J, Ng SC. Ultrastructural observations of enzymatically treated human blastocysts: zona-free blastocyst transfer and rescue of blastocysts with hatching difficulties. *Hum Reprod* 2001; **16**:540–546.
- Gardner DK, Schoolcraft WB. *In vitro* culture of human blastocysts. In: Jansen R, Mortimer D (eds). *Toward Reproductive Certainty: Fertility and Genetics Beyond 1999*. UK: Parthenon Publishing London, 1999, 378–388.
- Gardner DK, Lane M, Stevens J, Schlenker T, Schoolcraft WB. Blastocyst score affects implantation and pregnancy outcome: towards a single blastocyst transfer. *Fertil Steril* 2000; **73**:1155–1158.
- Hardarson T, Caisander C, Sjögren A, Hanson C, Hamberger L, Lundin K. A morphological and chromosomal study of blastocysts developing from morphologically suboptimal human preembryos compared to control blastocysts. *Hum Reprod* 2003; **18**:399–407.
- Hardy K. Cell death in the mammalian blastocyst. *Mol Hum Reprod* 1997; **3**:919–925.
- Hardy K. Apoptosis in the human embryo. *Rev Reprod* 1999; **4**:125–134.
- Hardy K, Handyside AH, Winston R. The human blastocyst: cell number, death and allocation during late preimplantation development *in vitro*. *Development* 1989; **107**:597–604.
- Hardy K, Warner A, Winston R, Becker L. Expression of intercellular junctions during preimplantation development of the human embryo. *Mol Hum Reprod* 1996; **2**:621–632.
- Kovacic B, Vlaisavljevic V, Reljic M, Cizek-Sajko M. Developmental capacity of different morphological types of day 5 human morulae and blastocysts. *Reprod Biomed Online* 2004; **8**:687–694.
- Meintjes M, Guerami AR, Rodriguez JA, Crider-Pirkle SS, Madden JD. Prospective identification of an in-vitro-assisted monozygotic pregnancy based on a double-inner-cell-mass blastocyst. *Fertil Steril* 2001; **76**:S172–S173.
- Payne D, Okuda A, Wakatsuki Y, Takeshita C, Iwata K, Shimura T, Yumoto K, Ueno Y, Flaherty S, Mio Y. Time-lapse recording identifies human blastocysts at risk of producing monozygotic twins. *Hum Reprod* 2007; **22**(Suppl.):i9–i10.
- Richter KS, Harris DC, Daneshmand ST, Shapiro BS. Quantitative grading of a human blastocyst: optimal inner cell mass size and shape. *Fertil Steril* 2001; **76**:1157–1167.
- Salas-Vidal E, Lomeli H. Imaging filopodia dynamics in the mouse blastocyst. *Dev Biol* 2004; **265**:75–89.
- Sathananthan H, Menezes J, Gunasheela S. Mechanics of human blastocyst hatching *in vitro*. *Reprod BioMed Online* 2003; **7**:228–234.
- Scott L. Oocyte and embryo polarity. *Semin Reprod Med* 2000; **18**:171–183.
- Shapiro BS, Daneshmand ST, Garner FC, Aguirre M, Thomas S. Large blastocyst diameter, early blastulation, and low preovulatory serum progesterone are dominant predictors of clinical pregnancy in fresh autologous cycles. *Fertil Steril* 2008; **90**:302–309.
- Van den Berg IM, Laven JS, Stevens M, Jonkers I, Galjaard RJ, Gribnau J, van Doorninck JH. X chromosome inactivation is initiated in human preimplantation embryos. *Am J Hum Genet* 2009; **84**:771–779.
- Watson AJ, Natale DR, Barcroft LC. Molecular regulation of blastocyst formation. *Anim Reprod Sci* 2004; **82–83**:583–592.
- Wyllie AH. Glucocorticoid-induced thymocyte apoptosis is associated with endogenous endonuclease activation. *Nature* 1980; **284**:555–556.
- Zaninovic N, Berrios R, Clarke RN, Bodine R, Ye Z, Veeck LL. Blastocyst expansion, inner cell mass (ICM) formation, and trophoctoderm (TM) quality: is one more important for implantation? *Fertil Steril* 2001; **76**:S8.